REPORT DOCUMENTATION PAGE

AFOSR-TR-97

1. AGENCY USE ONLY (Leave blank)	2. REPORT DATE	3. REPORT TYPE AND DATES COVERED
	April 1997	FINAL 1 Dec 1993 - 30 Apr 1997

4. TITLE AND SUBTITLE
Knowing the Depth of a Shallow Seismic Event, How Often Can We Find Depth Phases at Regional Distances?

5. FUNDING NUMBERS
PE 61102F
Proj 2309/AS
F49620-94-1-0086

6. AUTHOR(S)
James E. Zollweg
Dean M. Childs

7. PERFORMING ORGANIZATION NAME(S) AND ADDRESS(ES)
Department of Geosciences
Boise State University
Boise ID 83725

8. PERFORMING ORGANIZATION REPORT NUMBER
None

9. SPONSORING / MONITORING AGENCY NAME(S) AND ADDRESS(ES)
AFOSR/NM
110 Duncan Ave
Bolling AFB DC 20332

10. SPONSORING / MONITORING AGENCY REPORT NUMBER
Monograph Series of Seismic Research #97-12

11. SUPPLEMENTARY NOTES

12a. DISTRIBUTION AVAILABILITY STATEMENT
APPROVED FOR PUBLIC RELEASE
DISTRIBUTION UNLIMITED

12b. DISTRIBUTION CODE

13. ABSTRACT (Maximum 200 words)

Data from events (2.5 - 4.5M) in 2 U.S. Pacific Northwest earthquake sequences have been examined with a view toward improving the ability of small numbers of stations to accurately determine relative focal depth at near-regional distances (100-400km). Most phase arrivals predicted by regional crustal studies were not observed, including Pg in the range where it is a secondary phase. Pn was usually visible only for M3+ events. Of the observed phases, PmP and reflections from shallower discontinuties were most prevalent. An empirical method was established to identify depth-dependence of observed phases without the necessity of specifically identifying the phases. Using this method, it was found that approximately 1/3 of the stations that were examined recorded depth-dependent P phases. In some cases, time differences between pairs of stations at nearly the same source-to-receiver azimuth were found to be linear functions of focal depth. While the empirical method requires a calibration set of accurate depths and origin times, once a calibration is established a two-station, same-azimuth time-difference method would require no knowledge of the origin time, phase identification, or velocity structure, and is relatively weakly dependent upon epicenter.

14. SUBJECT TERMS
Seismology
Regional seismic phases
Earthquake focal depth

15. NUMBER OF PAGES
92

16. PRICE CODE

17. SECURITY CLASSIFICATION OF REPORT	18. SECURITY CLASSIFICATION OF THIS PAGE	19. SECURITY CLASSIFICATION OF ABSTRACT	20. LIMITATION OF ABSTRACT
UNCLASSIFIED	UNCLASSIFIED	UNCLASSIFIED	SAR

KNOWING THE DEPTH OF A SHALLOW SEISMIC EVENT, HOW OFTEN CAN WE FIND DEPTH PHASES AT REGIONAL DISTANCES?

D. M. Childs and J. E. Zollweg
Department of Geosciences
Boise State University
Boise, ID 83725

Prepared for

AIR FORCE OFFICE OF SCIENTIFIC RESEARCH
110 Duncan Avenue Suite B115
Bolling AFB, DC 20332-0001

1.0 Introduction

Accurate location of seismic events has emerged as an important goal for detection of potential violations of the Comprehensive Test Ban Treaty (CTBT). Accurate location serves two functions. First, a reliable location helps to identify natural seismicity and routine blasting activities. Since these two categories represent the vast majority of global seismic events, accurate location can reduce the monitoring work load by eliminating these events from further processing. Second, if an event is found to be interesting from the CTBT monitoring standpoint, accurate location improves the ability of an on-site inspection team to actually make a firm determination of the nature of the event.

For many events, focal depth is the least well-determined parameter. At the same time, accurately-determined focal depths can serve as excellent discriminants, since most natural seismicity occurs at depths greater than 3 km while explosions and rockbursts usually occur at shallower depths. Development of methodology for estimation of focal depth from small numbers of stations at near-regional distances has been the focus of our current work. To date, we have been examining data from a dense short-period seismic network for earthquake sequences whose events have well-controlled relative focal depths.

The U. S. Pacific Northwest is an area of complicated crustal structure. Epicenter-to-station paths often traverse more than one geologic province (or crustal model domain) for the data set we chose for analysis. Our interest in such data has been driven by the potential wide utility of depth-determination methods that could be applied in areas of complicated or unknown crustal structure.

We have found that regional crustal models, even when very detailed, do a mediocre-to-poor job of predicting and identifying *P* arrivals visible on

seismograms. In particular, P_g seems to be identifiable only in that distance range where it is a first arrival. We have also found that in the distance range where we have the most data (150-250 km), most recorded depth-dependent *P* waves arrive within so short a time window as to make separation and identification difficult. Single-station waveforms for different events in the same sequence are often only coherent over small ranges of depth and epicenter.

At approximately 1/3 of the stations examined for each of the two earthquake sequences studied to date, depth-dependent *P* phases can be identified from depth-order plots. For the 1981 Elk Lake, Washington, sequence, we have shown in previous reports that in some cases these phases could be exploited at same-azimuth (source to receiver) station pairs to estimate focal depths. Our analysis of the Scotts Mills sequence is not yet complete.

Our results to date, while not conclusive, suggest that: (1) arrays of seismometers which can identify arrivals based on their slowness are probably more useful than using single stations and resorting to travel-times; (2) depth-dependent arrivals are observed at a minority of sites and consequently the choice of station location may prove to be important.

2.0 The Scotts Mills Earthquake Sequence

2.1 Description of the Scotts Mills aftershock sequence

On March 25th 13:34 UT a M_{dur} 5.6 earthquake occurred near the town of Scotts Mills, Oregon. Eleven portable seismographs were installed by the U.S. Geological Survey (USGS) shortly after the mainshock (Carver *et al.*, 1993). In total, 33 sites were occupied with portable instruments at various time periods, 27 by the USGS, 3 by the University of Oregon, and 3 by Oregon State University. The maximum number of stations deployed on a given day was 22. Most USGS stations were removed by April 1st and the last were removed by mid-April. Technical details of the USGS monitoring effort can be found in Carver *et al.* (1993).

Using a single master event technique, Thomas *et al.* (1996) relocated 148 aftershocks. From these they selected a subset of 50 aftershocks for detailed analysis. These events all had some portable station coverage. The hypocentral depths of the 50 aftershocks ranged from 9.6 to 14.3 km. Focal solutions showed considerable variability ranging from pure strike slip to pure reverse motion (Thomas *et al.*, 1996; B. Schurr, personal communication, 1996). In cross section the 50 aftershocks formed a northwest trending plane striking 290 +/- 10 degrees and dipping 60 +/- 5 degrees to the northeast.

We decided to use the Scotts Mills sequence (SMS) in our analysis for the following reasons:

1. The SMS had the near-epicentral station coverage necessary to establish reasonably precise relative focal depths.
2. The SMS offered a good opportunity to test the applicability of depth phase

analysis techniques used by Zollweg and Childs (1996) for the 1981 Elk Lake sequence (ELS) to longer station offsets and a wider variety of raypaths.

3. Because the SMS is generally similar to the ELS in its geographic location, the magnitude of the mainshock and the depth range of aftershocks, it offers a good comparison set for Zollweg and Childs' (1996) analysis of the ELS.

2.1 Event relocations

Relocation of the SMS was necessary for two reasons:

1. Our investigation of depth-dependent phases required a more precise calibration set of earthquake hypocenters than was currently available.
2. Magnitude 2.0+ events have been found to be necessary in our analysis in order for there to be enough signal strength at distant stations for depth-dependent phase identification. Because there were not enough magnitude 2.0+ events with portable station coverage it was necessary to relocate events recorded solely by the permanent Pacific Northwest Seismic Network (PNSN). This required determining PNSN station corrections.

The following is a summary of the master event technique used to relocate the SMS. A detailed description may be found in appendix A.

Eight master events were relocated using data from 11 to 16 portable seismographs and PNSN station SSO (see figure 2-1). Because of the sporadic nature of the portable seismograph coverage (most stations used triggered digital recording) the 8 master events were not recorded by a consistent set of stations having good coverage of distance and azimuth. In an effort to reduce network bias errors, station corrections from the 8 events were averaged. Our 1D velocity model consists of a vertical profile taken from a 2D velocity model proposed by

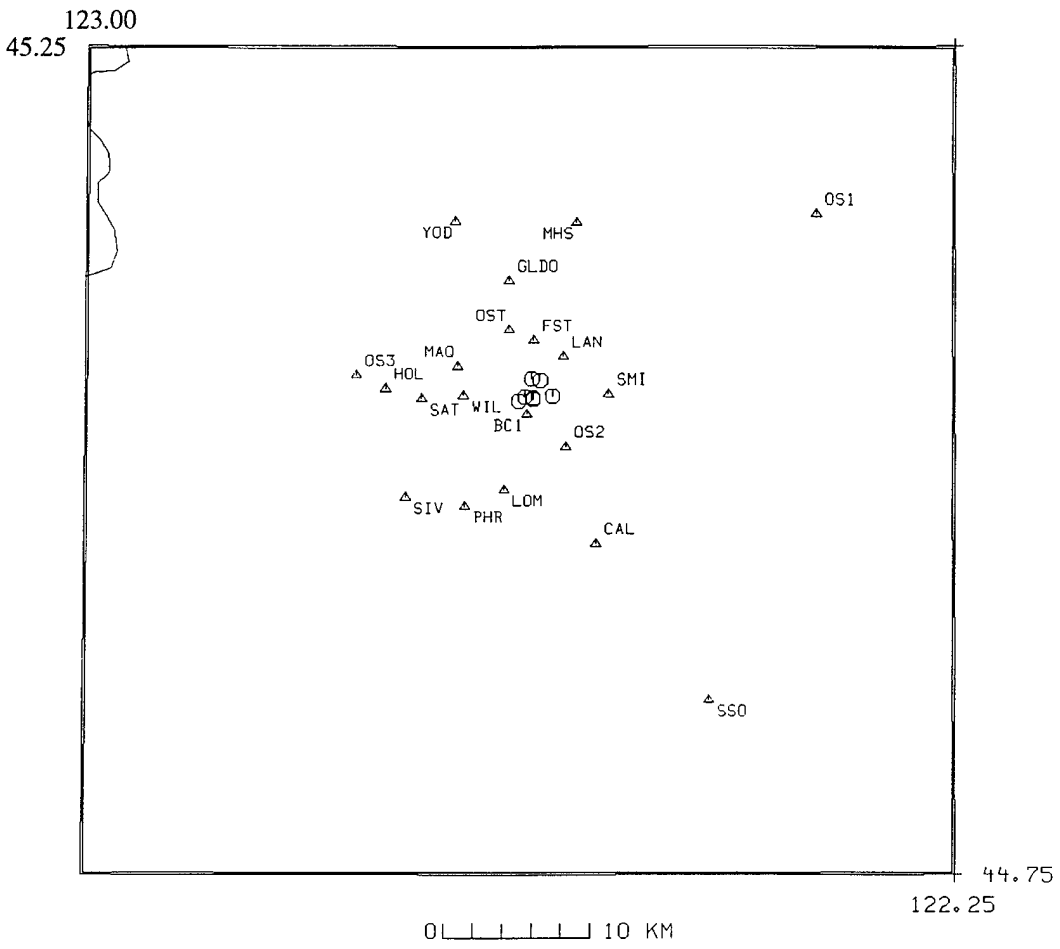

Figure 2-1. Location of 19 portable USGS seismic station sites and PNSN station SSO (lower right) used to relocate the 8 Scotts Mills sequence master events. Final master event locations are shown as octagons and stations as triangles.

Trehu *et al.* (1994). This 2D model was based upon an east-west crustal refraction and reflection study passing approximately 20 km to the south of the SMS. Based upon surface bedrock and alluvium velocities initial station delays were calculated with an elevation and focal depth datum of sea level. Corrections to these delays were calculated using an iterative procedure.

Eight permanent PNSN stations within 140 km of the Scotts Mills epicentral area which gave good azimuthal coverage were selected (see figure 2-2). At these 8 stations *P* arrivals for 40 events (32 mag 2.0 + events and the 8 master events) were re-timed by bandpass filtering the digital data between 1 to 5 Hz and then picking a consistently observed prominent peak or trough arriving within the first second. Using the 8 master events as a control set, station delays for that particular phase were determined at each of the 8 PNSN stations. Due to the low magnitudes of some of the master events not all were timeable at each of the 8 PNSN stations. Only picks of high confidence were used in the entire relocation effort. The 8 PNSN stations were then used to relocate the 32 magnitude 2.0+ events. As a test of the location method, 5 of the 8 master events were located using only the 8 PNSN stations. The average absolute value of depth change for the 5 events is 0.1 km indicating that our relocation procedure results produced stable relative depths.

Fifteen events representative of the SMS depth range and having magnitudes of 2.5 or greater were selected from the set of 40 relocated events. These events will be referred to in sections to follow as the "15 select events" and were analyzed in detail for depth related phases.

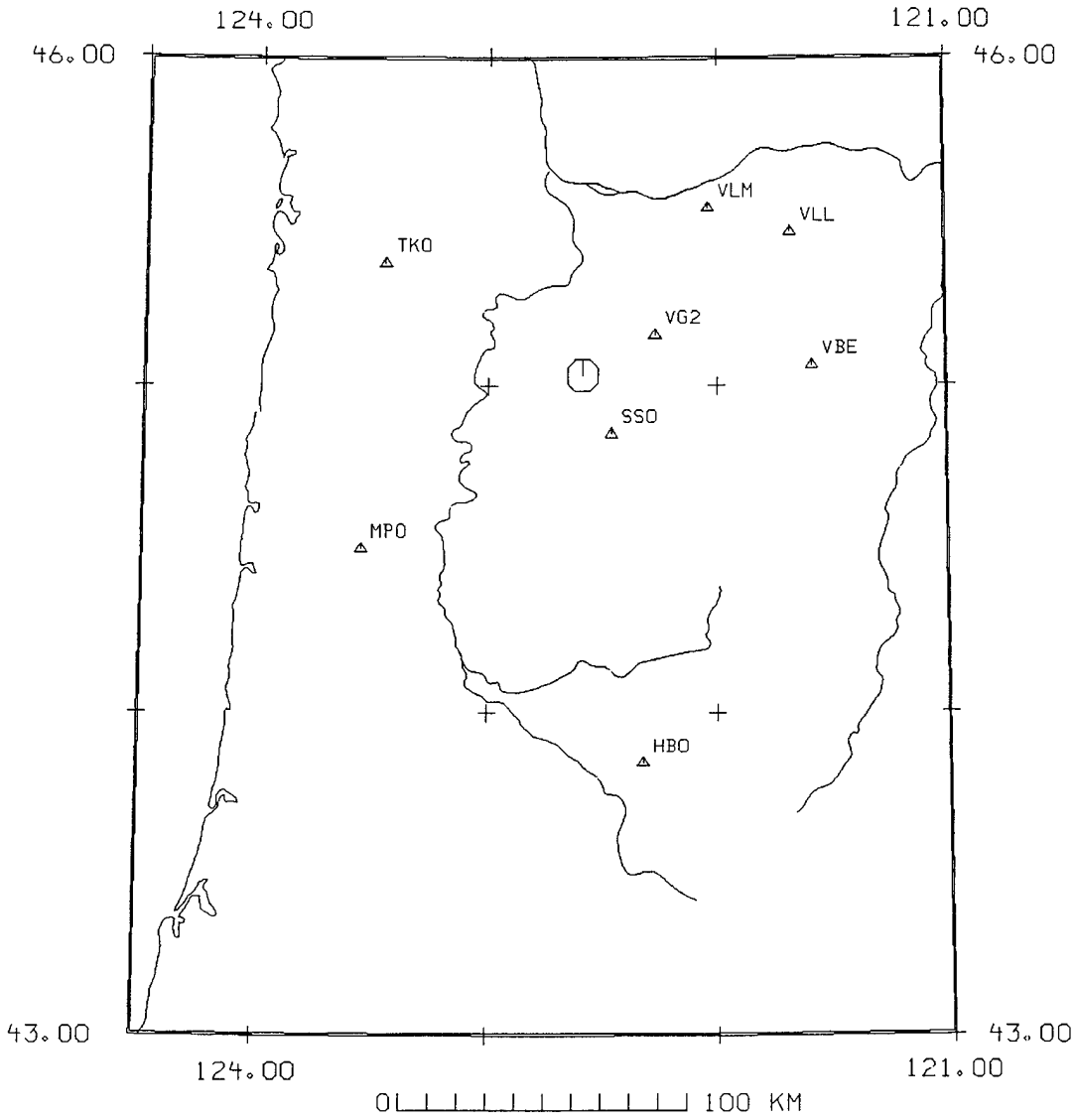

Figure 2-2. Eight PNSN stations used to relocate 32 magnitude 2.0+ events most of which do not have any portable coverage. PNSN station SSO, located 22 km from the Scotts Mills sequence epicentral area, provided good depth constraint. The mainshock of the Scotts Mills sequence is represented as an octagon.

3.0 Phase Prediction Forward Modelling of the Scotts Mills Earthquake Sequence

3.1 Introduction

We attempted to identify regional crustal phases based upon their predicted arrival times. Theoretical travel time plots were produced using the ray tracing program ***RAYINVR*** (Zelt and Smith, 1992). The plots were then compared to actual data from the SMS. Two velocity models were utilized, C3 for stations to the north of the SMS and LEAVER (Leaver *et al.* 1984) for stations to the south, southeast and east. In this section we present the procedure, the origin and description of each velocity model and the results of this methodology.

3.2 Procedure

Five earthquakes, listed in table 3-1 by depth and magnitude, were selected for the forward modelling analysis. These earthquakes were chosen because they have well constrained epicenters and depths (estimated to be accurate in a relative sense to +/- 0.5 km or better) are representative of the focal depth range found in the SMS and have magnitudes greater than or equal to 2.5. Using the ***RAYINVR*** seismic ray tracing and inversion program (Zelt and Smith, 1992) travel time and ray trace plots were created for each event using two distinct velocity models. Phases modelled include critically refracted, reflected, SP_mP and P_g.

A total of 18 stations shown in figure 3-1, with epicentral offsets ranging from 114 to 389 km, were chosen from the PNSN. To identify most of the predicted regional crustal *P* phases the initial 5.5 seconds of observed seismic data were bandpass filtered at 1 to 10 Hz (see appendix B) and then plotted together by station groups corresponding to each model. These were then compared with the appropriate

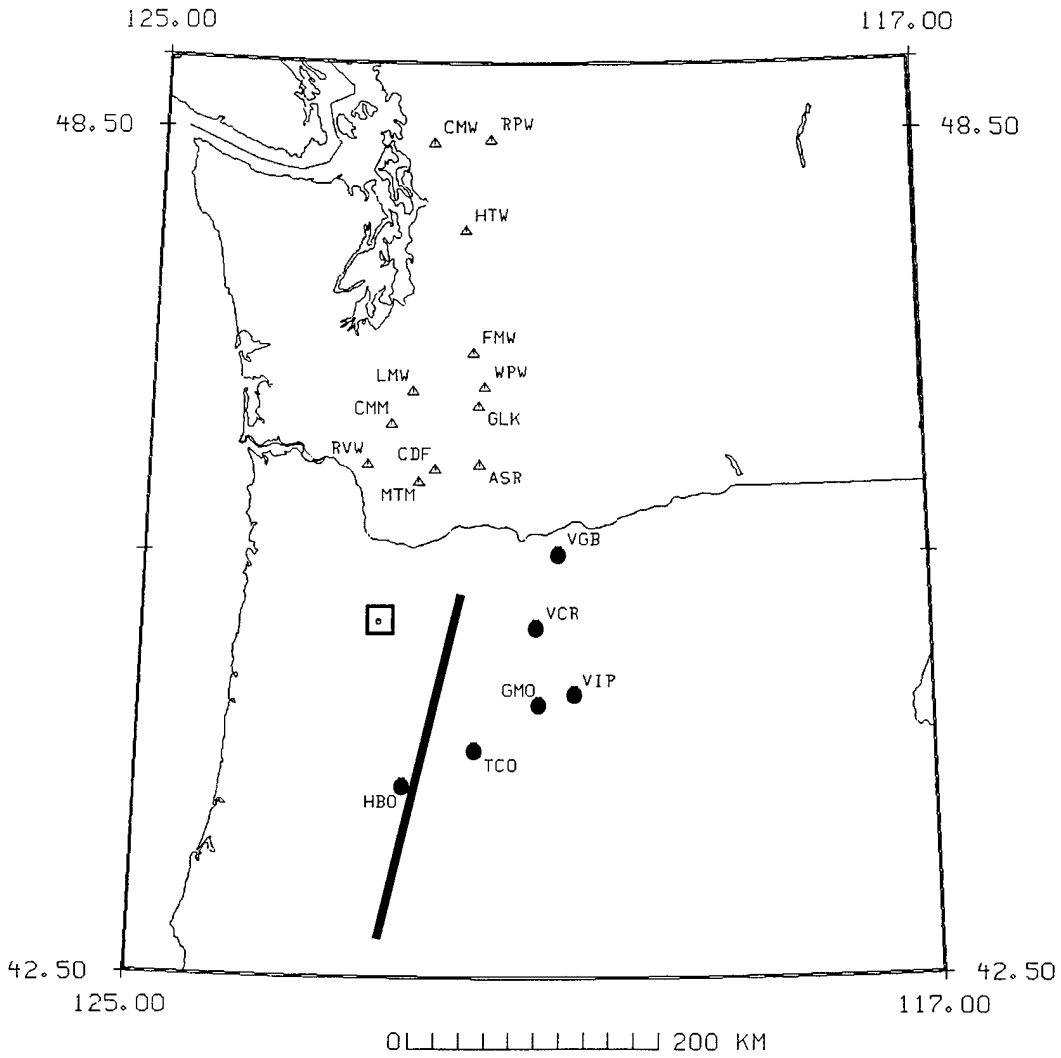

Figure 3-1. PNSN stations used in the forward modelling analysis of the Scotts Mills sequence. Stations modelled by the LEAVER and C3 velocity models are shown respectively as dots and triangles. The Scotts Mills sequence mainshock epicenter is shown as a dot surrounded by a box. The location of the crustal refraction study upon which the LEAVER model is based is shown as a bold black line.

Table 3-1
Five events used in the forward modelling analysis of the Scotts Mills sequence

Date (Yr. Mo Day)	Time (hr:min sec)	Latitude (deg. min)	Longitude (deg. min)	Depth (km)	M_{dur}
94 03 25	17:12 36.27	45N 4.03	122W 37.72	7.85	2.5
93 03 26	16:54 32.16	45N 2.16	122W 37.44	8.95	3.1
93 06 08	00:01 25.98	45N 2.10	122W 36.36	9.14	3.8
93 08 28	21:25 40.76	45N 3.08	122W 37.86	10.47	3.2
93 04 19	18:28 28.85	45N 3.30	122W 37.42	11.18	2.5

travel time curves both by sliding the seismic traces along the time axis and by comparing calculated arrival times (accounting for model elevation datum and station elevation corrections).

3.3 Description of velocity model LEAVER

Velocity model LEAVER (from Leaver *et al.*, 1984) is a 2-dimensional, 8-layer velocity model (see figure 3-2). It is primarily based upon a crustal refraction study with three shot points, one at each end and one in the middle. To constrain the lower layers of the model three earthquakes (2 to the north and one to the south) were used. The refraction line shown in figure 3-1 begins in the north approximately 70 km east-northeast of the SMS and runs south-southwest a distance of 270 km along the Oregon Cascades volcanic chain. The model's zero elevation datum corresponds approximately to the surface of the earth along the refraction line, fluctuating between 0.5 and 1.5 km above sea level (Mooney, personal communication, 1997). We chose an average model zero elevation datum of 1 km above sea level and used the model's surface velocity of 2.9 km/s

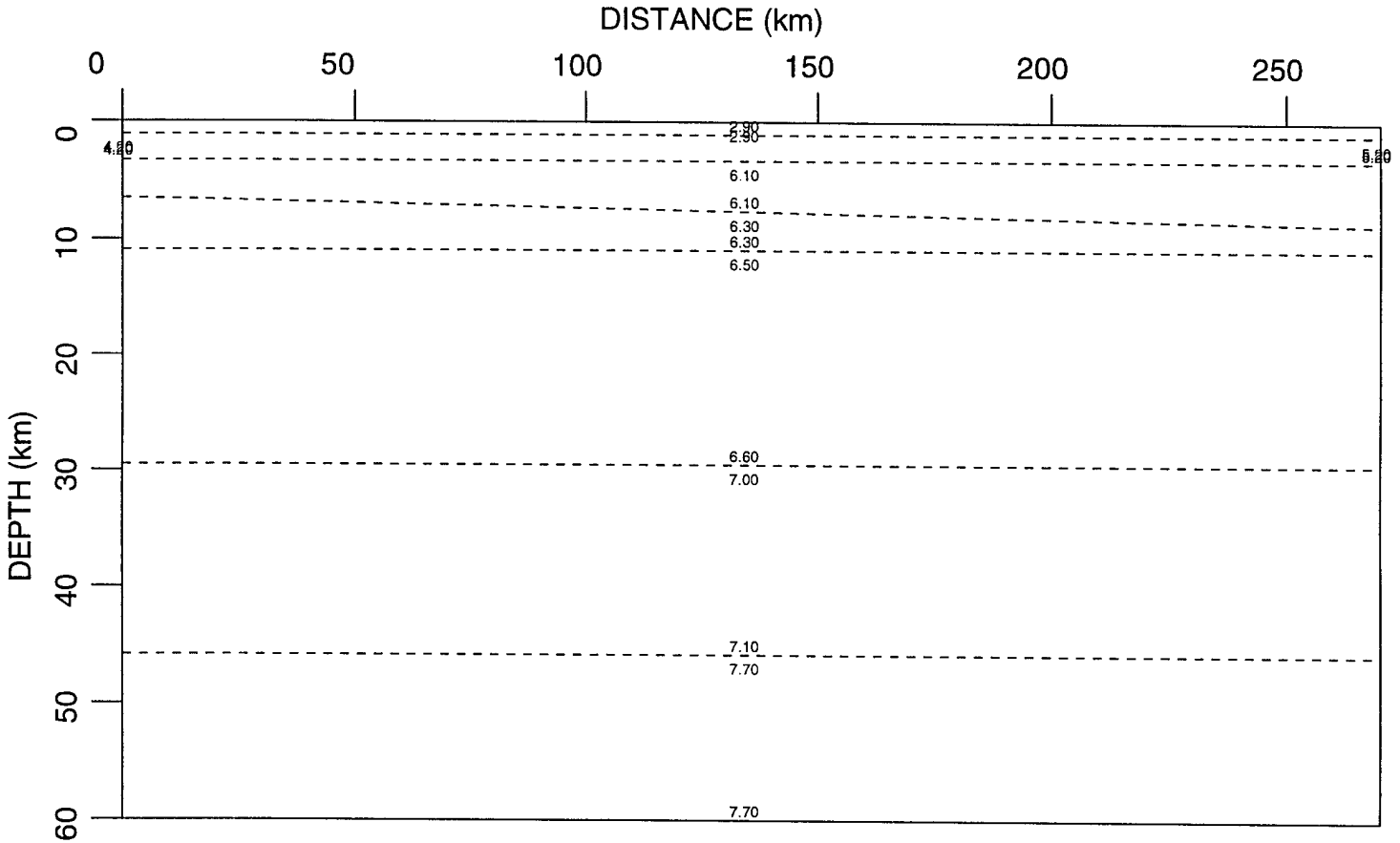

Velocity Model LEAVER

Figure 3-2. Velocity model LEAVER based upon a crustal refraction study in the Oregon Cascades and three regional earthquakes (Leaver *et al.*, 1984). Velocities are shown in each layer as km/s.

for station elevation corrections. Layer no. 7, which originally was a 2.2 km thick 7.1 to 7.7 km/s velocity transition zone, was replaced by an abrupt velocity boundary at the same depth. This modification was necessary in order to trace reflections and refractions from the moho using ***RAYINVR***. Because the location of the SMS is not in line with the LEAVER model, source to station paths have considerable azimuthal variation. Thus stations were chosen so that the majority of the travel path lay within the geologic domain of the model. The model was used to predict arrivals at 6 stations, VGB and VCR to the east and GMO, VIP, HBO and TCO to the southwest. Epicentral offsets range from 130 to 170 km.

3.4 Description of velocity model C3

Velocity model C3 (see figure 3-3) is a 1D model which is defined to a depth of 45 km and extends laterally 325 km. This model is used by the University of Washington to routinely locate earthquakes originating in the Cascades. It is based upon multi-azimuth earthquake and quarry blast data. The model's zero elevation datum is the average elevation of the stations used in its derivation, which is approximately 1 km above sea level (S. Malone, personal communication, 1996). The unmodified model was used to predict arrivals at 12 stations to the north of the Scotts Mills sequence (RPW, HTW, CMW, LMW, FMW, WPW, GLK, CMM, RVW, MTM, CDF and ASR). Station epicentral offsets range from 113 to 388 km.

3.5 SP_mP phase modelling

Partly due to a lack of P_g observations, (see Zollweg and Childs, 1996) most of our efforts have been focused upon refracted and reflected (downward directed) depth-dependent *P* phases arriving in the first few seconds of data. However the time difference between downward and upward directed phases, if observable,

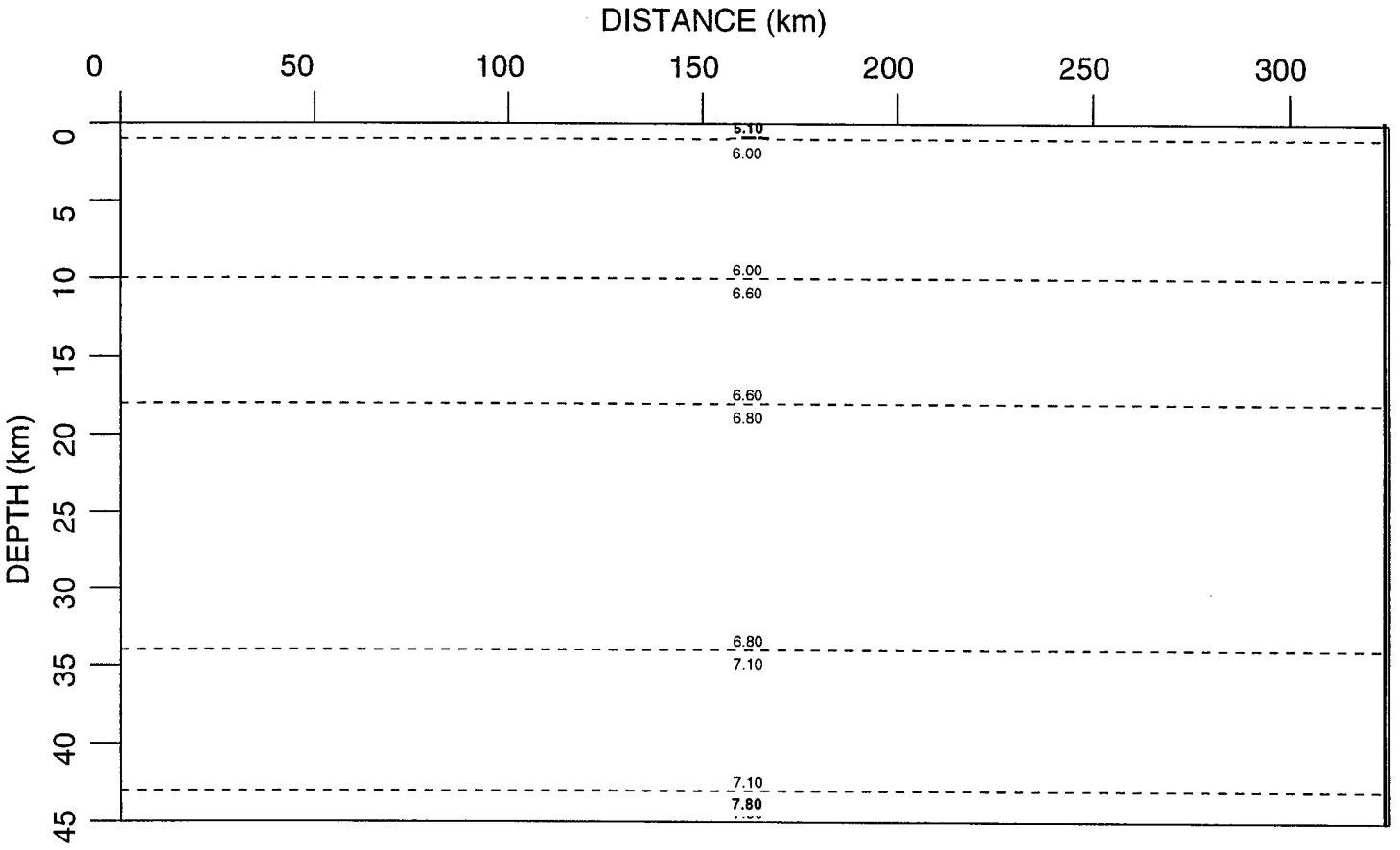

Velocity Model C3

Figure 3-3. This model is used by the University of Washington to routinely locate earthquakes originating in the Cascades. Velocity values are listed in each layer as km/s.

could possibly have a much greater change in time separation with respect to changes in source depth. As the source depth increases the downward directed phase arrives relatively earlier at a given station and the upward directed phase arrives relatively later. SP_mP phases were observed using broadband data from the 1993 Klamath Falls, Oregon earthquake sequence (D. Dreger, personal communication, 1996). Klamath Falls, Oregon is near our study area and thus we considered a search for this phase worthwhile. The C3 model and ***RAYINVR*** were used to predict the arrival of this phase (see appendix C). Observed data from the 15 select events at 22 stations were examined.

3.6 Synthetic seismograms

To better understand relative phase amplitudes, the effect of multiple phase arrivals and to test the validity of the C3 model, synthetic seismograms were produced using model C3 and the ***RAYINVR*** program (see appendix D) for the magnitude 3.2 event of August 28, 1993, 2125 UT. The synthetic seismograms were compared to observed data.

3.7 Observations of predicted P phases

To simplify the presentation of the forward modelling results, references to observed data will apply specifically to the event of August 28, 1993, 2125 UT, mag 3.2, depth 10.47 km. Our conclusions regarding the modelling of this event are representative of the remaining 5 events examined in the forward modelling analysis.

Prediction of first arrivals is a good general test of a model's validity. The C3 model predicted first arrivals to within an average absolute error of 0.1 s. Observed first arrivals were consistently early relative to those predicted by the

LEAVER velocity model by an average of 0.7 s. Discrepancies ranged from 0.0 s at station VGB to 1.1 s at station HBO (see figure 3-4). The early arrivals could be caused by errors in source depths but this is unlikely because the residuals between various predicted and observed arrivals are not consistent with focal depth changes. The large azimuthal variation in LEAVER station travel paths may be justification for poor model performance, but the travel path to station HBO, which strikes only 22 degrees relative to the LEAVER model, had the largest residual (1.1 s) while station VGB, which strikes 102 degrees relative to the LEAVER model, had the lowest residual (0.0 s).

The P_n crossover distance for both models is approximately 230 km. No P_n first arrival observations were available for the LEAVER model due to the lack of stations beyond the crossover distance. A weak and emergent P_n, as predicted by the C3 model, was observed at station HTW (epicentral offset of 315 km) for 3 of the 5 events analyzed exceeding magnitude 3.0. At stations CMW and RPW (epicentral offsets 377 and 389 km) P_n is not observed (see figure 3-5). The synthetic seismograms support observations of weak P_n phase arrivals (see appendix D).

The C3 stations RVW and CDF (epicentral offsets 122 and 127 km, respectively) show strong P_g arrivals. A weak P_g arrives at station CMM (offset 154 km). No P_g phases are seen beyond this offset (see figure 3-6). Zollweg and Childs (1996) and R. Crosson (personal communication, 1996) have previously observed lack of or poor propagation of the P_g phase in the Pacific Northwest.

No predicted SP_mP phases were observed at the 22 stations examined.

The C3 model-predicted P_mP and reflected arrivals from shallower velocity layers were most prevalent. Predicted P_mP arrivals were observed at stations WPW and

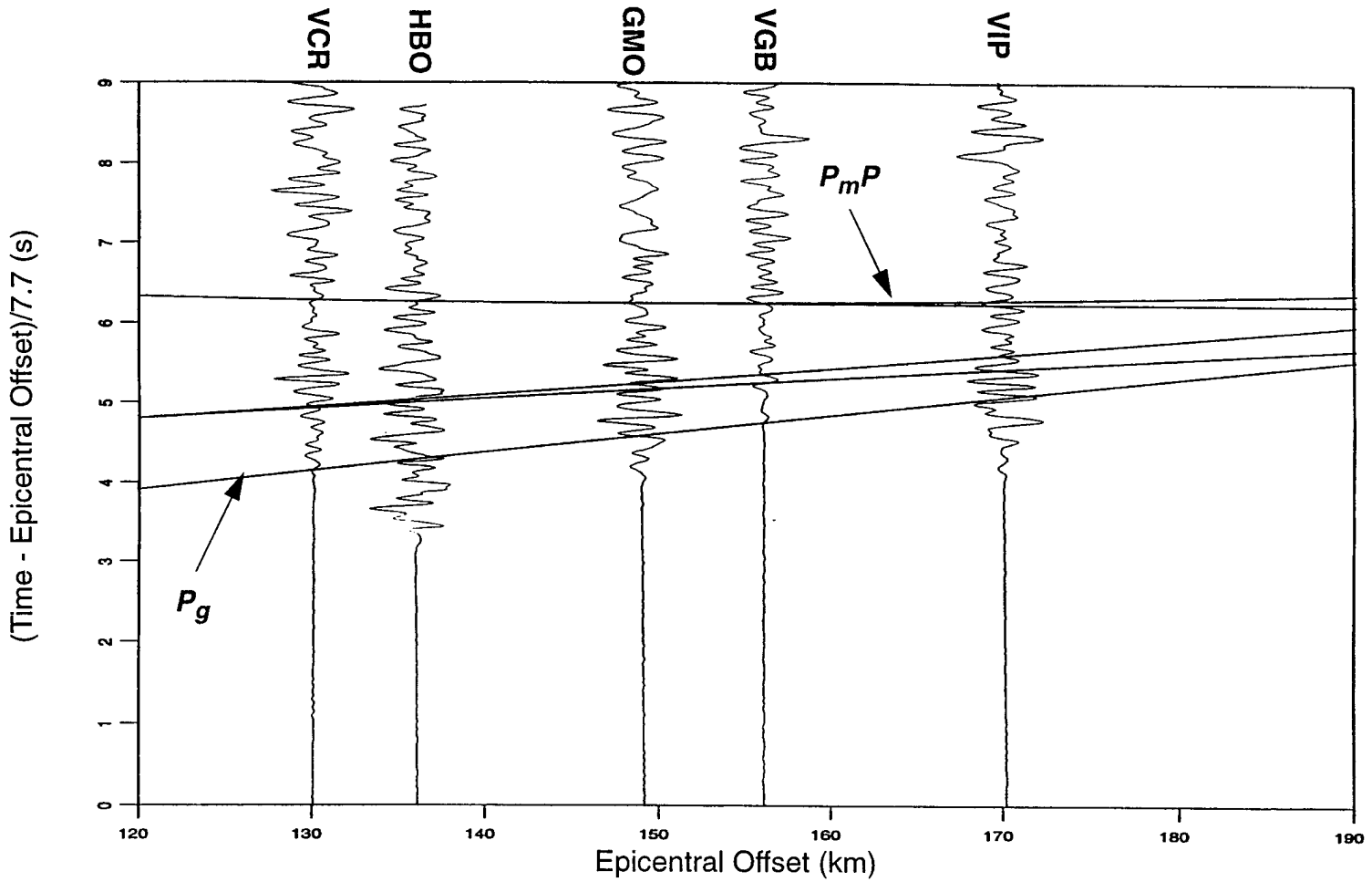

Figure 3-4. Traveltime plot using velocity model LEAVER for event (93/08/28, 2125 UTC) depth 10.47 km. Traces are bandpassed at 1-10 Hz. Travel-time curves plotted but not labeled include reflections and head waves off the base of velocity layer 5. Station codes are shown at the top of the plot. Notice early arrivals of up to a second at stations HBO, GMO and VIP.

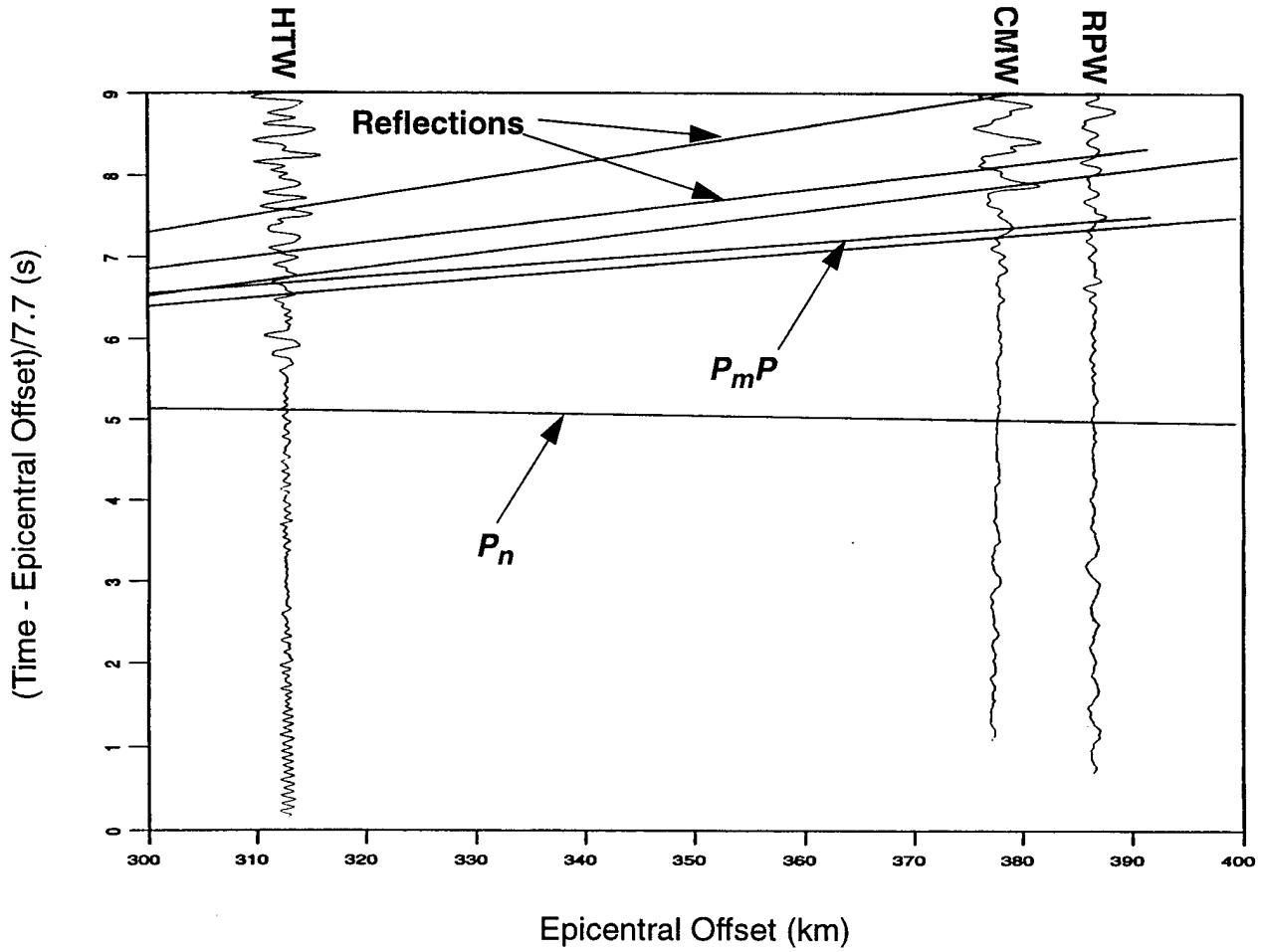

Figure 3-5. Traveltime plot of distant stations using velocity model C3 for event (93/08/28, 2125 UTC) depth 10.47 km. Traces are bandpassed at 1-10 Hz. Travel-time curves plotted but not labeled include reflections and head waves off the bases of velocity layer 3 and 4. Station codes are shown at the top of the plot. Notice very weak to unobservable predicted P_n at all 3 stations and unclear secondary reflected *P* phases.

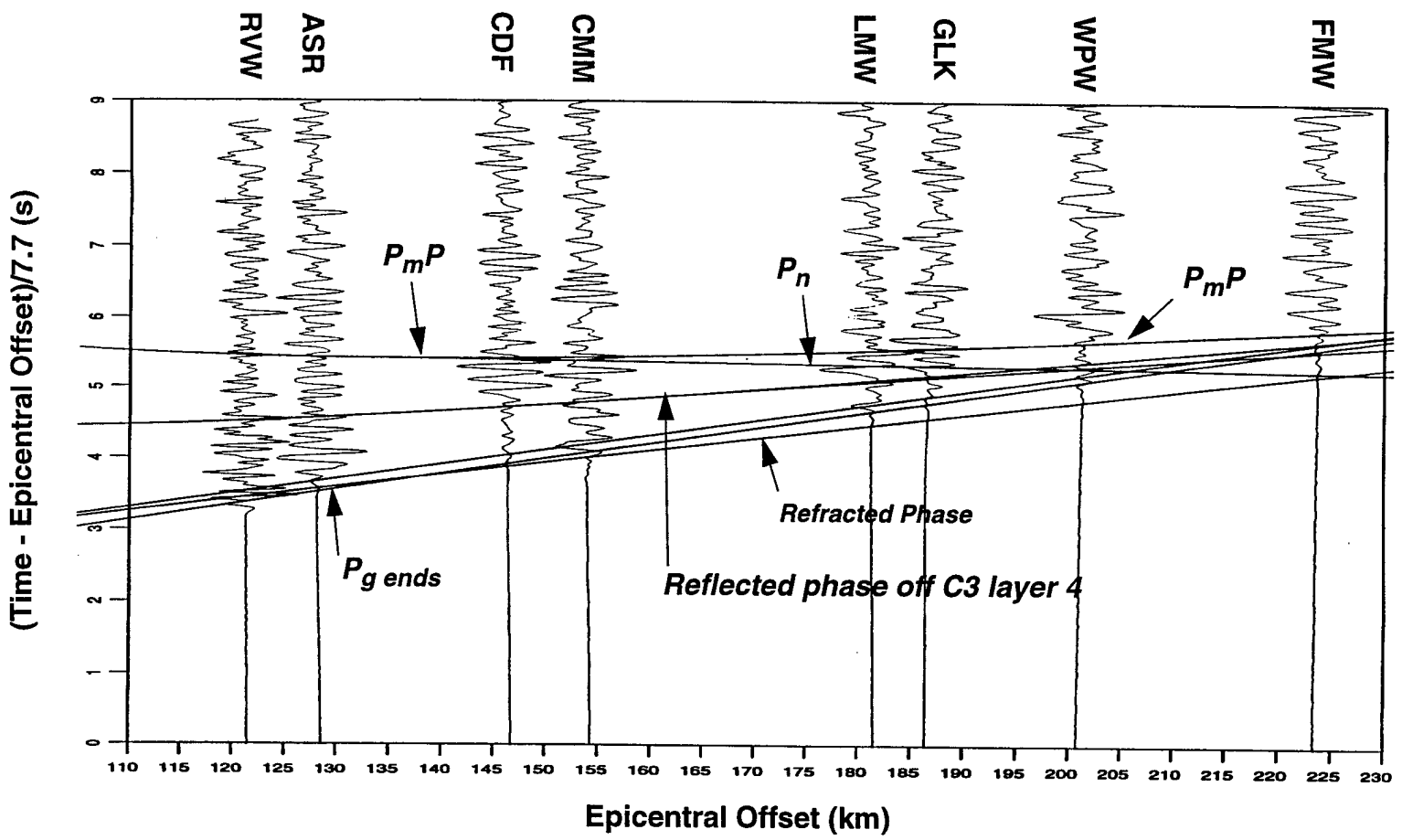

Figure 3-6. Traveltime plot using velocity model C3 for event (93/08/28, 2125 UTC), depth 10.47 km. Traces are bandpassed at 1-10 Hz. Travel-time curves plotted but not labeled include reflections and head waves off the bases of velocity layers 3 and 4. Notice P_mP arrivals at stations WPW and FMW and shallower reflected *P* phases at stations CDF and LMW. Also notice predicted arrivals converge to a 1 s window or less after 190 km offset.

FMW and shallower reflections off the base of C3 layer 4 were found at stations LMW and GLK (see figure 3-6). The reflected arrivals had relatively large amplitudes and most were emergent. These observations are supported by synthetic seismograms (see appendix D).

A closer examination of the phase offset time between the first arrival and the presumed P_mP arrival at station WPW (201 km epicentral offset) was conducted. Each of the 15 select events were bandpassed at 1 to 3 Hz and plotted in depth order. The presumed P_mP phase was timeable across source depths ranging from 10.09 to 11.18 km, but no depth dependence was found.

The lack of observed depth dependence of the presumed P_mP phase found at station WPW and the inability to correlate this phase across the 3.3 km SMS depth range raise two important points.

1. The magnitude of depth-dependent phase relative moveout time is a function of epicentral offset and velocity structure. The most prominent P_mP phase found at station WPW was only timeable across a depth range of approximately 1 km. The C3 model predicted relative moveout time between the first arrival and P_mP for this depth range is 0.016 s which is barely large enough to be seen above timing errors. For the entire SMS depth range of 3.33 km and at an offset of 201 km, the C3 model predicts a relative moveout time for the same phase pair of 0.05 s. In contrast, at an offset of 130 km, where predicted phase separation is more pronounced, a relative moveout time of 0.19 s is predicted for the 3.3 km depth range. Predicted phase separation also increases beyond 290 km, but signal to noise ratio for earthquakes of magnitude 2.5 or less is very low.
2. The presumed P_mP phase at station WPW was only timeable across a 1 km

depth range and was typical for many of the relatively coherent secondary *P* phases found in the SMS. This lack of phase coherency is probably related to the large variation of focal mechanisms found in the SMS (B. Schurr, personal communication, 1996; Thomas *et al.*, 1996) and/or the interference of multiple phase arrivals. At epicentral offsets from 183 to 245 +/- 15 km both models predict that all reflected, refracted and direct *P* phase arrivals converge within a 1 second time window making it difficult to distinguish any single phase. Between offsets of 126 to 295 km the C3 model predicts a convergence window of 2 s or less. At such offsets it may be very difficult to resolve separate phases. Observed phases, such as the presumed P_mP found at station WPW, may not be legitimate phases at all but "ghost" phases consisting of the constructive interference of several nearly coincident phases.

4.0 Analysis of Single Station Depth-dependent Phases and Interstation Phase Offset Time vs. Depth.

4.1 Procedure

Stations to be scrutinized for depth-dependent phase arrivals were selected from the PNSN according to the following criteria:

1. Their epicentral offset had to exceed 100 km.
2. The original event analyst at the University of Washington must have picked the station for at least 10 of the 40 relocated events.

A total of 57 stations with epicentral offsets ranging from 114 to 462 km met these criteria (see figure 4-1). Theoretical P_g arrival times for the 57 stations were calculated for each of the 15 select events using an assumed average P_g velocity of 6.0 km/s (see appendix E). Depth order plots of the 15 select events were made for each station and examined for any waveform correlatable across most of the 3.3 km depth range. Each trace was 8 seconds in length, bandpass filtered at 1 to 3 Hz, and aligned upon the predicted P_g phase arrival (whose travel time is relatively independent of depth). Same-azimuth station pairs with correlatable waveforms were timed and interstation phase offset time vs. source depth plots were created.

4.2 Observations

Twenty-one of the 57 stations examined had waveforms correlatable across most of the depth range, arriving in the first couple of seconds after the first arrival (see figure 4-2). Most of the stations were concentrated to the north around Mt. St. Helens, primarily due to high station density in that area. Twenty of the 22 had offsets of 200 km or less. Phases that exhibit depth dependence were found at 14

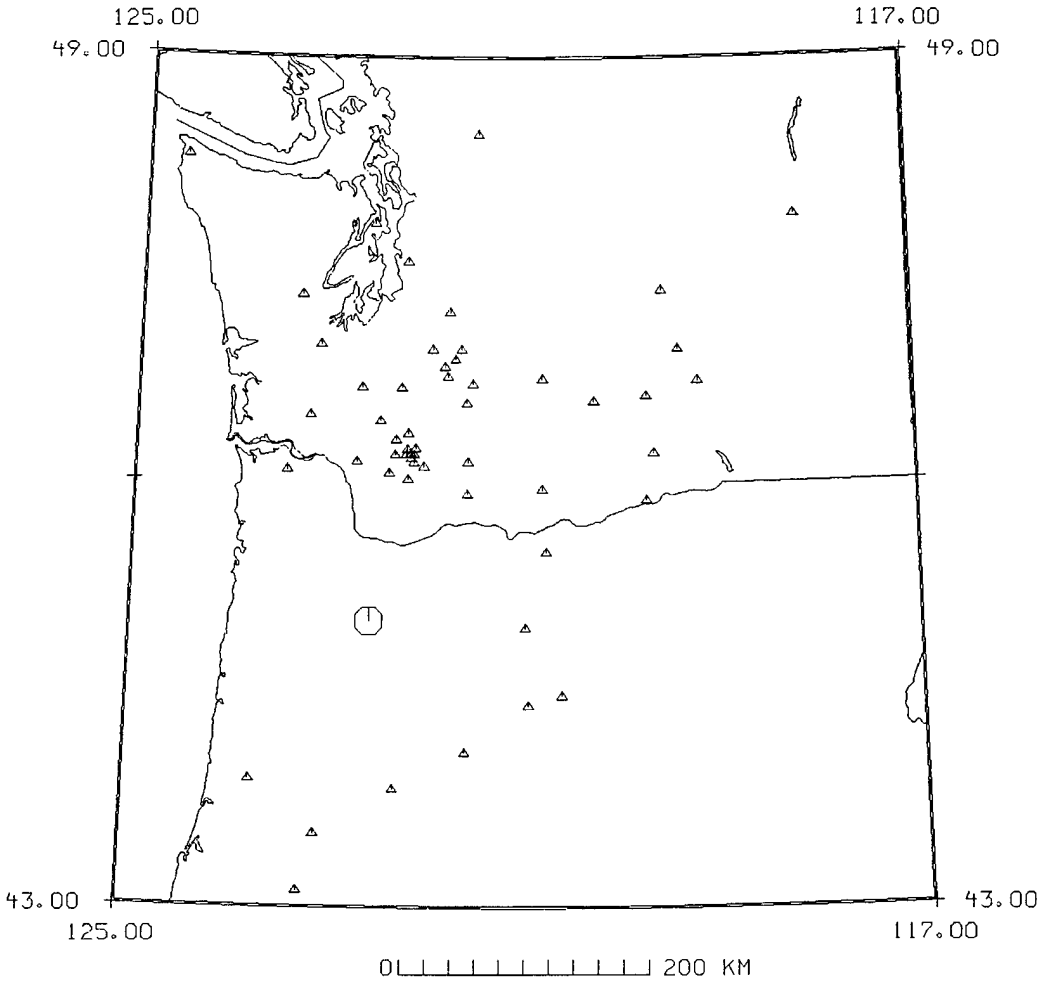

Figure 4-1. Fifty-seven regional PNSN seismic stations analyzed for depth-dependent phases. Octagon represents the Scotts Mills sequence mainshock epicenter.

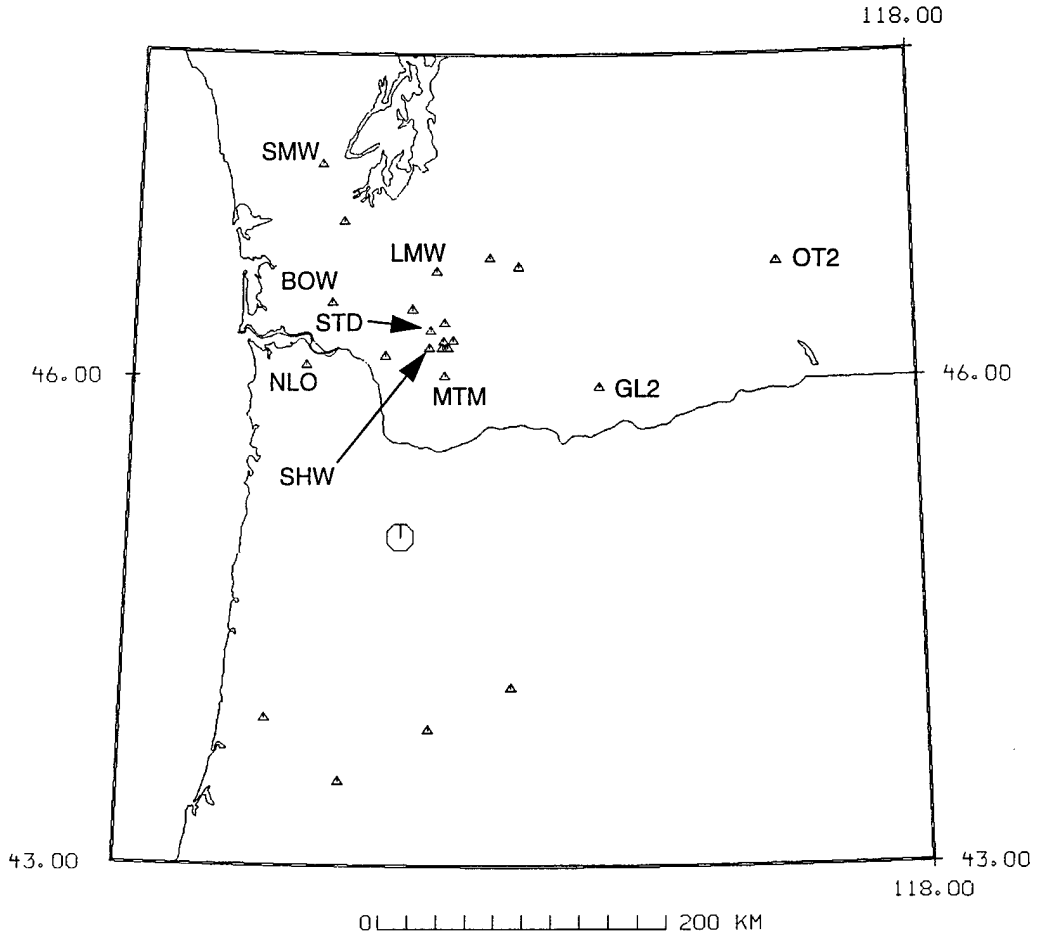

Figure 4-2. Twenty-one of the 57 regional PNSN seismic stations analyzed that had observable phases across most of the Scotts Mills sequence 3.3 km depth range. Stations used in the interstation phase offset time analysis are labeled. The octagon represents the Scotts Mills sequence mainshock epicenter.

of 57 stations from the Scotts Mills sequence. Station STD, typical of the 14 stations with depth dependent phase arrivals, can be seen plotted by increasing depth order in figure 4-3 with aligned phase arrivals sloping to the left. Because the traces are aligned upon a theoretical P_g arrival time which is relatively depth independent the slope is indicative of depth dependence. The same data are plotted by increasing epicentral offset in figure 4-4 and lack any clear phase alignment.

Phase offset time vs. hypocentral depth plots were made for 9 stations aligned upon similar azimuthal paths. These plotted station pairs are BOW-NLO, OT2-GL2, SMW-BOW, STD-MTM, LMW-STD, SHW-MTM and SMW-NLO. None of these plots exhibited depth dependence. A typical phase offset time vs. hypocenter depth plot for station pair STD and MTM is shown in figure 4-5. This lack of depth dependence may be the result of picking the same phase at each station pair or small depth-dependent phase relative moveout times. Prominent peaks or troughs were picked at the 9 stations mentioned above at an average time of 0.5 s after first arrival onset, with a range of 0.3 to 0.8 s. We were unable to use 12 of the 22 stations with prominent phase arrivals because there were no other stations along the same azimuth.

Secondary *P* phases arriving 2 to 4 seconds after the first arrival were found at stations OT2 (3 out of 15 events), WPW (7 out of 15 events), RNO(10 out of 15 events), STD (12 out of 15 events), NLO (10 out of 15 events), and HSO (5 out of 15 events) and timed relative to the first arrival; however, no depth dependence was found.

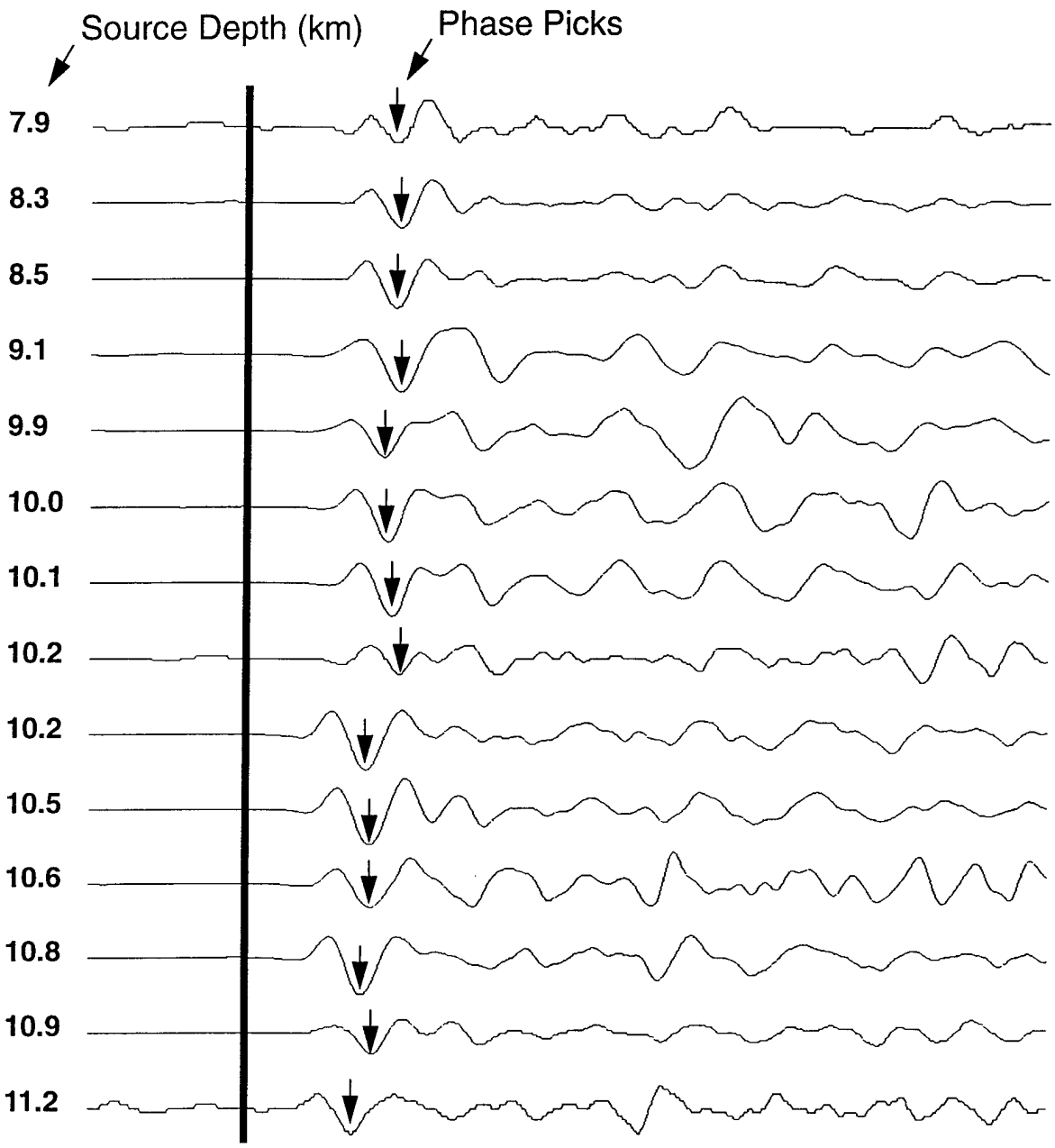

Figure 4-3. Station STD (epicentral offset 136 km) phase picks of the 15 select events ordered relative to increasing focal depth. Seismograms are 4.4 seconds in length, aligned upon calculated ***Pg*** arrival times and bandpassed at 1 to 3 Hz. Note cant of phase picks to the left with increasing focal depth

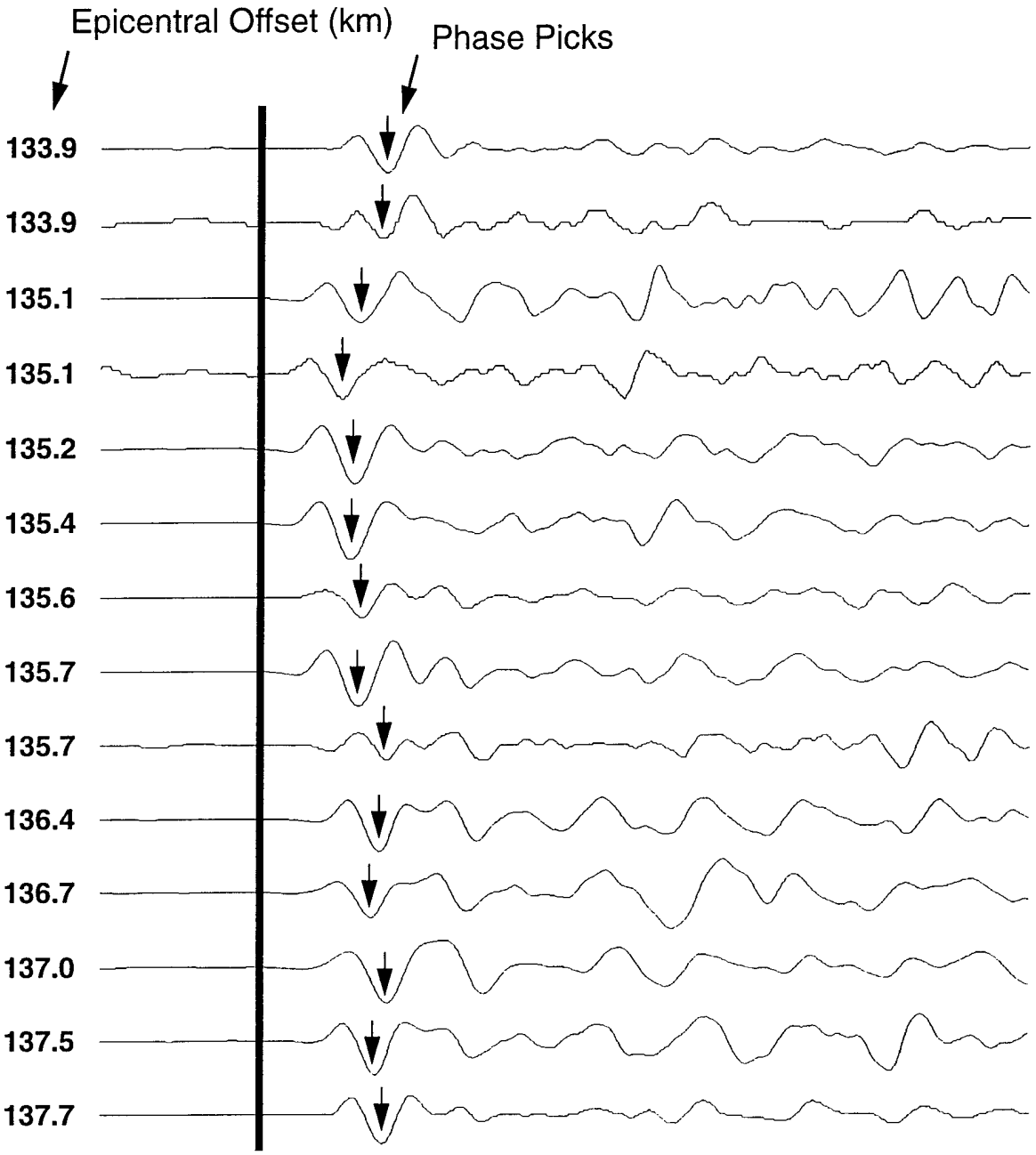

Figure 4-4. Station STD phase picks of the 15 select events ordered relative to increasing epicentral offset. Seismograms are 4.3 seconds in length, aligned upon calculated P_g arrival times and bandpassed at 1 to 3 Hz. Note lack of clear alignment of phase picks.

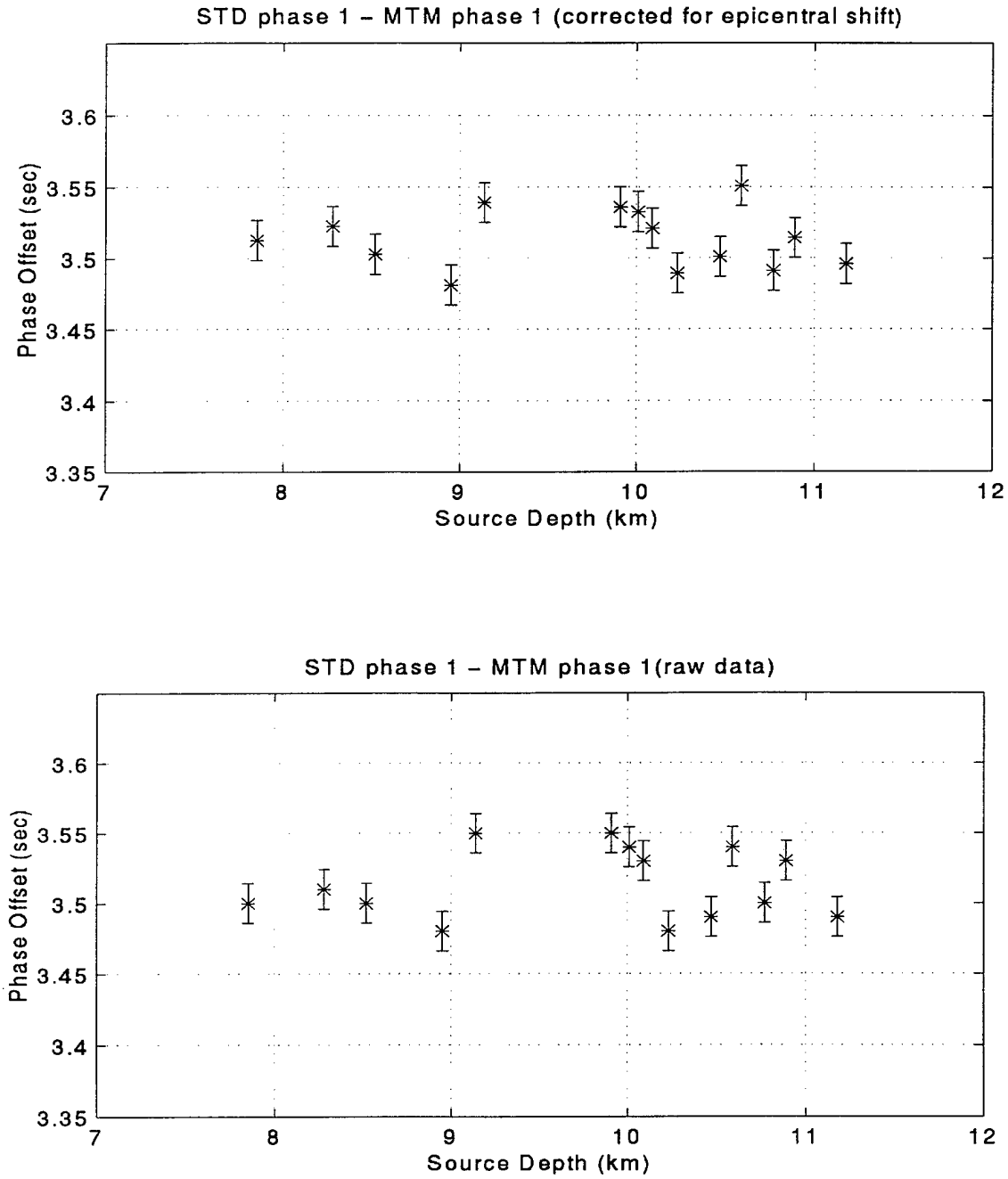

Figure 4-5. Phase offset plots between station STD and station MTM for 15 select events in the Scotts Mills sequence. The top plot has been corrected for inter-station epicentral shift, bottom shows uncorrected data. Error bars represent a standard deviation of +/- 0.014 s. Notice no clear change in offset times relative to depth. Probably, the same phase has been picked at each station.

5.0 Discussion of the Scotts Mills Sequence Depth Phase Analysis

Of the *P* phases modelled P_mP and shallower reflected phases are the most prevalent. They have relatively large amplitude emergent onsets that are difficult to time. These observations are supported by synthetic seismograms.

Velocity model C3, derived from a large multi-azimuth, multi-depth data set composed of earthquakes and surface quarry blasts more accurately predicts first arrivals than velocity model LEAVER which is based upon a small, single-azimuth data set of 3 surface blasts and 3 regional earthquakes.

Choice of receiver offset is an important consideration with regard to recording depth-dependent phases. Based upon theoretical travel time curves from the C3 and LEAVER velocity models attempts to observe depth-dependent *P* phases between epicentral offsets of 183 to 245 +/-15 km may be hampered for two reasons:

a) Predicted *P* phase arrivals converge within a one second time window making it difficult to resolve single phases.

b) The depth controlled phase pair relative moveout time is so small that it cannot be resolved above timing errors.

At offsets less than 126 and greater than 295 km maximum phase separation is greater than 2 seconds and phase pair depth controlled moveout times are resolvable. However at offsets exceeding 295 km signal strength is reduced to near background noise for events of magnitude less than 2.5. On the other hand sensors placed at offsets less than 126 km may be impractical for CTBT compliance monitoring.

Similar waveforms from several events arriving at a single station were often timeable across a very small depth range. This may be the result of:

a) The wide variability of source mechanisms observed in the SMS.

b) The phase may be a ghost phase consisting of the constructive interference of several phases.

Neither SMS interstation phase offset times nor single station phase offset times between onset and secondary *P* phase arrivals showed conclusive depth dependence. Explanations may include picking the same phase in the interstation analysis and/or lacking a sufficiently large depth-dependent phase pair relative moveout time that can be resolved above timing errors. In contrast depth-dependent interstation phase offset times were found in the ELS using primary and secondary *P* phases. Analysis of secondary *P* phases from the SMS is continuing.

6.0 Discussion of the Scotts Mills and the Elk Lake sequences

The depth calibration earthquake data sets derived from the ELS and the SMS have the following similarities:

Both earthquake sequences occurred in the Pacific Northwest. The ELS occurred within the Cascade Volcanic Range and the SMS occurred on the western edge of the Cascade Volcanic Range

Both sequences have a similar mainshock magnitude. The ELS and SMS have mainshock magnitudes of 5.5 and 5.6 respectively.

The depth ranges of both sets of relocated depth calibration events are less than 5 km. The ELS has a depth range of 4.1 km (7.5 to 11.6 km) and the SMS has a depth range of 3.3 km (7.9 to 11.2 km).

The SMS and the ELS are different in the following ways:

The ELS has relatively consistent set focal plane solutions whereas the SMS is highly variable.

The ELS has a constant set of master stations and only one master event was used. In contrast the SMS has a variable set of master stations and eight master events were used

The forward modelling analysis of both earthquake sequences revealed the following important observations:

1. Velocity models based upon a small data set of first and secondary *P* arrivals from single azimuth surface shots and a few regional earthquakes such as

models NWPS (Zollweg and Childs, 1996) and LEAVER are consistently late in their prediction of first arrivals. In contrast velocity model C3, which is based upon first arrival picks from a large multi-azimuth multi-depth data set consisting of earthquakes and quarry blasts, consistently predicts observed first and some secondary *P* arrivals.

2. The predicted P_g phase is not observed beyond an offset exceeding 130 +/- 15 km.

3. Predicted P_mP and reflected phases off shallower velocity layers are observed frequently. However they are usually not traceable to adjacent stations. These phases have large amplitudes and emergent arrivals which are consistent with synthetic seismogram observations. Phases with these characteristics are easy to identify but difficult to time at high resolution.

4. Predicted P_n crossover distances range from 185 to 256 km. Observed P_n first arrivals are weak and emergent. For events less than magnitude 2.5 and offsets exceeding 300 km P_n is frequently not observed above the noise.

5. Varying source mechanisms and multiple interfering phase arrivals hamper efforts to correlate phases from event to event.

6. For the small depth ranges found in the SMS and ELS depth calibration sets predicted depth controlled phase pair relative moveout times can range from 0.02 to 0.20 s. Observed phase pair relative moveout times ranging from undetectable to 0.15 s are consistent with model predictions. With such small relative moveouts timing resolution is a critical and sometimes limiting factor in determining source depths from depth phase arrival times. Predicted phase pair relative moveout times are a function of source depth range, receiver offset, phases timed and velocity structure.

7. Observations of interstation phase offset times from the ELS have variously revealed depth dependence, depth independence and unclear relation to depth. Observations of interstation phase offset times from the SMS to date have revealed only depth independence.

In contrast to the ELS analysis no observed secondary *P* phases from the SMS were included in the interstation phase offset time analysis. Further work with SMS secondary *P* phases is planned.

7.0 Conclusion

Our studies of depth-dependent *P* phases from U. S. Pacific Northwest earthquake sequences have:

- helped to define the problems that are encountered in analysis,
- suggested the kinds of data that may be most useful,
- developed a methodology that is useful in identifying depth-dependent phases,
- developed a methodology for extracting depth information from pairs of same azimuth stations,
- shown that only about 1/3 of the stations record usable depth-dependent *P* phases and,
- found that rather precise relative depth determinations are possible in at least one earthquake sequence.

These results are further discussed below.

One of the most serious problems we encountered in attempting to develop a robust methodology for depth-dependent phase identification was our inability to confidently identify specific arrivals on the seismograms. We found that even relatively detailed crustal models based upon extensive refraction experiments generally did a poor job of explaining the observed *P* arrivals. Because the data we examined came from a network of single-component short period stations with inter-station spacings of the order of 25 to 75 km, we could not use either slowness or polarization information to identify phase arrivals. Not surprisingly, we conclude that array data would be more useful than widely-spaced single-component data. Since polarization data from three-component stations is of

comparatively less value in distinguishing arrivals having relatively small differences in the angles of incidence, the type of data that appears to be most useful is that from one or more arrays.

A problem that may be insurmountable even with array data is the tendency of multiple *P* phases to arrive within such small time intervals in certain distance ranges that they interfere with each other. Such interference can lead to "ghost" arrivals caused by chance constructive interference. We have shown that distance ranges exist in which same-station seismograms may show low coherence for slight changes in source depth and epicenter. While there is a great deal of event location information in such phenomena, we are not yet at a knowledge stage where we can extract such information from the recordings.

The difficulties we encountered in making positive phase identifications led us to base our analysis methodology upon empirical identification of depth-related phases. If a calibration set of seismograms exists for events with well-determined focal depths, then phase identification is unimportant compared to demonstrating depth dependence. We have developed a straightforward method of making such identifications from calibration sets. We plot same-station seismograms in order of increasing source depth, vertically aligned upon the expected arrival time of some depth-independent phase (we used P_g, whose arrival time is virtually independent of focal depth at distances greater than several times the focal depth). From these plots a phase whose arrival is depth-dependent can be identified on the basis of the inclination of its arrivals with respect to those of the vertically-aligned P_g.

For each of the two earthquake sequences we have examined to date, we found that approximately 1/3 of stations whose data we examined show depth-dependent phases. In nearly all cases, only one such phase was recorded at a

given station, precluding single-station depth determinations unless the origin time is known independently to a high degree of accuracy. However, if the time difference between two distinct phases, each recorded at different stations along the same source to receiver azimuthal path, can itself be shown to be a function of focal depth, we have the basis for a precise and easily computed depth indicator which does not require highly accurate information on the event's location. For the Elk Lake earthquake sequence, some such station pairs were found (see Zollweg and Childs, 1996). We believe that relative depth determinations with an accuracy of about 0.5 km may be possible, based upon the observed source depth versus time difference functions. The usable station pairs must be observing depth-dependent phases with differing depth dependence. We infer that such phases also differ in slowness.

In summary, we feel that we are developing a promising methodology for making accurate relative depth determinations from small numbers of stations. We do not yet understand what siting criteria may apply to predicting optimal recording locations, nor do we yet know much about the scale length of coherence of depth-dependent phases. We believe at this time that our methodology may prove most applicable to source depth determinations over areas of a few kilometers. While this may seem restrictive, it should prove useful in sorting out relative depths of clustered events. Rockbursts are examples of such events that are important in CTBT monitoring scenarios.

8.0 Appendices

Appendix - A

The SMS master event relocation procedure

The following is a detailed description of our efforts to more precisely relocate select events of the Scotts Mills sequence (SMS). In the entire relocation effort only high quality picks were used. The procedure is broken into two parts:

First, 8 master events were located using only portable seismographs located very near the epicenter.

Second, using the 8 master events as a control, station delays were determined for a set of 8 permanent stations from the Pacific Northwest Seismograph Network (PNSN). These 8 stations and any existing portable seismograph data were then used to locate 32 events greater than magnitude 2.0. Most of the 32 events lacked portable station coverage.

On 25 March 1993 a M_{dur} 5.6 earthquake occurred near Scotts Mills, Oregon (Thomas *et al.*, 1996). To record aftershocks digital and analog seismographs were deployed by the U.S. Geological Survey (USGS), University of Oregon, and Oregon State University. The SMS was also recorded continuously by the PNSN including two stations within 28 km of the epicentral area. Technical details of USGS portable instrumentation and monitoring may be found in papers by Carver *et al.* (1993) and Thomas *et al.* (1996). The 8 master events were located by a select set of up to 19 portable stations and PNSN station SSO (see table A-1). The number of stations used (including PNSN station SSO) to locate each of the 8 master events ranged from 12 to 17. Compression and shear wave picks from the USGS, Oregon State University, and the University of Oregon stations were

Table A-1
Stations used to locate the 8 Scotts Mills sequence master events

Station Name	North Latitude (deg. min. sec.)	West Longitude (deg. min. sec.)	Elevation (km)	Station Delay (s)	Station Type *
BC1	45 01 44.10	122 37 04.80	0.192	-0.10	portable USGS
CAL	44 57 03.80	122 33 29.20	0.615	-0.21	portable USGS
HOL	45 02 39.12	122 44 26.40	0.092	-0.05	portable USGS
LAN	45 03 48.80	122 35 12.48	0.207	-0.09	portable USGS
LOM	44 59 00.60	122 38 14.40	0.277	-0.15	portable USGS
OST	45 04 46.80	122 38 01.10	0.159	-0.03	portable USGS
SAT	45 02 17.10	122 42 33.50	0.181	-0.03	portable USGS
WIL	45 02 24.60	122 40 23.10	0.216	-0.03	portable USGS
FST	45 04 24.00	122 36 44.40	0.240	-0.07	portable USGS
GLDO	45 06 33.00	122 38 02.00	0.091	-0.13	portable USGS
MAQ	45 03 27.60	122 40 41.40	0.116	-0.03	portable USGS
MHS	45 08 37.80	122 34 32.90	0.117	-0.09	portable USGS
PHR	44 58 25.20	122 40 17.40	0.390	-0.08	portable USGS
SIV	44 58 44.40	122 43 22.75	0.308	-0.15	portable USGS
SMI	45 02 27.30	122 32 53.52	0.415	-0.05	portable USGS
YOD	45 08 40.50	122 40 51.75	0.067	-0.00	portable USGS
OSU1	45 08 55.61	122 22 07.07	0.530	-0.20	portable OSU
OSU2	45 00 33.95	122 35 03.55	0.256	-0.13	portable OSU
OSU3	45 03 07.38	122 45 57.10	0.107	-0.02	portable OSU
CHUO	45 21 19.44	122 59 18.60	0.436	0.00	portable UO
DPUO	45 06 23.76	122 31 21.00	0.137	-0.05	portable UO
WHUO	45 10 59.52	122 44 14.28	0.043	-0.09	portable UO
SSO	44 51 21.60	122 27 37.80	1.242	-0.44	permanent PNSN

* Station ownership
(UO) University of Oregon
(OSU) Oregon State University
(USGS) U. S. Geological Survey
(PNSN) Pacific Northwest Seismograph Network

generously provided by Mr. George Thomas, of the University of Washington, Dr. John Nabelek of Oregon State University and Mr. Bill Zediker of the University of Oregon. Because portable station coverage was sporadic we chose to average the station correction results of the 8 master events in an effort to reduce network bias errors. The velocity model used was taken from a vertical transect of an east west crustal velocity model by Trehu *et al.* (1994) at the point where the model intersects the longitude of the SMS epicentral zone. Vertical velocity gradients were averaged to form a 1D model shown in table A-2. This was necessary for hypocenter location using the University of Washington's ***SPONG*** least squares inversion software. Initial portable station delays were calculated to force the zero

Table A-2
Velocity model for SMS relocations

Depth (km)	V_p (km/s)	V_s (km/s)
0.0 - 1.25	2.85	1.50
1.25 - 2.5	4.4	2.3
2.5 - 3.5	5.06	2.7
3.5 - 6.5	5.63	3.0
6.5 - 7.5	6.20	3.3
7.5 - 11.5	6.40	3.4
11.5 - 15.5	6.63	3.5
15.5 - 19.5	6.86	3.6
19.5 - 23.5	7.09	3.7
23.5 -	7.32	3.9

elevation reference plane to sea level. Alluvial thicknesses were taken from isopach maps by Hampton (1972) and Werner *et al.* (1992). Average alluvial and

bedrock velocities of 1800 m/s and 2850 m/s respectively were based upon reflection and refraction work done by Lee Liberty (personal communication, 1996) and Trehu *et al.* (1994). Through an iterative process the final station delays for the 19 stations shown in table A-1 were determined. The final locations of the 8 master events are shown in table A-3. A V_p/V_s ratio of 1.9 was necessary in order to reduce shear wave residuals. This high ratio is a result of low shear wave velocities also observed by Nabelek (personal communication, 1996) and Thomas *et al.* (1996).

The 8 master events were then used as a control set to determine station delays at 8 PNSN stations. Forty events (the 8 master events and 32 additional events with magnitudes exceeding 2.0) were picked at the 8 PNSN stations. To avoid questionable picks on noisy and emergent first arrivals the traces were bandpassed at 1 to 5 Hz and a prominent peak or trough was picked that could be seen across the majority of events. This was not necessary for station SSO, which was 22 km from the epicentral area and had clear impulsive first arrivals. Not all of the 8 PNSN stations were picked for each master event due to occasional down time or low signal to noise ratio (half of the master events had magnitudes ranging from 1.7 - 1.9). The eight PNSN stations and their delays are shown in table A-4.

Table A-3
Final locations of 8 Scotts Mills sequence master events

Date (Yr. Mo Day)	Time (hr:min sec)	Latitude (deg. min.)	Longitude (deg. min)	Depth (km)	Magnitude	Gap (degrees)	RMS residual (sec)	Number of stations used in the relocation *
93 03 27	05:40 33.50	45N 2.40	122W 35.76	10.41	2.5	63	0.01	15
93 03 27	14:38 59.03	45N 2.96	122W 36.39	10.77	2.9	56	0.01	15
93 03 27	22:24 16.01	45N 2.32	122W 36.75	9.89	2.5	58	0.01	15
93 03 27	23:34 13.36	45N 2.36	122W 37.20	9.23	1.8	52	0.01	14
93 03 28	05:22 56.63	45N 2.27	122W 36.74	10.03	2.0	58	0.01	16
93 03 28	07:43 51.48	45N 2.33	122W 36.74	9.98	1.7	58	0.01	17
93 03 29	00:16 31.73	45N 3.01	122W 36.83	10.83	1.9	54	0.01	15
93 03 29	10:39 00.15	45N 2.21	122W 37.52	9.29	1.7	67	0.02	12

* This number includes PNSN station SSO which was used in the relocation of all the master events.

Table A-4
PNSN stations used to locate 32 magnitude 2.0+ events.

Station Name	North Latitude (deg. min. sec.)	West Longitude (deg. min. sec.)	Elevation (km)	Station Delay (s)	Number of master events used to determine station delay
SSO	44 51 21.60	122 27 37.80	1.242	-.044	8
HBO	43 50 39.55	122 19 11.88	1.615	0.04	7
MPO	44 30 17.40	123 33 00.60	1.249	-0.17	5
TKO	045 22 16.73	123 27 14.02	1.024	0.05	7
VBE	45 03 37.20	121 35 12.60	1.544	-0.01	6
VG2	45 09 20.00	122 16 15.00	0.823	-0.14	3
VLL	45 27 48.00	121 40 45.00	1.195	-0.06	4
VLM	45 32 18.60	122 02 21.00	1.150	0.02	3

As a test of the reliability of the 8 PNSN stations in accurately determining hypocenter depth, 5 of the 8 master events were relocated solely by these stations. The average absolute variation in depth from the initial master locations was 0.1 km (see table A-5). The 32 events were then relocated using the 8 PNSN stations and any available portable seismographs. The final locations shown in table A-6 revealed hypocenter depths ranging from 7.85 to 11.18 km. Fourteen of the 32 events along with one master event, all with magnitudes equal or exceeding 2.5 and representative of the total depth range, were selected for detailed analysis. These are referred to in the text as "the 15 select events" (see table A-7). An epicentral plot of the 8 master and 32 additional events is shown in figure A-1. A cross section plot shown in figure A-2 shows a clear alignment of the 40 events along a plane striking 310 +/- 5 degrees and dipping 35 +/- 5 degrees to the northeast. Our results are generally consistent with those of Thomas *et al.* (1996), who found a plane striking 290 +/- 10 degrees and dipping 60 +/- 5

Table A-5
Five master events located solely with the 8 PNSN stations

Date (Yr. Mo Day)	Time (hr:min sec)	Latitude (deg. min.)	Longitude (deg. min)	Depth (km)	Magnitude	Gap (degrees)	RMS residual (sec)
93 03 27	05:40 33.50	45N 2.39	122W 35.66	10.22	2.5	99	0.01
93 03 27	14:38 59.02	45N 2.99	122W 36.34	10.76	2.9	101	0.02
93 03 27	22:24 16.03	45N 2.26	122W 36.74	9.92	2.5	99	0.01
93 03 27	23:34 13.33	45N 2.42	122W 37.33	9.44	1.8	129	0.00
93 03 28	05:22 56.64	45N 2.27	122W 36.82	9.97	2.0	148	0.00

Table A-6

32 Scotts Mills sequence events located with 8 PNSN stations and available portable stations. Fourteen of the fifteen select events are italicized.

Date (Yr. Mo Day)	Time (hr:min sec)	Latitude (deg. min.)	Longitude (deg. min)	Depth (km)	Magnitude	Gap (degrees)	RMS residual (sec)
93 03 25	13:55 12.34	45N 3.25	122W 38.17	10.11	2.2	102	0.01
93 03 25	14:00 36.79	45N 3.49	122W 38.01	10.45	2.1	102	0.03
93 03 25	*14:20 56.89*	*45N 2.09*	*122W 36.24*	*9.91*	*3.2*	*99*	*0.01*
93 03 25	14:58 6.06	45N 2.88	122W 36.16	10.64	2.3	100	0.01
93 03 25	*15:35 12.90*	*45N 230*	*122W 36.59*	*10.09*	*3.1*	*99*	*0.03*
93 03 25	15:44 13.00	45N 3.52	122W 37.95	10.48	2.2	128	0.01
93 03 25	18:08 55.37	45N 1.73	122W 35.85	9.72	2.3	98	0.03
93 03 25	20:25 6.41	45N 3.51	122W 37.87	10.74	2.2	102	0.02
93 03 25	*21:03 60.71*	*45N 3.31*	*122W 37.73*	*10.23*	*2.7*	*102*	*0.03*
93 03 26	01:42 46.76	45N 3.44	122W 37.77	10.41	2.1	102	0.02
93 03 26	05:18 26.90	45N 2.49	122W 37.06	10.07	2.9	68	0.04
93 03 26	*07:59 65.97*	*45N 2.58*	*122W 37.16*	*10.16**	*3.0*	*70*	*0.01*
93 03 26	*16:54 32.16*	*45N 2.16*	*122W 37.44*	*8.95*	*3.1*	*51*	*0.03*
93 03 26	*17:39 22.47*	*45N 3.39*	*122W 37.76*	*10.59*	*3.2*	*54*	*0.03*
93 03 26	*18:43 48.52*	*45N 4.04*	*122W 37.72*	*8.28*	*2.7*	*125*	*0.05*
93 04 05	06:38 37.94	45N 1.96	122W 35.56	10.17	2.1	98	0.02
93 04 07	04:32 35.63	45N 3.33	122W 37.73	10.51	2.4	102	0.04

Table A-6

32 Scotts Mills sequence events located with 8 PNSN stations and available portable stations. Fourteen of the fifteen select events are italicized.

Date (Yr. Mo Day)	Time (hr:min sec)	Latitude (deg. min.)	Longitude (deg. min)	Depth (km)	Magnitude	Gap (degrees)	RMS residual (sec)
93 04 08	06:24 17.66	45N 2.90	122W 37.79	10.10	2.2	146	0.04
93 04 15	06:44 45.96	45N 1.77	122W 35.87	10.29	2.4	148	0.01
93 04 19	*18:28 28.85*	*45N 3.30*	*122W 37.42*	*11.18*	*2.5*	*102*	*0.02*
93 06 02	*21:09 52.70*	*45N 1.91*	*122W 36.82*	*10.01*	*2.9*	*98*	*0.03*
93 06 08	*00:01 25.98*	*45N 2.10*	*122W 36.36*	*9.14*	*3.8*	*99*	*0.04*
93 07 15	23:37 16.42	45N 2.22	122W 36.86	9.98	2.7	99	0.01
93 07 19	*05:10 28.43*	*45N 2.77*	*122W 35.70*	*10.89*	*2.6*	*100*	*0.01*
93 07 21	20:56 47.66	45N 2.75	122W 35.62	11.02	2.2	100	0.02
93 08 28	*21:25 40.76*	*45N 3.08*	*122W 37.86*	*10.47*	*3.2*	*101*	*0.02*
93 09 18	01:49 44.62	45N 3.77	122W 39.51	8.07	2.1	121	0.01
93 09 25	03:12 44.50	45N 2.30	122W 36.73	10.11	2.3	117	0.00
93 10 02	06:49 11.47	45N 2.25	122W 36.60	10.25	2.6	110	0.02
93 10 12	*00:14 30.93*	*45N 1.93*	*122W 37.68*	*8.52*	*2.6*	*99*	*0.02*
94 02 01	12:39 10.84	45N 2.24	122W 36.25	10.08	2.5	117	0.01
94 03 25	*17:12 36.27*	*45N 4.03*	*122W 37.72*	*7.85*	*2.5*	*121*	*0.06*

Table A-7
Fifteen Scotts Mills sequence events selected for detailed analysis.

Date (Yr. Mo Day)	Time (hr:min sec)	Latitude (deg. min.)	Longitude (deg. min)	Depth (km)	Magnitude	Gap (degrees)	RMS residual (sec)
94 03 25	17:12 36.27	45N 4.03	122W 37.72	7.85	2.5	121	0.06
93 03 26	18:43 48.52	45N 4.04	122W 37.72	8.28	2.7	125	0.05
93 10 12	00:14 30.93	45N 1.93	122W 37.68	8.52	2.6	99	0.02
93 03 26	16:54 32.16	45N 2.16	122W 37.44	8.95	3.1	51	0.03
93 06 08	00:01 25.98	45N 2.10	122W 36.36	9.14	3.8	99	0.04
93 03 25	14:20 56.89	45N 2.09	122W 36.24	9.91	3.2	99	0.01
93 06 02	21:09 52.70	45N 1.91	122W 36.82	10.01	2.9	98	0.03
93 03 25	15:35 12.90	45N 230	122W 36.59	10.09	3.1	99	0.03
93 03 26	07:59 65.97	45N 2.58	122W 37.16	10.16*	3.0	70	0.01
93 03 25	21:03 60.71	45N 3.31	122W 37.73	10.23	2.7	102	0.03
93 08 28	21:25 40.76	45N 3.08	122W 37.86	10.47	3.2	101	0.02
93 03 26	17:39 22.47	45N 3.39	122W 37.76	10.59	3.2	54	0.03
93 03 27	14:38 59.03	45N 2.96	122W 36.39	10.77	2.9	56	0.01
93 07 19	05:10 28.43	45N 2.77	122W 35.70	10.89	2.6	100	0.01
93 04 19	18:28 28.85	45N 3.30	122W 37.42	11.18	2.5	102	0.02

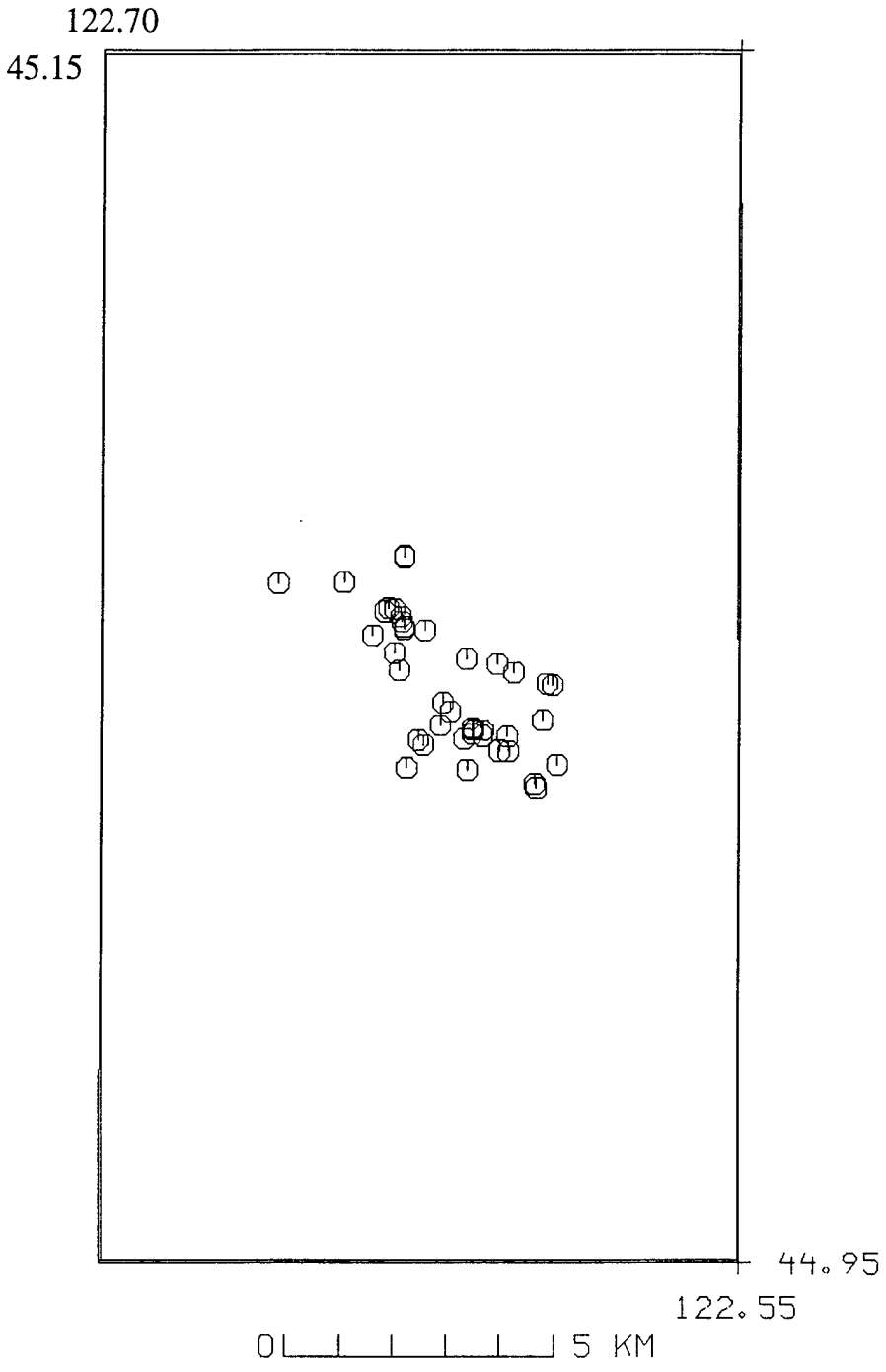

Figure A-1. Epicenter plot of the 40 relocated Scotts Mills sequence events.

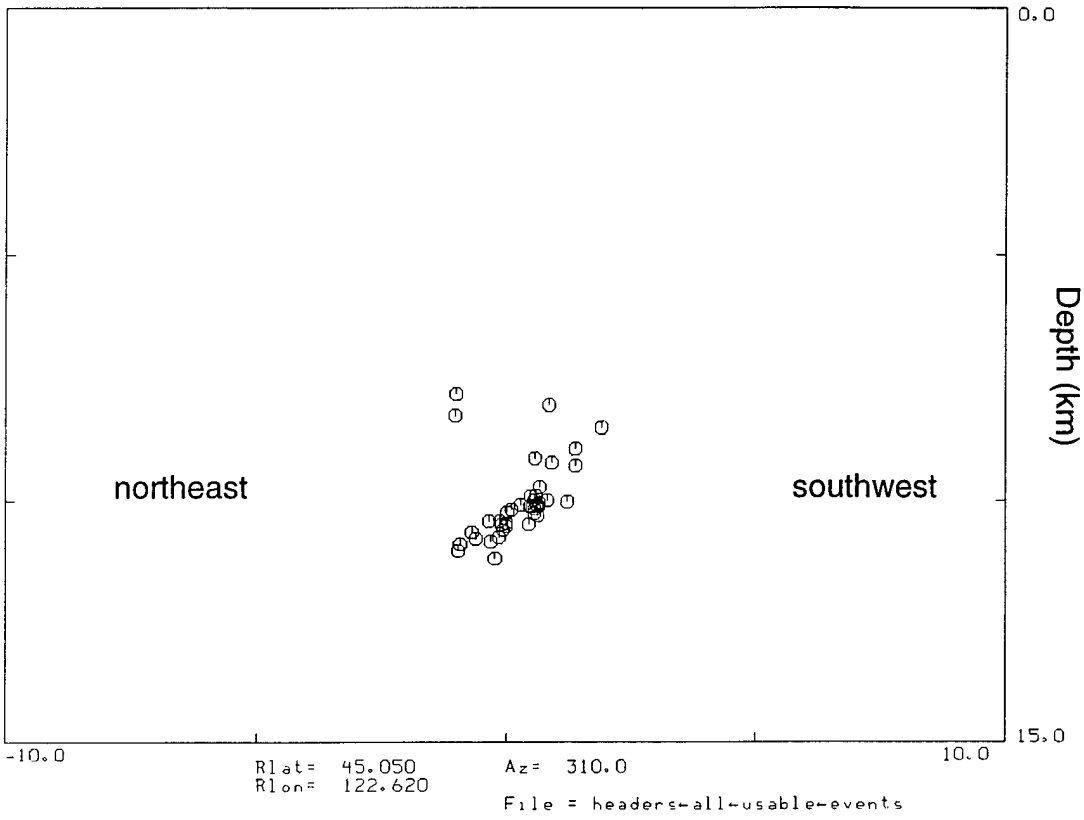

Figure A-2. Cross sectional plot with no vertical exaggeration of the 40 relocated events viewed from an azimuth of 310 degrees. Events fall on a plane dipping approximately 35 degrees to the northeast.

degrees to the northeast. The variation in dip is a function of Thomas *et al.* (1996) using a lower V_p/V_s ratio of 1.78 compared to ours of 1.9. This higher V_p/V_s ratio effectively compresses the vertical depth axis resulting in a lower dip angle. With exception of the 8 master events, we relocated 32 events that were not included in Thomas's final analysis.

Appendix - B

Filtering

Seismogram filtering performs two useful functions. First, it suppresses background and telemetry noise that interfere with the desired signal. The analog telemetry systems employed by the University of Washington add significant high frequency electronic noise to the amplified seismometer signals and some of the stations occasionally record wind noise. Low pass and bandpass filtering often improved the observed signal. Second, low pass filtering enhances same-station similarity of events arriving from the same source area. All usable data we examined were the result of bandpass filtering the recorded data.

Filtering was performed using a two pole Butterworth filter, part of the University of Washington's interactive phase picking program ***PING***. Stations were examined in a variety of frequency bands. For matching observed data with predicted arrivals we found that bandpass filtering between 1 and 10 Hz was optimal. The 10 Hz high cut passed enough high frequency content to resolve separate phases while eliminating most of the unwanted high frequency noise. The modelled travel time plots required the resolution of up to seven phases in time windows ranging from 1 to 3 seconds. High cuts below 10 Hz reduced our resolving power whereas high cuts above 15 Hz were complicated by their excessive high frequency component.

When the objective was to improve similarity from one event to the next at a single station in order to correlate phases across the entire depth range, phases were found to be most enhanced at low pass bands ranging from 0-3 Hz to 0-6 Hz. Examples of the effectiveness of different filter settings can be found in Zollweg and Childs (1996).

Appendix - C

SP_mP phase modelling using the C3 velocity model, Scotts Mills

Because ***RAYINVR*** was not capable of producing travel time curves for a free surface reflection the SP_mP curves were produced in two stages. First RAYINVR was used to create a P_mP reflection travel time curve for a hypothetical surface source using the C3 model. Using a V_p/V_s ratio of 1.9 the added travel time for an upward directed shear wave with a source depth of 10 km was calculated at 3.4 and 3.6 s corresponding to offsets of 111 and 381 km respectively. Similar calculations were conducted for source depths of 7.85 and 11.18 km. A time delay window of 2.7 to 4.0 s after the ray traced arrival of the surface source P_mP phase was determined. Depth order plots for 22 regional stations bandpassed at 0.01 to 4.0 Hz with 18 s of data were produced to search the SP_mP predicted arrival time window. These stations were selected because they had already been observed to have prominent early ***P*** phase arrivals.

Appendix - D

Production of Scotts Mills Synthetics

Synthetics were produced using the C3 model and the ***RAYINVR*** program for the SMS event of August 28, 1993, 2125 UTC, source depth of 10.47 km. To avoid contamination by later non ***P***-phases, spectral analysis of the first 8 seconds of

observed data was performed on each of the 11 C3 stations analyzed in the forward modelling process. Peak energy was found in a 2.5 to 7.5 Hz band. The source wavelet was then produced by convolving a 500 point spike at time zero with a 2.5 to 7.5 Hz Butterworth bandpass filter. This wavelet was then input into the ***RAYINVR*** program to produce an amplitude normalized record section plot of the synthetics shown in figure D-1).

Appendix E

Procedure for calculation of theoretical P_g arrival times

Theoretical P_g arrival times were calculated to be used as a depth independent reference frame used in single station depth order plots. The travel distance is calculated as the hypotenuse of a right triangle where the hypocenter depth and epicentral offset serve as the two remaining sides. The travel time is calculated by dividing the travel distance by an average P_g velocity of 6.0 km/s. This result is then added to the origin time. Arrival times were calculated at each station for all 40 events analyzed.

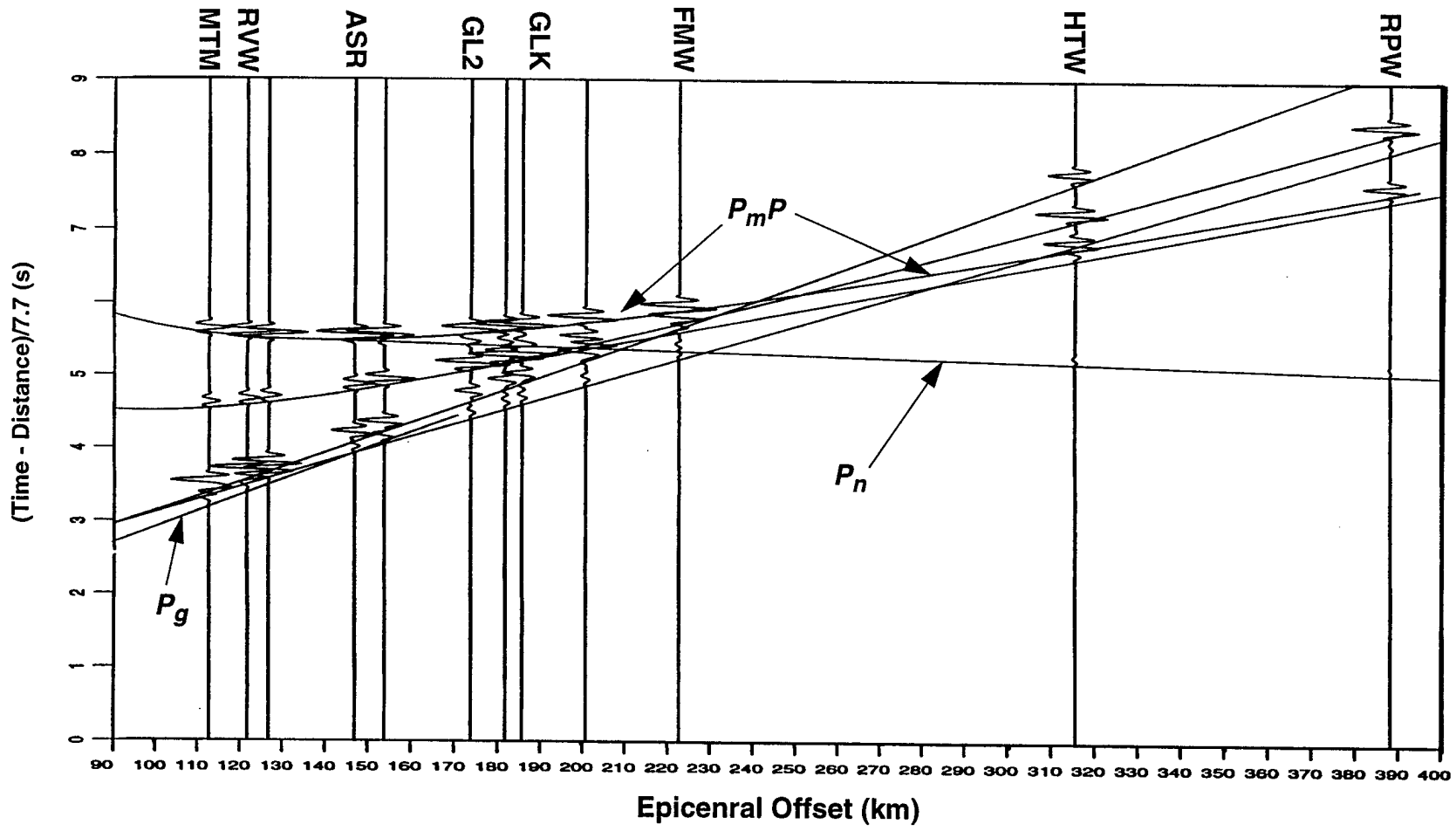

Figure D-1. Record section plot of synthetics overlain by a travel time curve produced using velocity model C3 and *RAYINVR* program *xpltsyn* for the event of August 26, 1993, 21:25 UT, source depth of 10.47 km. Stations modelled are shown at the top of the plot. Predicted phases are labeled. Notice strong but emergent arrivals of the *PmP* phase and weak arrivals of *Pn* and *Pg*

9.0 References

Carver, D., D. Worley, and T. Yelin (1993). Digital recordings of the March 25, 1993, Scotts Mills, Oregon earthquake, U.S. Geol. Surv. Open File Rept. 93-535.

Grant, W. C., C. S. Weaver, and J. E. Zollweg (1984), The 14 February 1981 Elk Lake, Washington, earthquake sequence, *Bull. Seism, Soc. Am.* **74**, 1289-1309.

Hampton, E. R. (1972). Geology and ground water of the Molalla-Salem slope area, northern Willamette Valley, Oregon, U.S. Geol. Surv. Water Supply Pap. 1977.

Leaver, D., W. D. Mooney, and W. M. Kohler (1984), A seismic refraction study of the Oregon Cascades, *J. Geophys. Res.* **89**, 3121-3134.

Thomas, G. C., R. S. Crosson, D. L. Carver, and T. S. Yelin (1996), The 25 March Scotts Mills, Oregon, earthquake and aftershock sequence: spatial distribution, focal mechanisms, and the Mount Angel Fault, *Bull. Seism, Soc. Am.* **86**, 925-935.

Trehu, A. M., I. Asudeh, T. M. Brocher, J. H. Luetgert, W. D. Mooney, J. L. Nabelek, and Y. Nakamura (1994), Crustal architecture of the Cascadia Forearc, *Science* **265**, pp. 237-243.

Werner, K., J. Nabelek, R. Yeats, and S. Malone (1992), The Mt. Angel fault: implications of seismic-reflection data and the Woodburn, Oregon, earthquake sequence of August, 1990, *Oregon Geol.* **54**, 112-117 (published by the Oregon Department of Geology and Mineral Industries).

Zelt, C. A., and R. B. Smith (1992), Seismic traveltime inversion for 2-D crustal velocity structure, *Geophys. J. Int.* **108**, 16-34.

Zollweg, J. E. and D. M. Childs (1996), Empirical identification of depth related phases at regional distances, in Lewkowicz, J. F., J. M. McPhetres, and D. T. Reiter (eds), Proceedings of the 18th Annual Seismic Research Symposium on Monitoring a Comprehensive Test Ban Treaty, 4-6 September, Phillips Laboratory Report PL-TR-96-2153, 809-818.

1. INTRODUCTION

Discrimination between explosions and earthquakes in a Comprehensive Nuclear Test Ban monitoring scenario is in part dependent on accurate event location. Accurate event location serves a critical function by separating potentially interesting events from the tens of thousands of industrial explosions and natural earthquakes that occur annually around the world. An important and still largely unsolved problem in location is the determination of focal depth for small events recorded at regional distances. Focal depth is an important discriminant in its own right. Most explosions and rockbursts occur at depths less than 3 km, while most natural earthquakes occur at depths greater than 4 km. Focal depth determination at regional distances depends on the ability to either directly identify depth-related phases such as P_mP, or else find some other characteristic of the recorded seismograms that can be shown to be depth-related (for example, surface wave excitation).

We are examining earthquake sequences in the Pacific Northwest of the United States in an effort to improve capabilities of determining focal depths at regional distances. The Pacific Northwest is an interesting test platform for several reasons. First, earthquakes and explosions are widely distributed throughout the crust, rather than being confined to zones of small areal extent as is often the case elsewhere. Second, seismograph coverage is good, allowing many events to be considered as having "known" focal depth and providing broad spatial sampling of the earthquake wavefield. Third, there are many crustal geological provinces, giving us a chance at evaluating how well regional phases propagate along paths through a mixture of geological environments.

Our efforts to date have been directed toward the 1981 Elk Lake, Washington earthquake sequence (see Figure 1-1), as described in the previous annual report. We have concentrated on a group of the larger aftershocks having a good distribution in depth. We have found that most depth-related phases predicted by crustal model studies are unidentifiable on the seismograms, in part because the complicated structure leads to multiple phase arrivals within very short time windows. Propagation of other phases (particularly P_g) seems to be blocked at relatively short distances. However, by plotting the observed seismograms at a single station as a function of focal depth of the events, we have been able to identify depth-dependent phases at nearly half

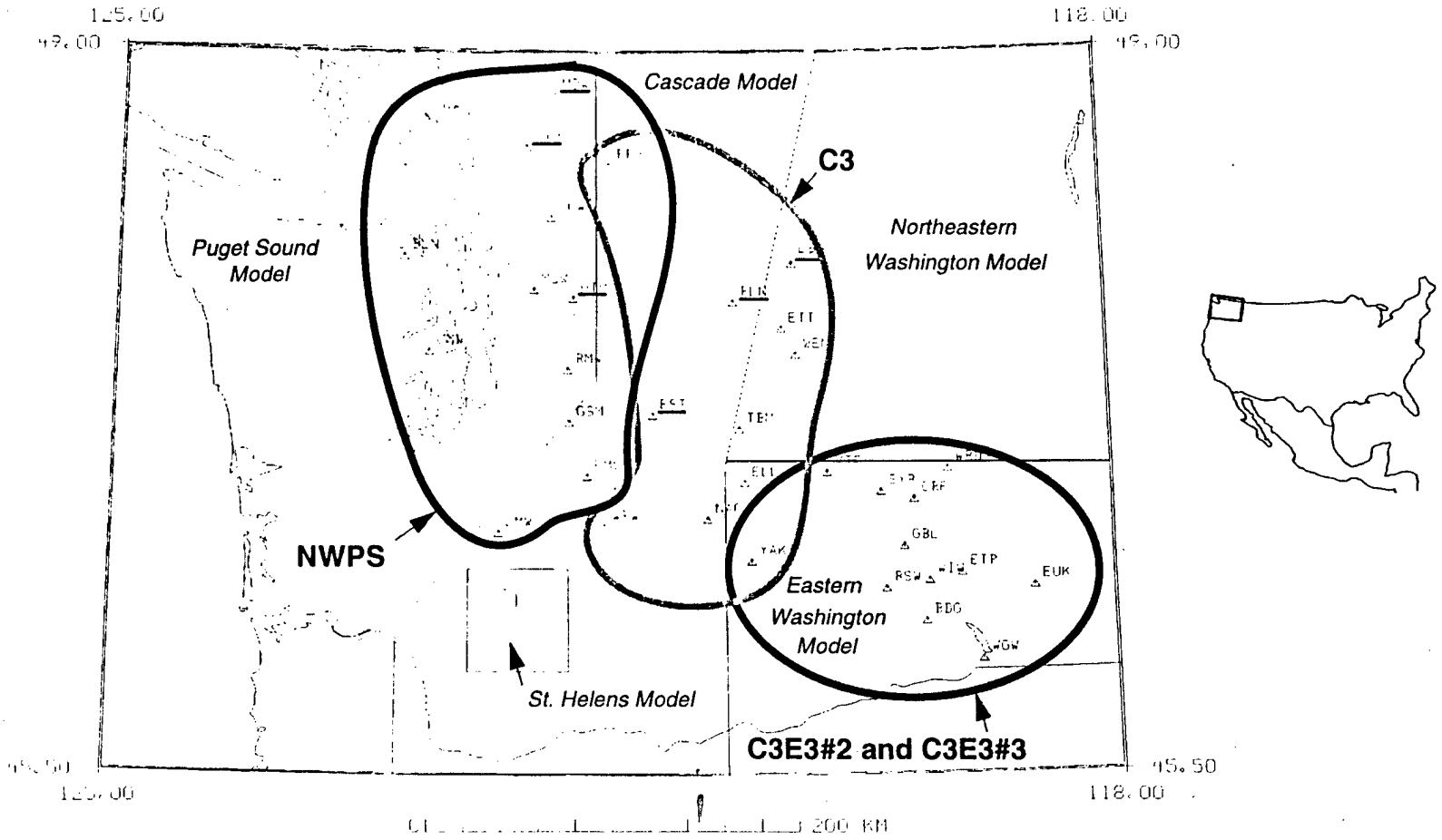

Figure 1-1. Regions of validity of the University of Washington velocity models (italicized) used in routine seismic event location. Recording stations whose data have been examined in this study are shown by triangles. Stations whose data are discussed in detail are underlined. Station groups are enclosed by solid lines according to the corresponding velocity model (NWPS, C3, C3E3#2 or C3E3#3) used to predict crustal phase arrivals. The epicenter of the 1981 Elk Lake main shock is shown by an octagon.

of the stations examined to date. We may not know what these phases are at this time, but they still may serve as useful indicators of relative depth.

In nearly all of the cases of depth-related phases we have observed, only one such depth-related phase is apparent on any seismogram. This problem has led us to examine the utility of time differences between depth-related phases at two stations along the same azimuth as measures of focal depth. We have found a few cases where such time differences are functions of depth. In some other cases, however, the observed relationship is difficult to interpret.

In the following sections we describe our efforts to identify depth-related phases from forward modelling based on crustal structure studies, and then discuss the more empirical approach we adopted when the modelling approach proved a disappointment. We note that we have examined only one earthquake sequence in detail and our upcoming studies of other sequences may still show the forward modelling approach to be of use.

2. REGIONAL CRUSTAL PHASE IDENTIFICATION UTILIZING FORWARD MODELLING

Introduction

We attempted to identify regional crustal phases based upon their predicted arrival times. Theoretical travel time plots were produced using the raytracing program *RAYINVR* (Zelt and Smith, 1992). The plots were then compared to data from the 1981 Elk Lake, Washington earthquake sequence (Grant *et al.*, 1984). Use of several different velocity models was necessary due to variations in velocity structure for station groups lying to the north, northeast, and east of Elk Lake (Figure 1-1). In this section we present the procedure, the origin and description of each velocity model, and our evaluation of the utility of the raytracing exercise for phase identification.

Procedure

Four earthquakes (magnitude 3.0 - 4.5) of differing focal depth (7.83, 8.56, 9.69, and 10.33 km) were studied in detail. These earthquakes have well constrained epicenters and depths, estimated to be accurate within about 0.5 km in a relative sense. Their focal depths are representative of the range found in the Elk Lake sequence. Travel time and ray trace plots were created for each event using *RAYINVR* and each of four distinct velocity models. Phases modelled included critically refracted, reflected, and direct *P* and *S*, as well as *S*-to-*P* reflection boundary conversions. When possible all phases were traced for each velocity layer. *S*-to-*P* reflection boundary conversions were traced for at least one event for each model but are not shown in the ray trace plots presented below. Four velocity models were used corresponding to three station groups lying to the north (model NWPS), the northeast (model C3), and the east (models C3E3#2 and C3E3#3) of Elk Lake. Models were based upon current interpretations of crustal refraction and earthquake data and are discussed later in this section. A total of 34 stations was chosen from the University of Washington's seismic network to form the three station groups. Epicentral offsets range from 35 to 285 km. To identify regional crustal phases 5 to 10 seconds of data around the observed first arrivals were plotted together by station groups. These were then compared with the appropriate travel time curves both by their calculated arrival times and by visual inspection, the latter being a means of accounting for station delays. Observed data were bandpassed at 1 to 10 Hz. Details of the filtering procedure are discussed in Appendix A.

Origins and Descriptions of Velocity Models

Due to the variation in structure along the three azimuthal paths it was necessary to use several 2 dimensional velocity models. Both C3 (University of Washington's standard processing model for events in the Cascades), and NWPS (Miller *et al.*, 1995) are existing models, whereas we developed transitional model C3E3#1 from the University of Washington's C3 and E3 models (E3 is the University of Washington's standard processing model for events in southeastern Washington). Other studies of crustal structure in Oregon and southeastern Washington (Leaver *et al.*, 1984; Glover, 1985; Catchings and Mooney, 1988) were used to develop transitional models C3E3#2 and C3E3#3.

Models C3E3#1, C3E3#2 and C3E3#3, Eastern Washington

Twelve stations (YAK, VTG, RSW, SYR, GBL, CRF, BDG, WIW, ETP, WRD, WGW, and EUK) were used in conjunction with the C3E3 models (Figure 1-1). These models were used at stations around a line running from the Elk Lake epicenters slightly north of east across the Cascades into eastern Washington. Station offset distances range from 133 to 283 km. The development of a velocity model was complicated by the fact that the path encompasses two major geologic provinces, the Cascades to the west and the Columbia Plateau to the east, and that no single refraction study covers the entire azimuthal path.

The seven layer C3E3#1 model was created using University of Washington's one dimensional C3 and E3 routine earthquake location models. We joined the two models across a 75 km transition zone where layers of similar velocity were connected (Figure 2-1). No travel time curves were produced for this model because we felt the transition zone was unrealistic, particularly with regard to the pinching out of layer 5 on the west end of the model. However, this model was used as a basis for the development of C3E3#2.

Model C3E3#2 (Figures 2-2 and 2-3), is essentially a hybrid of C3E3#1 and results from a refraction study by Catchings and Mooney (1988). The abruptness of the transition zone had to be smoothed out to make the raytracing realistic. The smoothing was accomplished by extending the 6.8 km/s layer to the model's eastern terminus, raising the bottoms of layers 2, 3, and 4 in the east, and raising layer 5 both to the east and west. Velocities in layer 6 and the eastern half of layers 7 and 8 match velocities proposed by Catchings and Mooney (1988).

The 7 layer, C3E3#3 model is 325 km long and 46 km deep (Figures 2-4 and 2-5). It is based upon refraction studies from southeastern Washington (Catchings and Mooney, 1988; Glover, 1985) and the Oregon Cascades (Leaver *et al.*, 1984). At 0 km offset, referenced to the Elk Lake sequence epicenters, velocities and layer boundary depths are taken from the north end of the model proposed by Leaver *et al.* with the exception of the lower layer at 45 km depth in which the C3E3#3 model has an immediate transition from 7.1 to 7.7 km/s as opposed to a 2.7 km thick transition zone proposed by Leaver *et al.* Moving east there is a substantial gap in the coverage

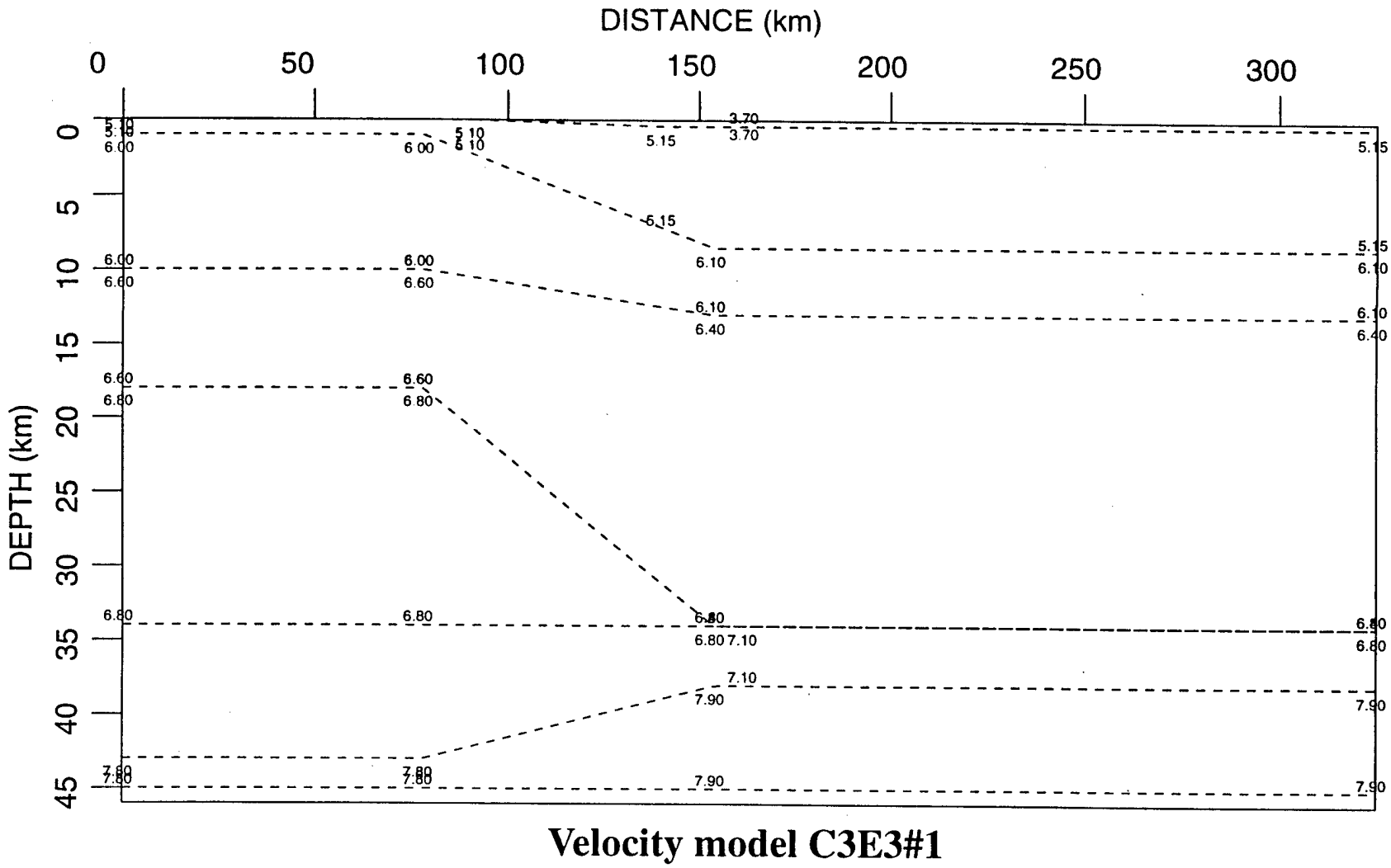

Figure 2-1. Initial velocity model for eastern Washington station group. This model is based upon velocity models used for routine earthquake location by the University of Washington for earthquakes originating in the Cascades (model C3) and eastern Washington (model E3). This model, considered to crude to warrant ray tracing, was used as a basis for model C3E3#2. Numbers are velocity values in km/s.

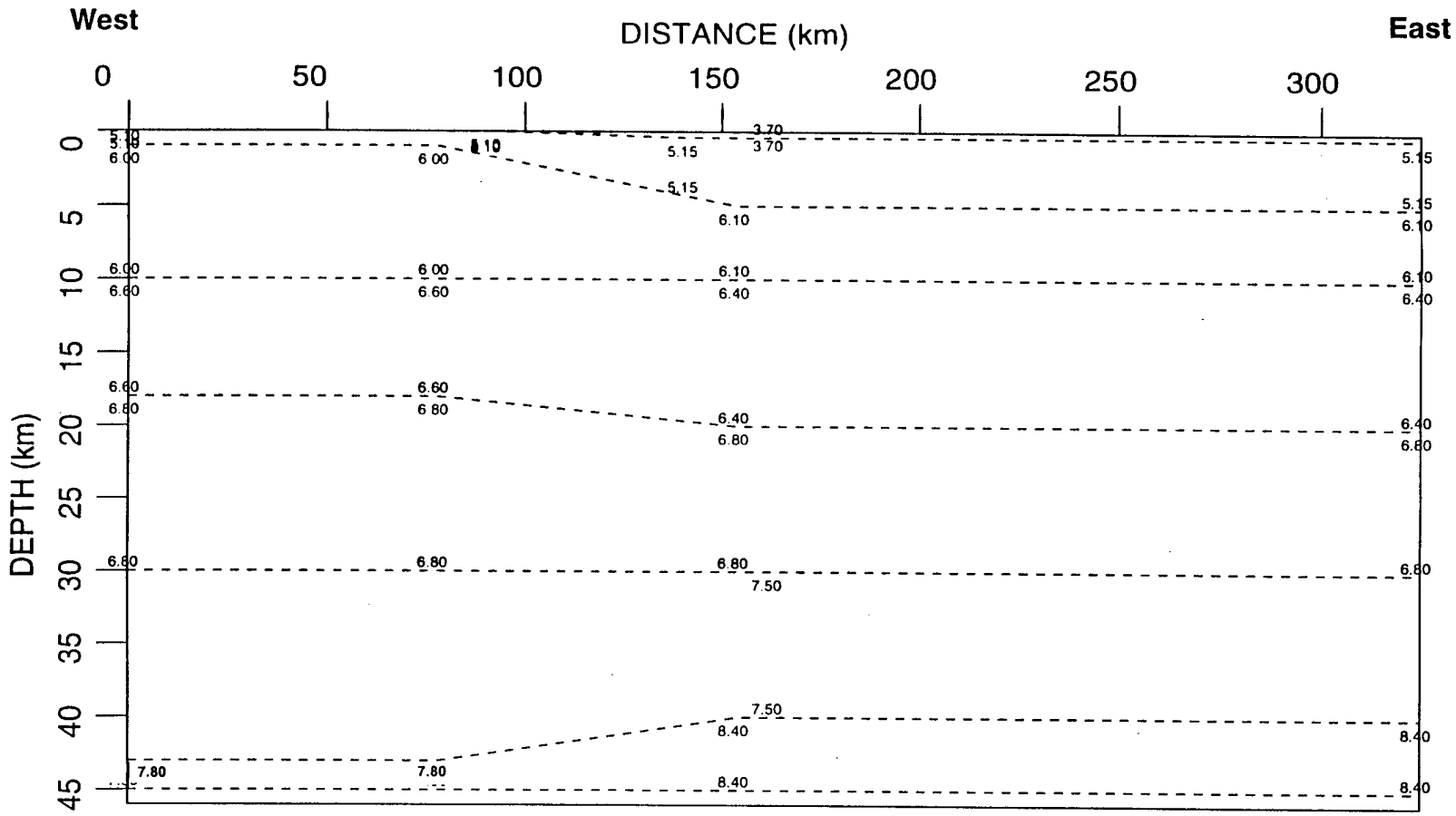

Figure 2-2. One of two models used to predict phase arrivals for 12 stations to the east of the Elk Lake earthquake sequence. Stations are YAK, VTG, RSW, SYR, GBL, CRF, BDG, WIW, ETP, WRD, WGW, and EUK. Station epicentral offsets range from 133 to 283 km. Numbers are velocity values in km/s.

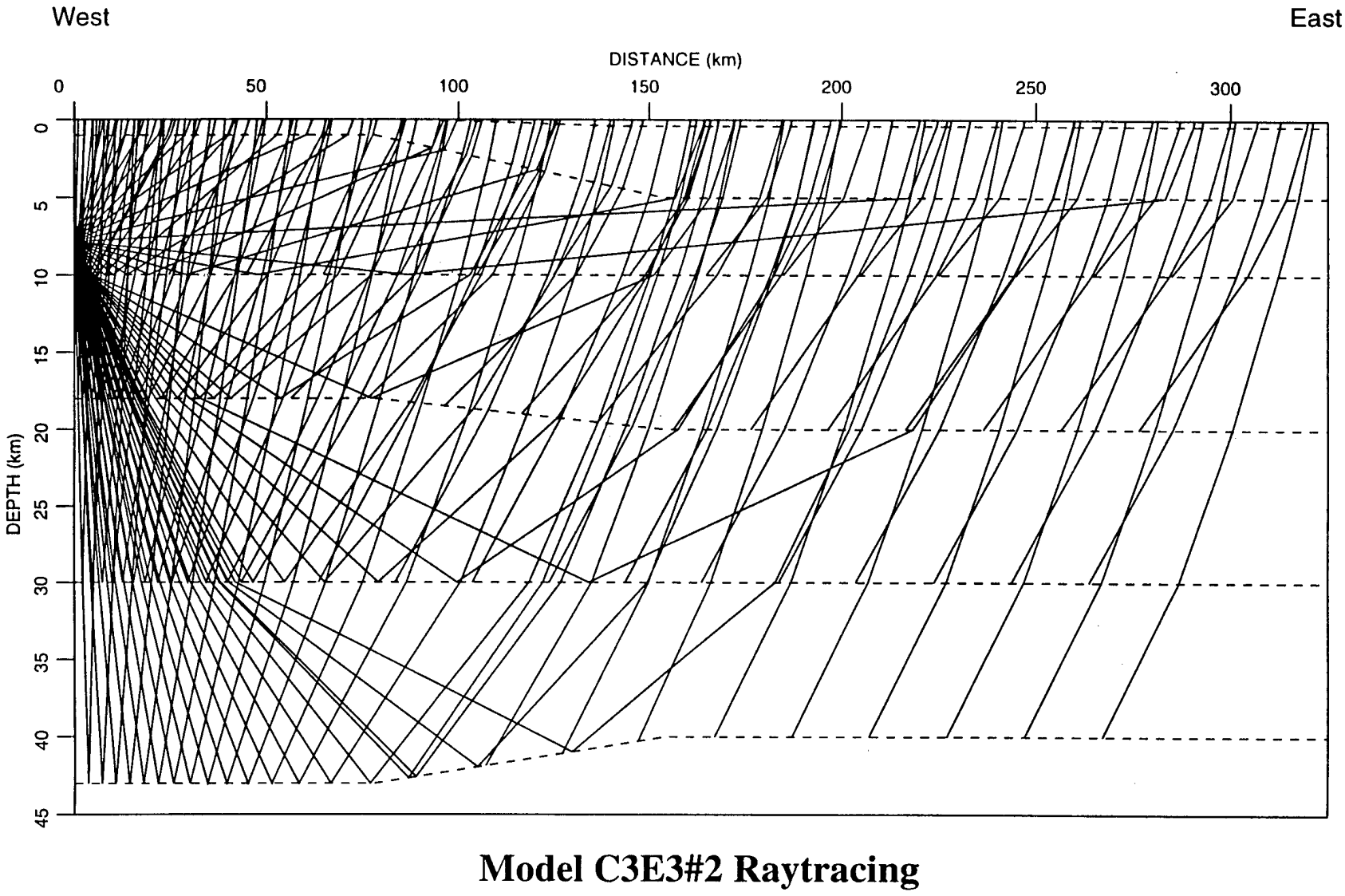

Figure 2-3. *RAYINVR* raytracing results for 7.83 km deep event (81/02/14, 2127 UTC). Phases traced include P_n, P_mP, P_g, and both reflections and head waves off the bases of velocity layers 3, 4 and 5.

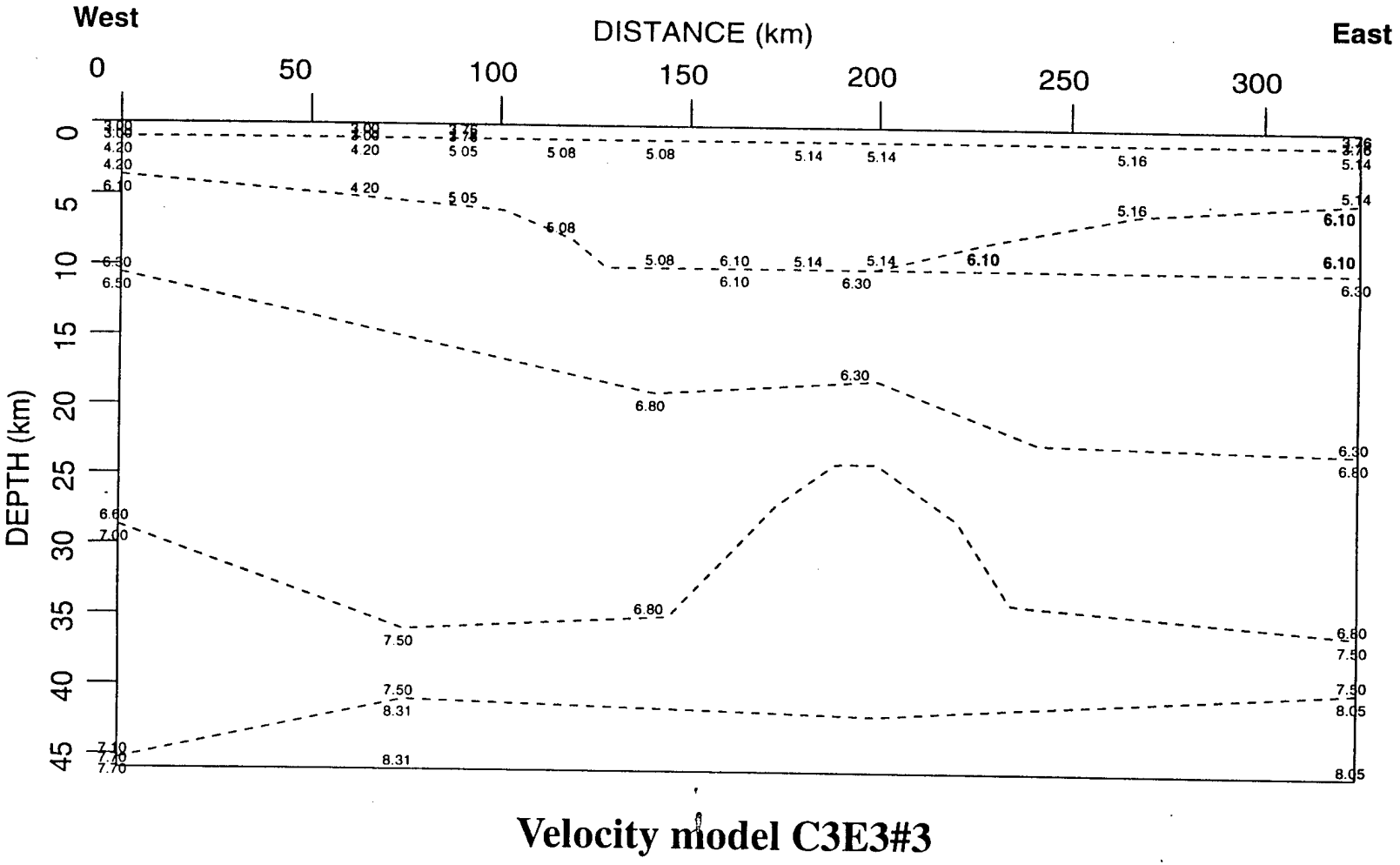

Figure 2-4. One of two models used to predict phase arrivals for 12 stations to the east of the Elk Lake earthquake sequence. Stations are YAK, VTG, RSW, SYR, GBL, CRF, BDG, WIW, ETP, WRD, WGW, and EUK. Station epicentral offsets range from 133 to 283 km. Numbers are velocity values in km/s.

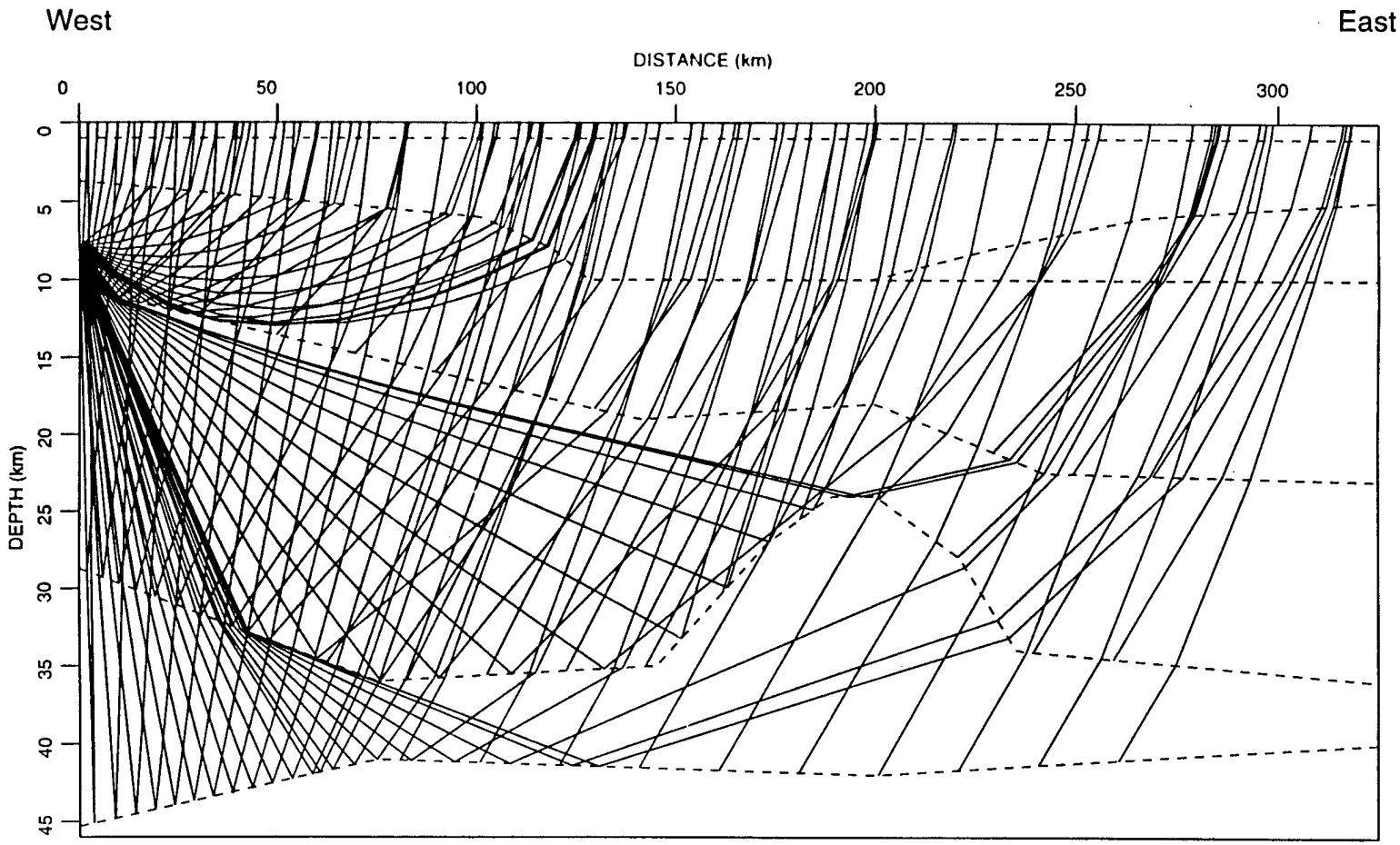

Figure 2-5. *RAYINVR* raytracing results for 7.83 km deep event (81/02/14, 2127 UTC). Phases traced include P_n, P_mP, P_g, and both reflections and head waves reflected from and refracted across the bases of velocity layers 4 and 5.

by crustal studies which is overcome as best as possible by matching velocity layers of similar values with those proposed in the refraction studies by Glover (1985) and Catchings and Mooney (1988). This transition zone spans the first 100 km of the model. At 100 km the model enters the area of the refraction studies undertaken by Glover (1985) and Catchings and Mooney (1988). There is reasonable agreement between the velocity structure proposed by these two studies, although Glover's data lose resolution at around 20-25 km depth whereas Catchings and Mooney present their model to a depth of 54 km. From 100 to 290 km offset the depths of the layers 1 through 3 are based upon velocity contour maps proposed by Glover. The 3.76 km/s velocity in layer one is an average of both studies whereas that of layer 2 is a thickness-weighted average of alternating fast and slow layers proposed by Catchings and Mooney. Layer 2 velocities were averaged vertically to preserve lateral velocity variations while simplifying the process of ray tracing through a single layer rather then several thin ones. The layer 3 velocity of 5 km/s, as well as boundaries and velocities from layers 4, 5, and 6 are all taken directly from Catchings and Mooney. Velocities in layer 7, 8.31 and 8.05 km/s, were determined by us by inverting P_n picks from the magnitude 5.2 Elk Lake main shock.

Velocity model C3, Northeastern Washington

Velocity model C3 is a simple one dimensional model which reaches to a depth of 45 km and extends laterally 325 km (Figures 2-6 and 2-7). This model is used by the University of Washington to routinely locate earthquakes originating in the Cascades. The unmodified model was used to predict arrivals at eleven stations to the Northeast of the Elk Lake sequence (ETT, FPW, WEN, RPW, PLN, EST, TBM, ELL, NAC, YAK and WPW). Station epicentral offsets range from 66 to 241 km.

Velocity Model NWPS, Northwestern Washington

The NWPS velocity model was derived from a refraction study undertaken in 1991 in collaboration with the USGS Deep Continental Studies Group. The line ran from the U.S./Canadian border south through the Puget Sound Basin terminating south of Mt. Rainer in Washington state (Miller and Keller, 1993). The thirteen stations used in conjunction with this model are MCW, MBW, LYW, JCW, RPW, BLN, MOW, HTW, GMW, RMW, GSM, FMW,

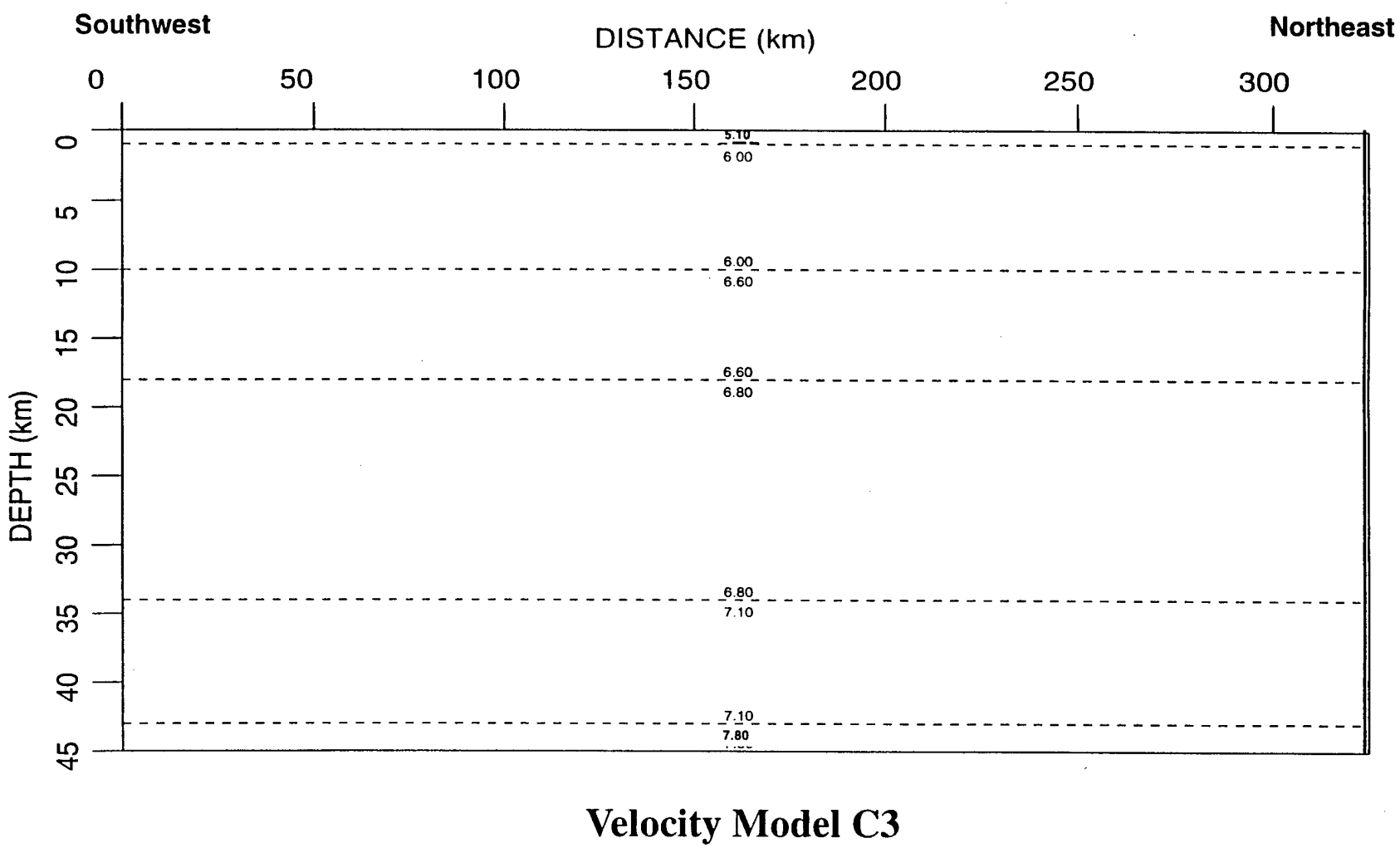

Figure 2-6. This model is used by the University of Washington to routinely locate earthquakes originating in the Cascades. The unmodified model was used to predict arrivals at eleven stations to the northeast of the Elk Lake earthquake sequence (ETT, WEN, RPW, PLN, EST, TBM, ELL, NAC, YAK, FPW and WPW). Numbers are velocity values in km/s.

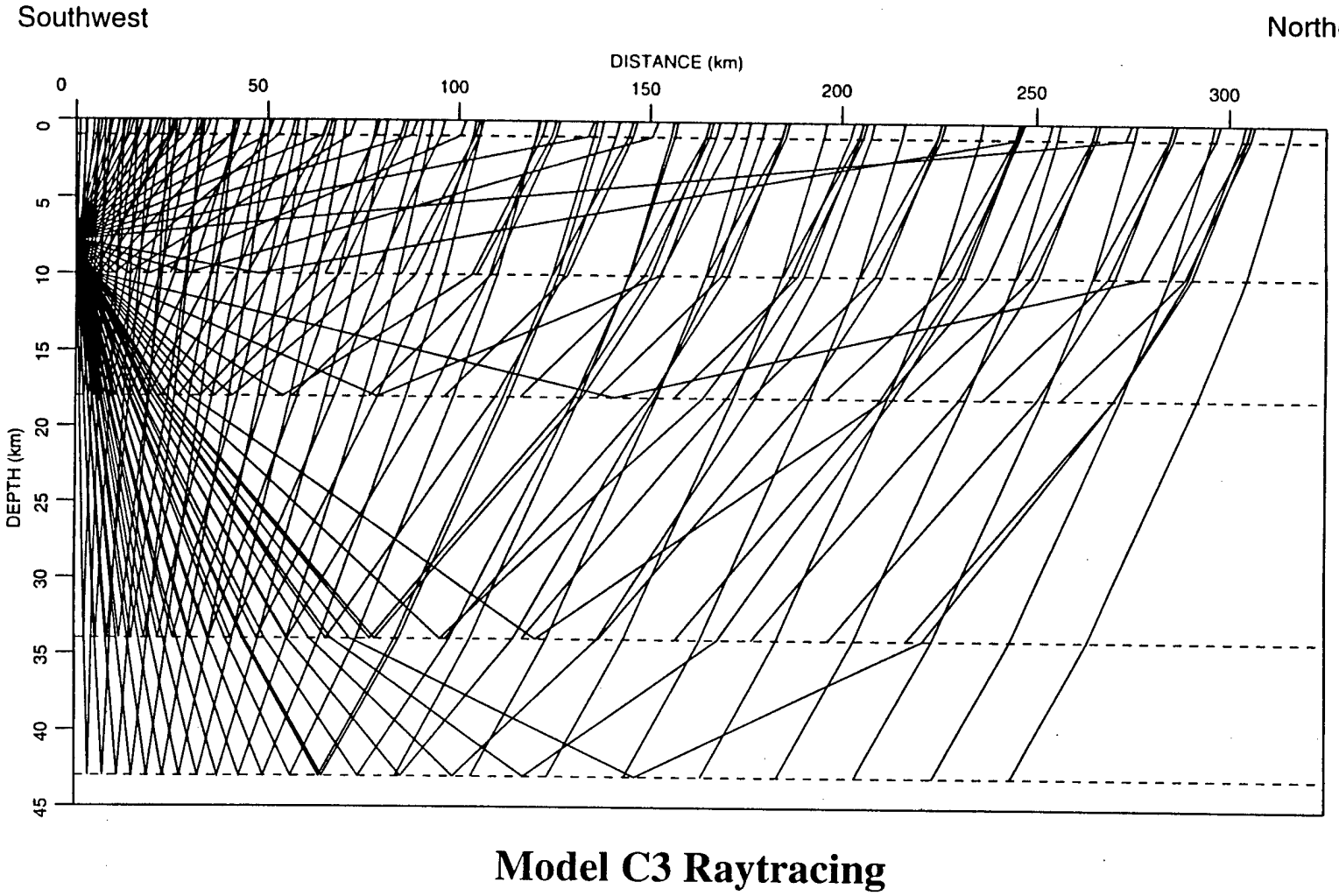

Figure 2-7. *RAYINVR* raytracing results for 7.83 km deep event (81/02/14, 2127 UTC). Phases traced include P_n, P_mP, P_g, and both reflections and head waves reflected off and refracted across the bases of velocity layers 2, 3 and 4.

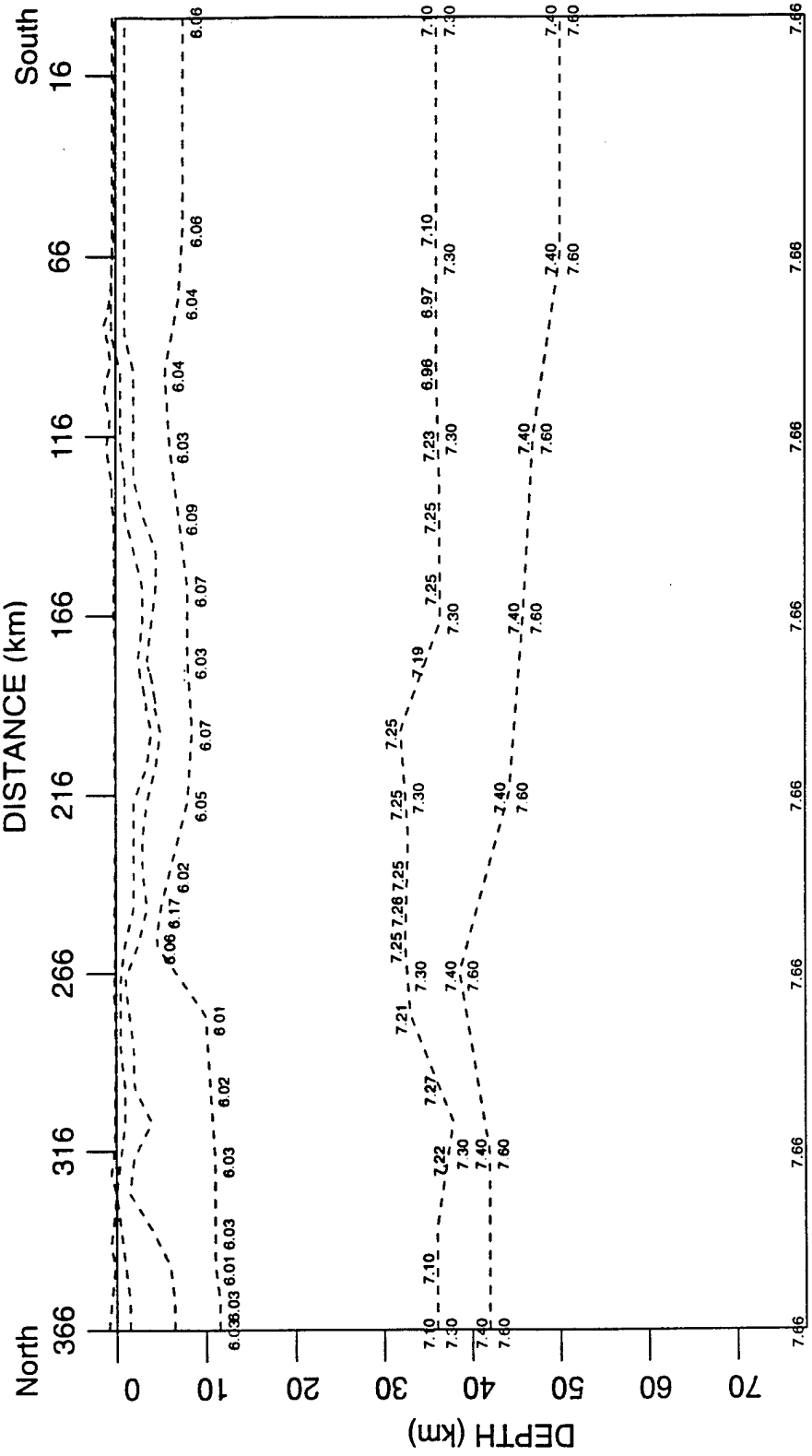

Figure 2-8. This model, taken from Miller *et. al* (1995) with minor modifications, was used for thirteen stations lying to the north of the Elk Lake earthquake sequence, including MCW, MBW, LYW, JCW, RPW, BLN, MOW, HTW, GMW, RMW, GSM, FMW, and LMW. Station epicentral offsets ranged from 36 to 273 km. Velocity values are in km/s. Velocity values in layer one, two and three range from 3.3 to 4.9, 4.29 to 5.30 and 5.02 to 6.00 km/s respectively.

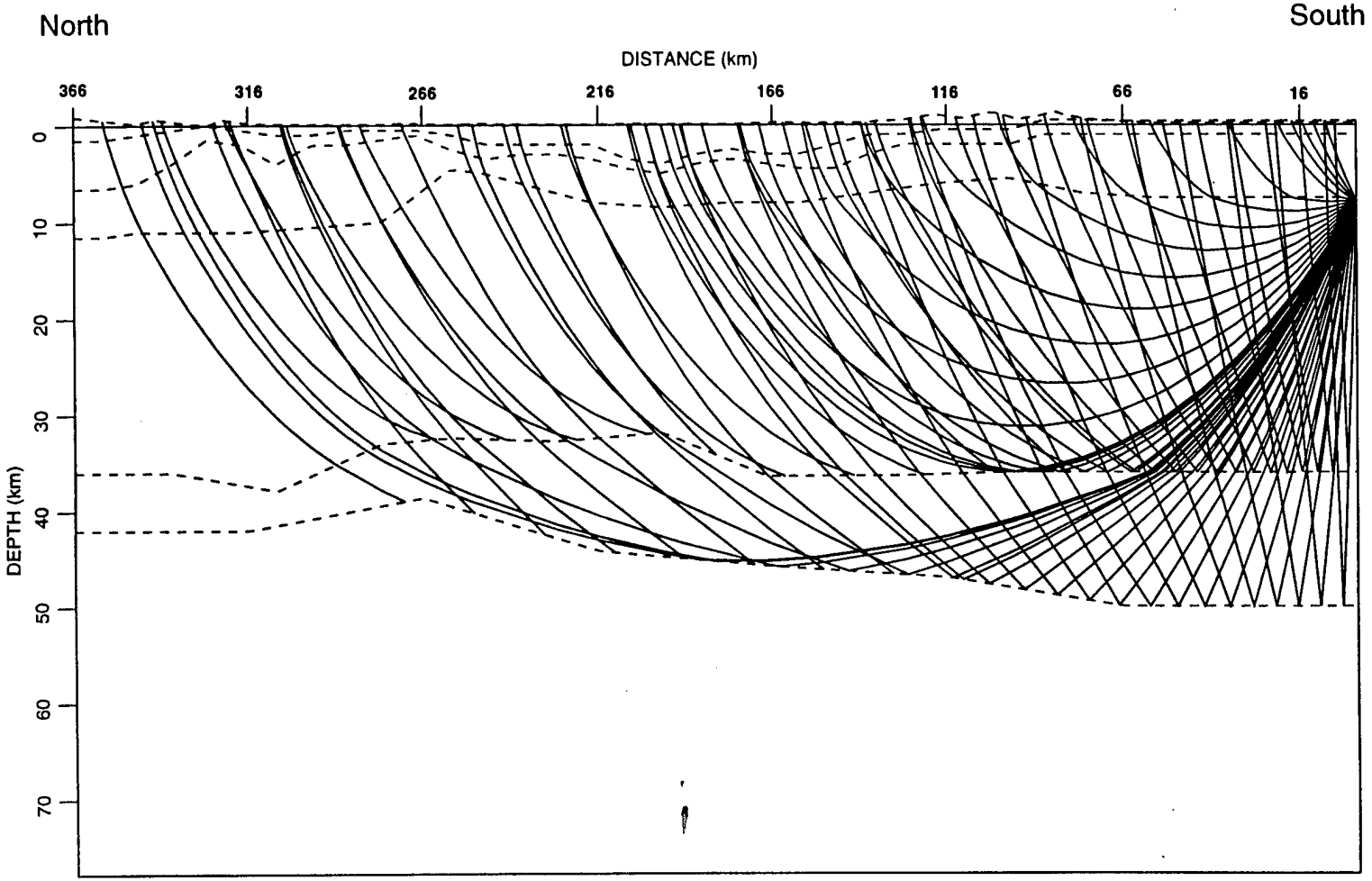

Figure 2-9. *RAYINVR* raytracing results for 7.83 km deep event (81/02/14, 2127 UTC). Phases traced include P_n, P_mP, P_g, and both reflections and head waves reflected off and refracted across the base of

and LMW. Station epicentral offsets range from 36 to 273 km. Based upon this refraction study several models have been proposed by Miller *et al.* (1995). The selected model was considered the most appropriate by its authors (Miller, personal communication, 1995). Sixteen kilometers were added to the southern model terminus to account for the average north-south offset between the south end of the model and the epicentral area of the Elk Lake sequence, giving the model a total length of 366 km and depth of 77.69 km (Figures 2-8 and 2-9). Velocities and depths within this 16 km extension are the same as at the original southern terminus of the model. Layer one upper velocities from 98.10 to 238.1 km offset underlying the Puget Sound region of Washington were raised to the velocities that exist at the base of layer one. This increase in surface velocity is justified because our station group for this model mainly lies to the east of the Puget Sound Basin, in the area transitional to the Cascades where surface velocities are higher.

Results of Velocity Modeling

Amplitude-normalized record sections overlying travel time curves from velocity models C3E3#2, C3E3#3, C3 and NWPS are shown for the aftershock of 14 February 1981 2127 UTC (magnitude 3.8, depth 7.8 km) in Figures 2-10 through 2-13. Trace plots were also made for aftershocks at other depths, and the observations we will present based on the one aftershock were found to apply to events over the whole range of aftershock focal depths.

Observations are as follow:

1. P_n is weak, very emergent and often not visible at all on some of the smaller events. This can be seen at all of the station groups. Model C3E3#3 (Figure 2-11) has very good agreement with the P_n first arrival whereas NWPS (Figure 2-13) predicts times that are late by 0.2-0.6 s at stations MBW, MCW, and LYW. Emergent P_n waveforms are also illustrated in an eastern Washington amplitude normalized station group trace plot of the 14 February 1981 2127 UTC aftershock (Figure 2-14).

2. P_g as predicted by the models is seen with model C3 (Figure 2-12) at stations TBM, RPW and arguably WEN with a 0.4 s delay. However, there appears to be no correlation with models

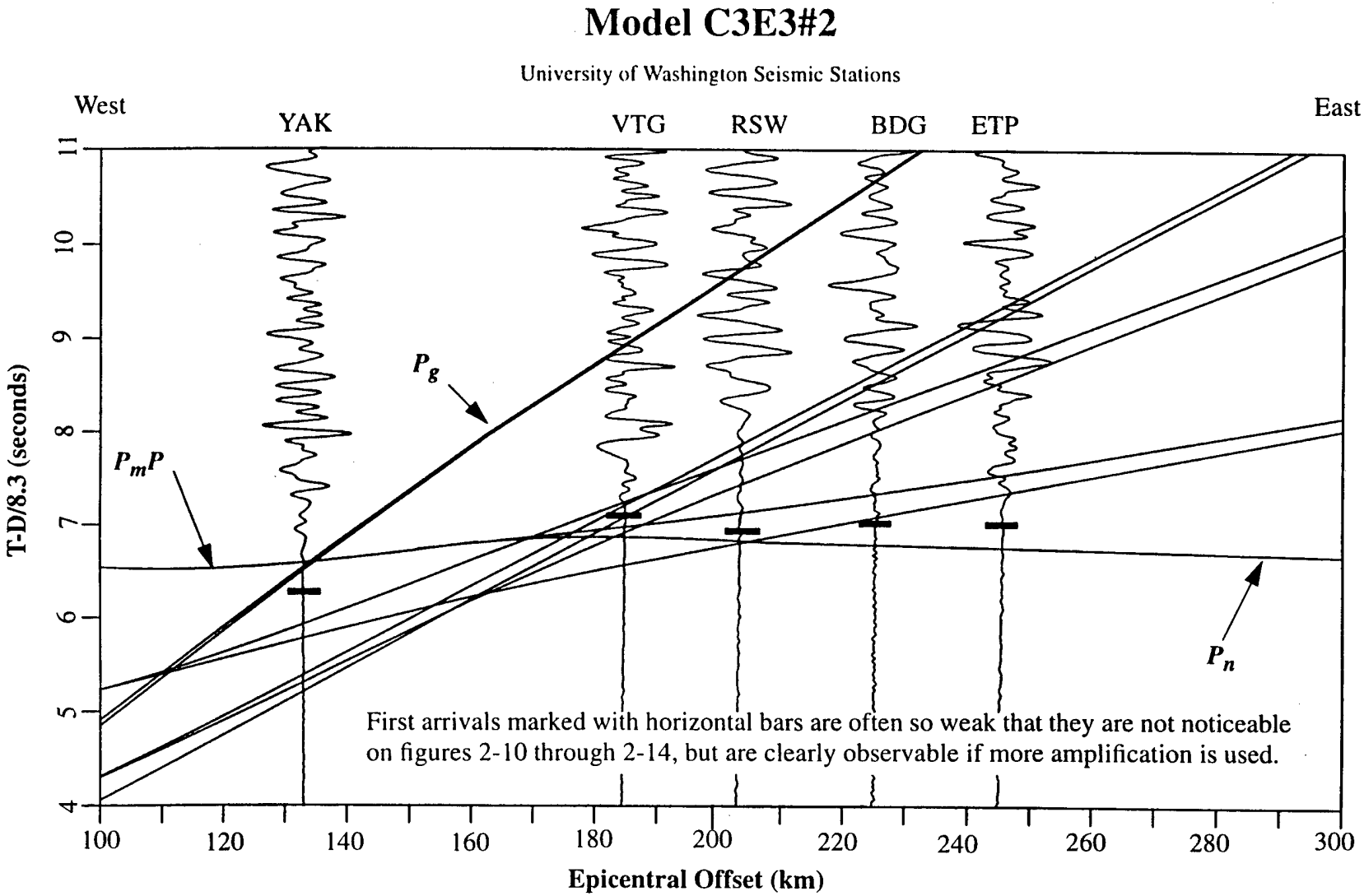

Figure 2-10. Traveltime plot using velocity model C3E3#2, event (81/02/14, 2127 UTC), depth 7.83 km. Traces are bandpassed at 1-10 Hz. Travel-time curves plotted but not labeled include reflections and head waves off the bases of velocity layers 3, 4 and 5. Traces are positioned based upon a 8.3 km/s reduced travel time. Horizontal bars across each trace mark the observed first arrival pick (see note on plot).

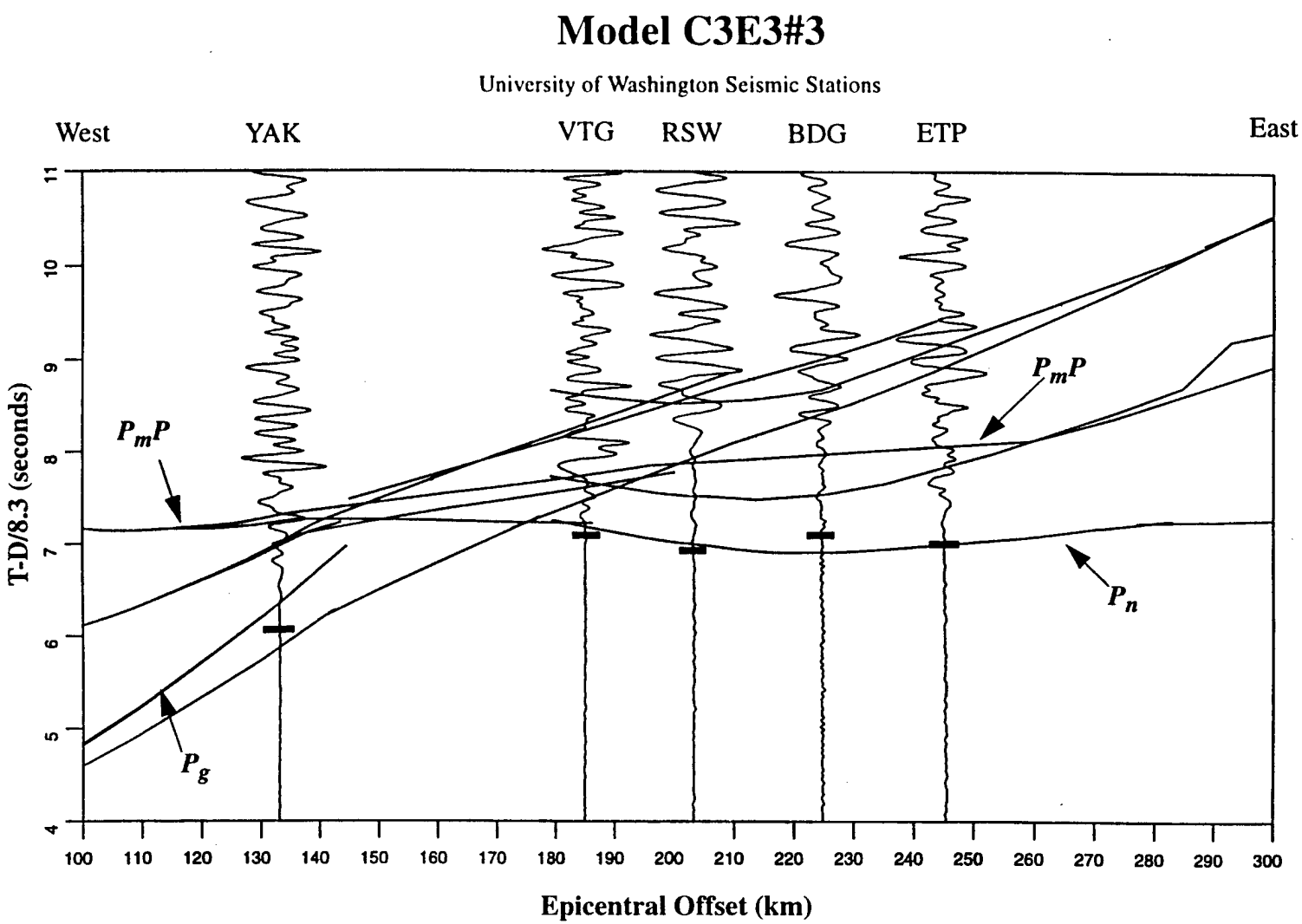

Figure 2-11. Traveltime plot using velocity model C3E3#3, event (81/02/14, 2127 UTC), depth 7.83 km. Traces are bandpassed at 1-10 Hz. Travel-time curves plotted but not labeled include reflections and head waves off the bases of velocity layers 4 and 5. Traces are positioned based upon a 8.3 km/s reduced travel time. Horizontal bars across traces represent observed time of first arrival. See note regarding first arrival amplification (Figure 2-10).

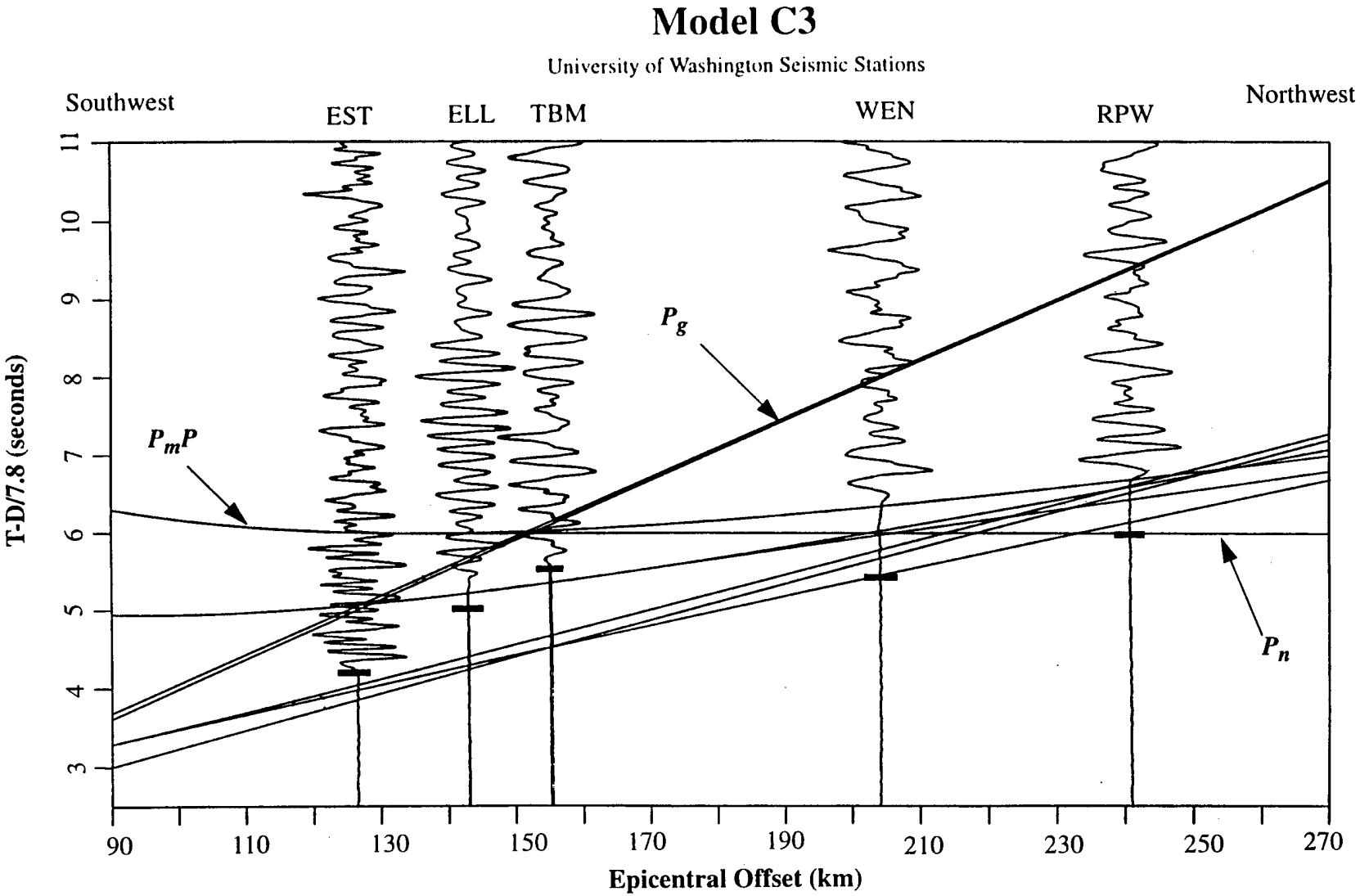

Figure 2-12. Traveltime plot using velocity model C3 for event (81/02/14, 2127 UTC), depth 7.83 km. Traces are bandpassed at 1-10 Hz. Travel-time curves plotted but not labeled include reflections and head waves off the bases of velocity layers 2, 3 and 4. Traces positioned based upon a 7.8 km/s reduced travel time. Horizontal bars across each trace represent observed time of first arrival. See note regarding first arrival amplification (Figure 2-10).

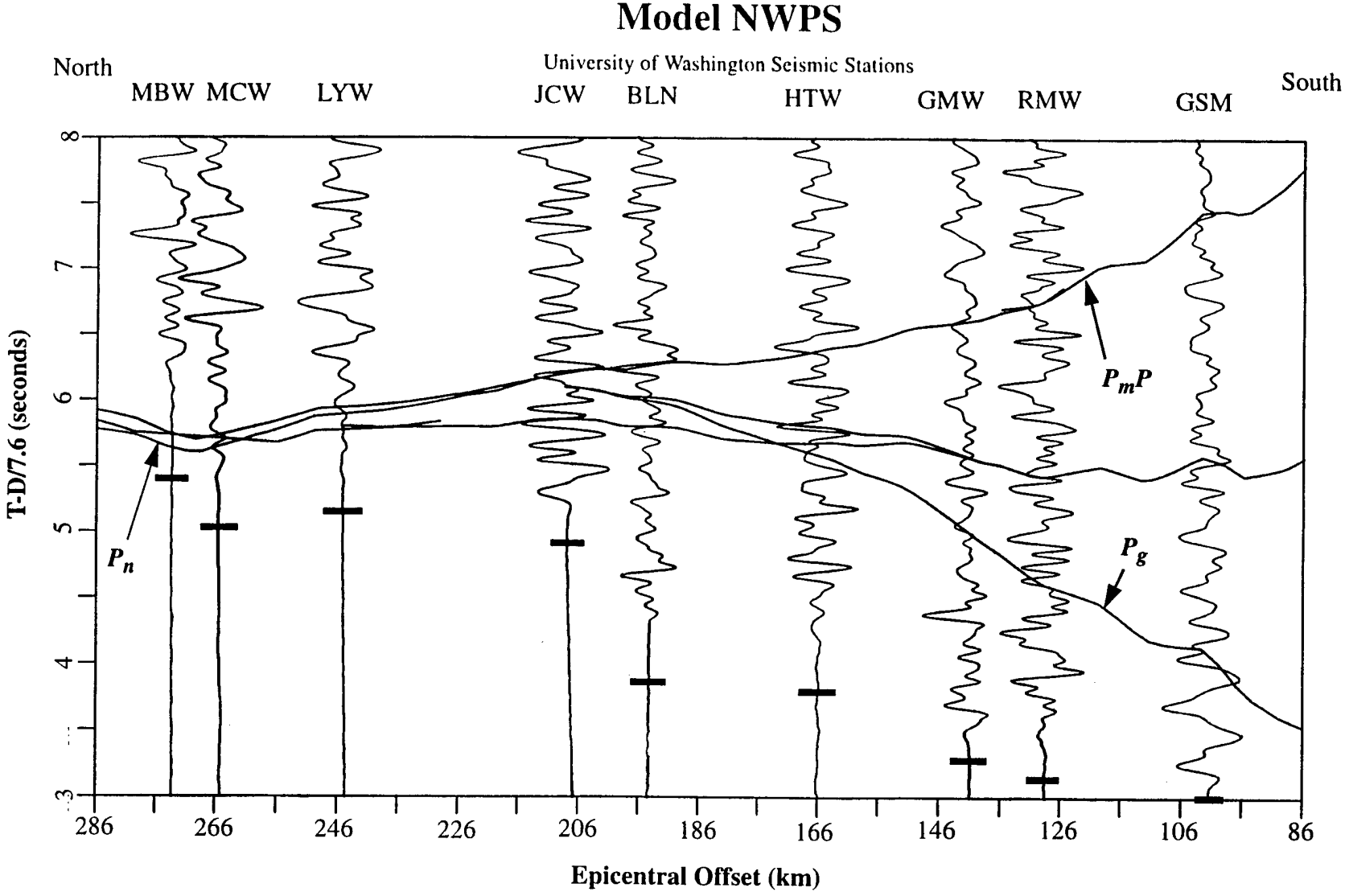

Figure 2-13. Traveltime plot using velocity model NWPS, event (81/02/14, 2127 UTC), depth 7.83 km. Traces are bandpassed at 1-10 Hz. Travel-time curves plotted but not labeled include reflections and head waves off the base of velocity layer 4. Traces positioned based upon a 7.6 km/s reduced travel time. Horizontal bars across each trace represent observed time of first arrival. See note regarding first arrival amplification (Figure 2-10).

Emergent P_n Waveforms, Eastern Washington

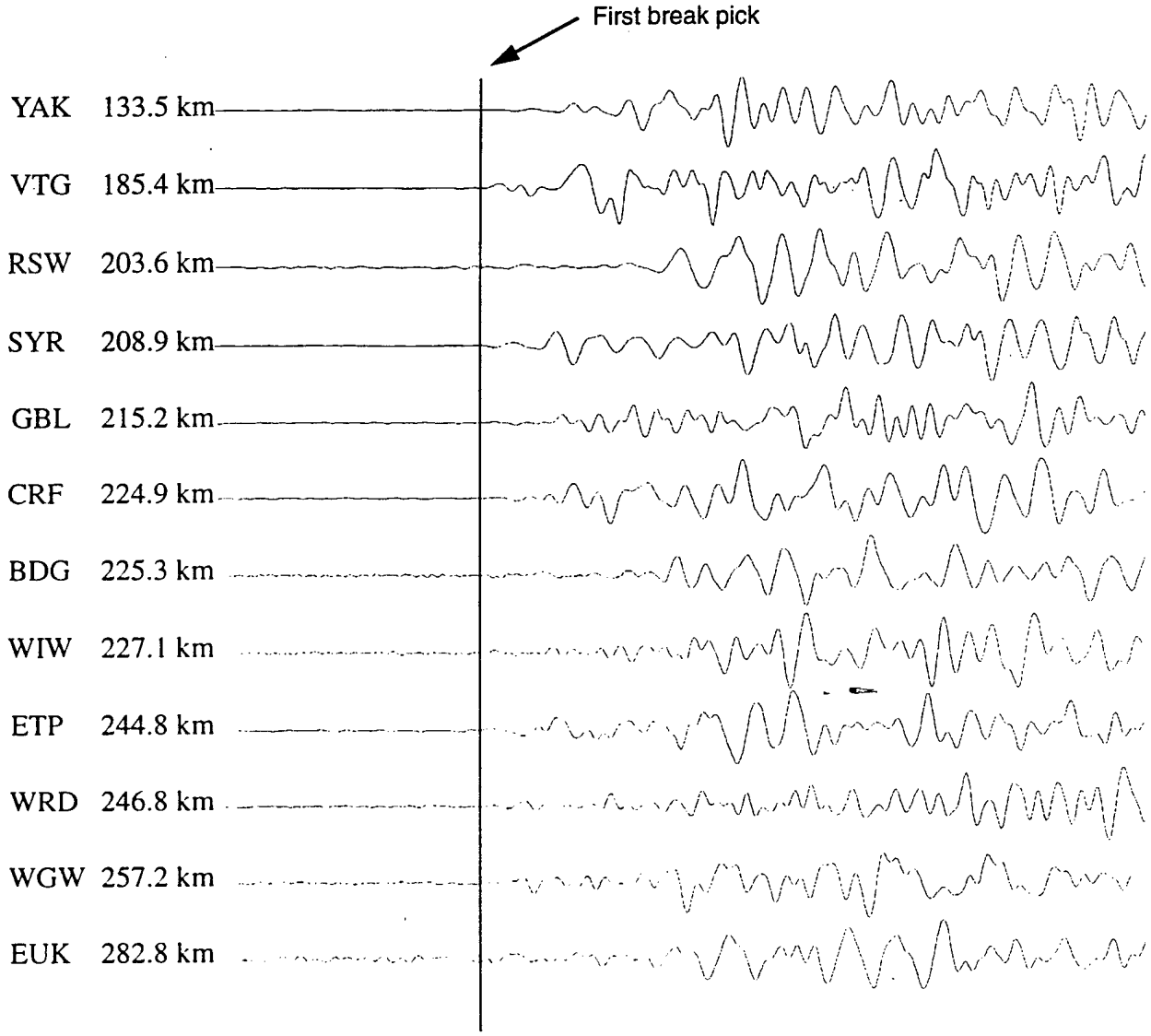

Figure 2-14. Seismograms from eastern Washington stations for aftershock of 14 February 1981 2127 UTC (magnitude 3.8, depth 7.8 km). Seismograms are 6.0 seconds in length, bandpassed at 1-10 Hz and are aligned on the observed first arrival time. Note weak and emergent first arrivals. See note regarding first arrival amplification (figure 2-10).

C3E3#2 and C3E3#3 (Figures 2-10 and 2-11) where P_g fails to propagate beyond 150 km offset due to its angle of approach causing it to critically refract. Predicted arrivals for model NWPS (Figure 2-13) have considerable error; what appear to be the proper phases arrive one to two seconds early.

3. Relatively strong P_mP arrivals may be seen in Figure 2-12 (model C3) at stations TBM, WEN, and RPW allowing a slight station delay. P_mP may also be present in Figure 2-10 (model C3E3#2) at stations YAK, RSW, BDG, and ETP. In Figure 2-11 (model C3E3#3) a weak P_mP phase may be seen at stations YAK, VTG, RSW, BDG and ETP, but this is not the same phase predicted to be P_mP by model C3E3#2.

4. The remaining reflected and critically refracted phases often arrive close together in short time windows (often one second or less), hampering efforts to identify distinct phases. This can be seen in Figure 2-10 (model C3E3#2) from offsets of 120 to 280 km, Figure 2-11 (model C3E3#3) at offsets between 140 and 240 km, and Figure 2-12 (model C3) between offsets of 195 and 260 km. Resolvable theoretical reflected phase arrival times occur between 100 to 130 km on all models. However, with the exception of some P_mP phases, arrivals are not recognizable. Filtering, which is discussed in Appendix A, is relevant to the topic of resolution of phases which arrive close together in time.

5. Several travel time plots were made for *S*-to-*P* conversions, but such phases are not obvious in the observed data.

6. Synthetic seismograms were produced but were oversimplified when compared to the actual data, and did not aid in the identification of regional crustal phases.

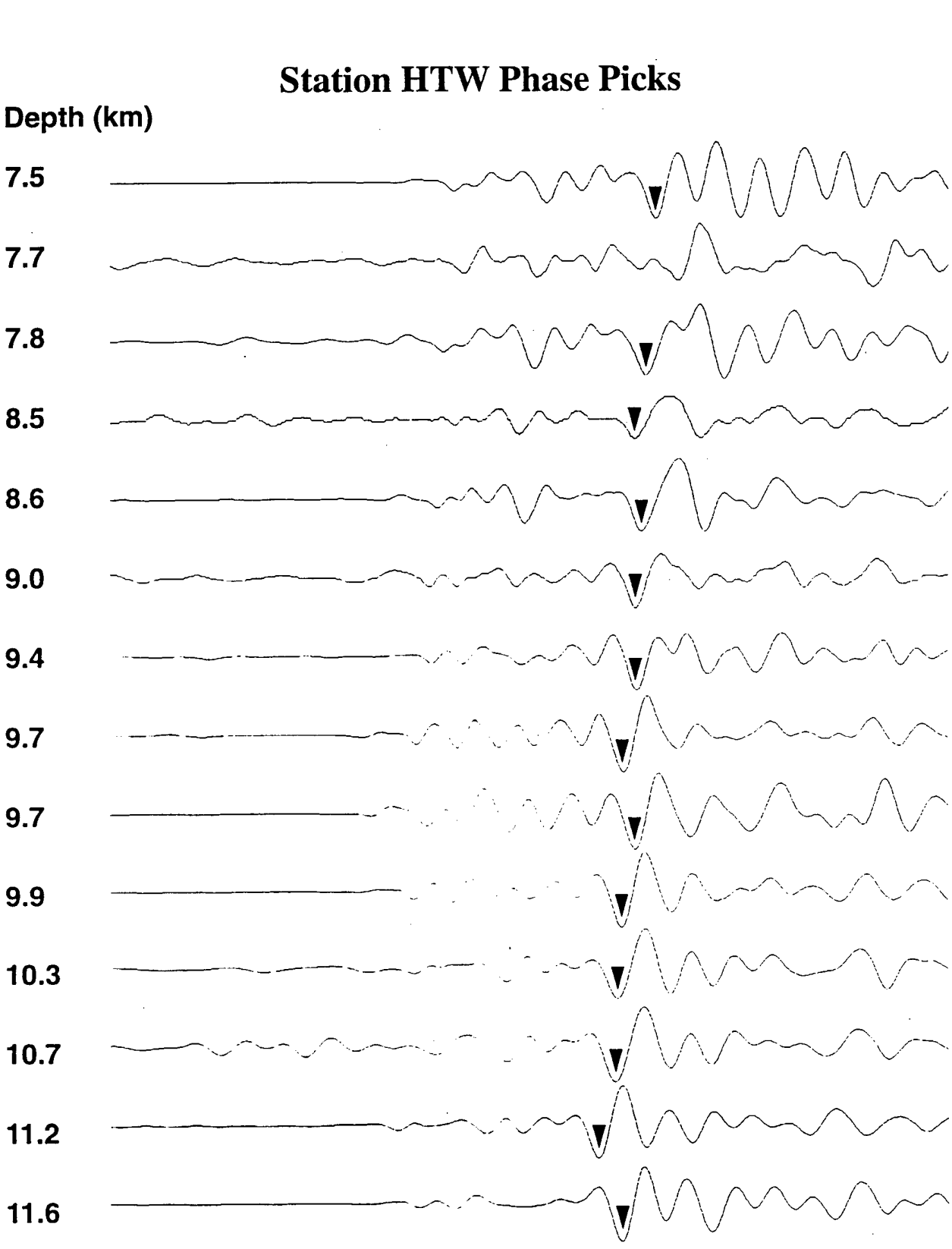

Figure 3-1. Seismograms and phase picks (arrows) from station HTW plotted in order of increasing hypocenter depth. Depths (in km) are listed to the left of the traces. Traces are: bandpassed at 1 to 3 Hz with a two pole Butterworth filter; 6 seconds in length; amplitude normalized; and aligned according to calculated P_g arrival times using a velocity of 6.0 km/s.

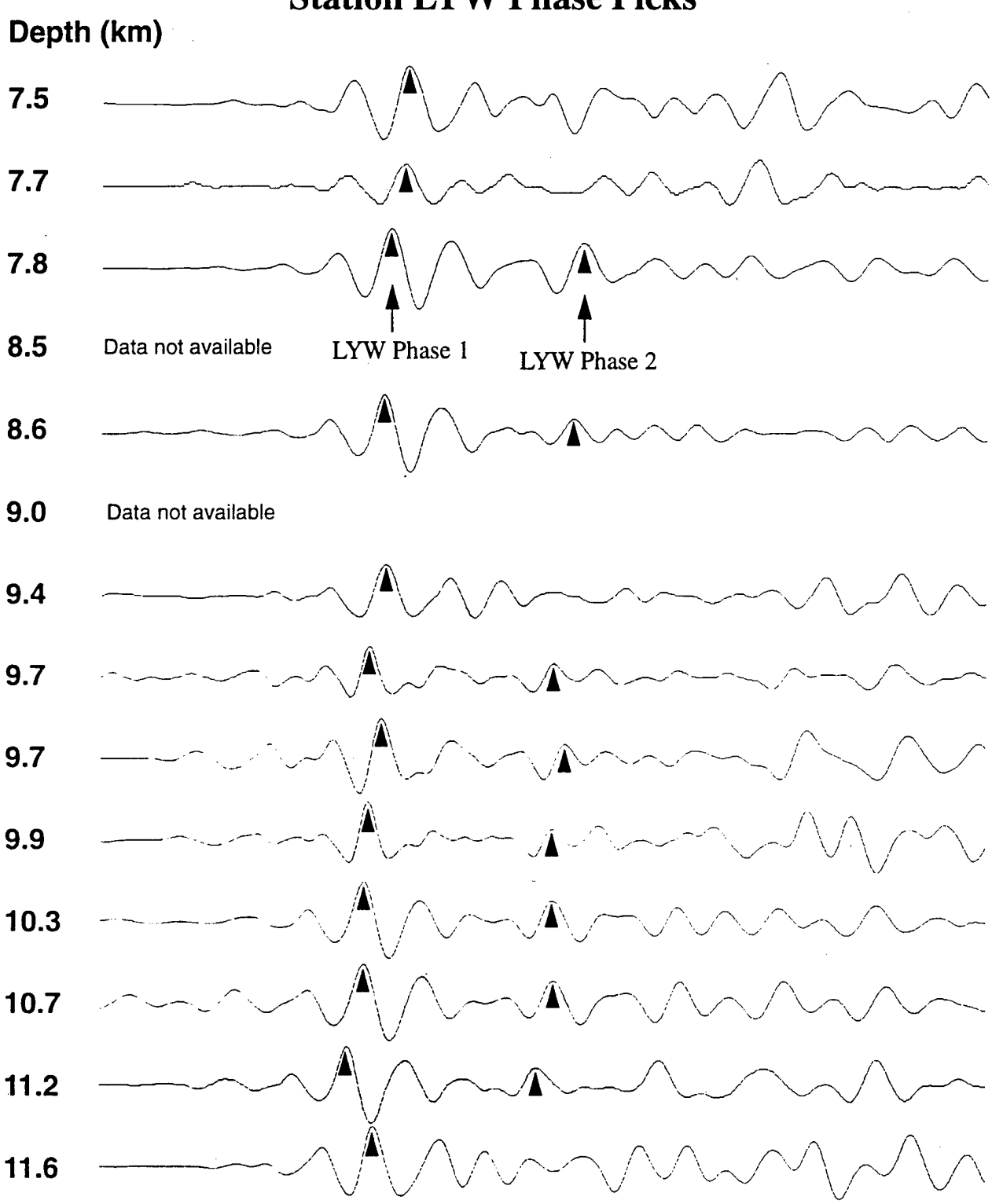

Figure 3-2. Seismograms and phase 1 and 2 picks from station LYW plotted in order of increasing hypocenter depth. Depths (in km) are listed to the left of the traces. Traces are: bandpassed at 1 to 3 Hz with a two pole Butterworth filter; 6 seconds in length; amplitude normalized; and aligned according to calculated P_g arrival times using a velocity of 6.0 km/s.

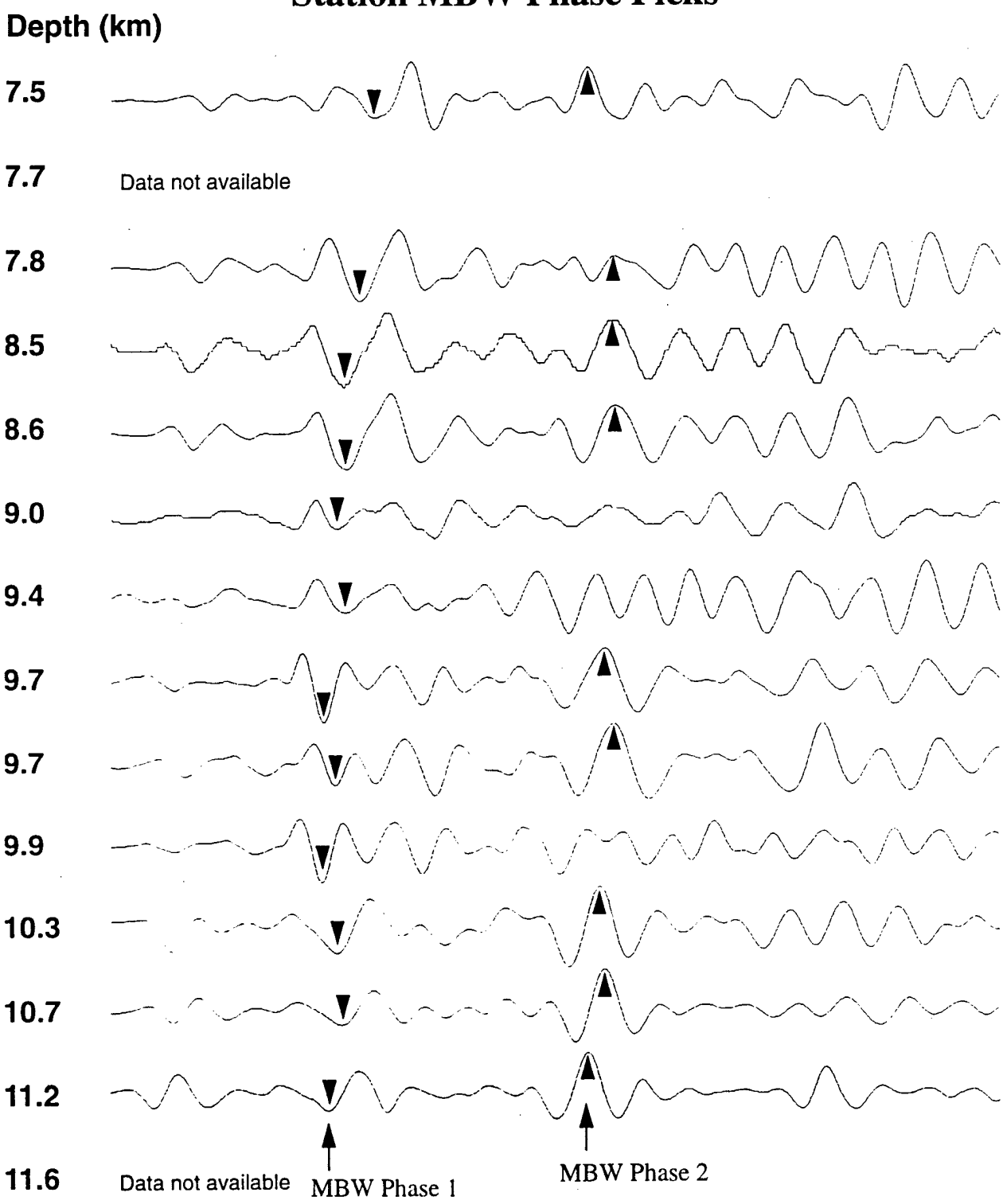

Figure 3-3. Seismograms and phase 1 and 2 picks from station MBW plotted in order of increasing hypocenter depth. Depths (in km) are listed to the left of the traces. Traces are: bandpassed at 1 to 3 Hz with a two pole Butterworth filter; 6 seconds in length; amplitude normalized; and aligned according to calculated P_g arrival times using a velocity of 6.0 km/s.

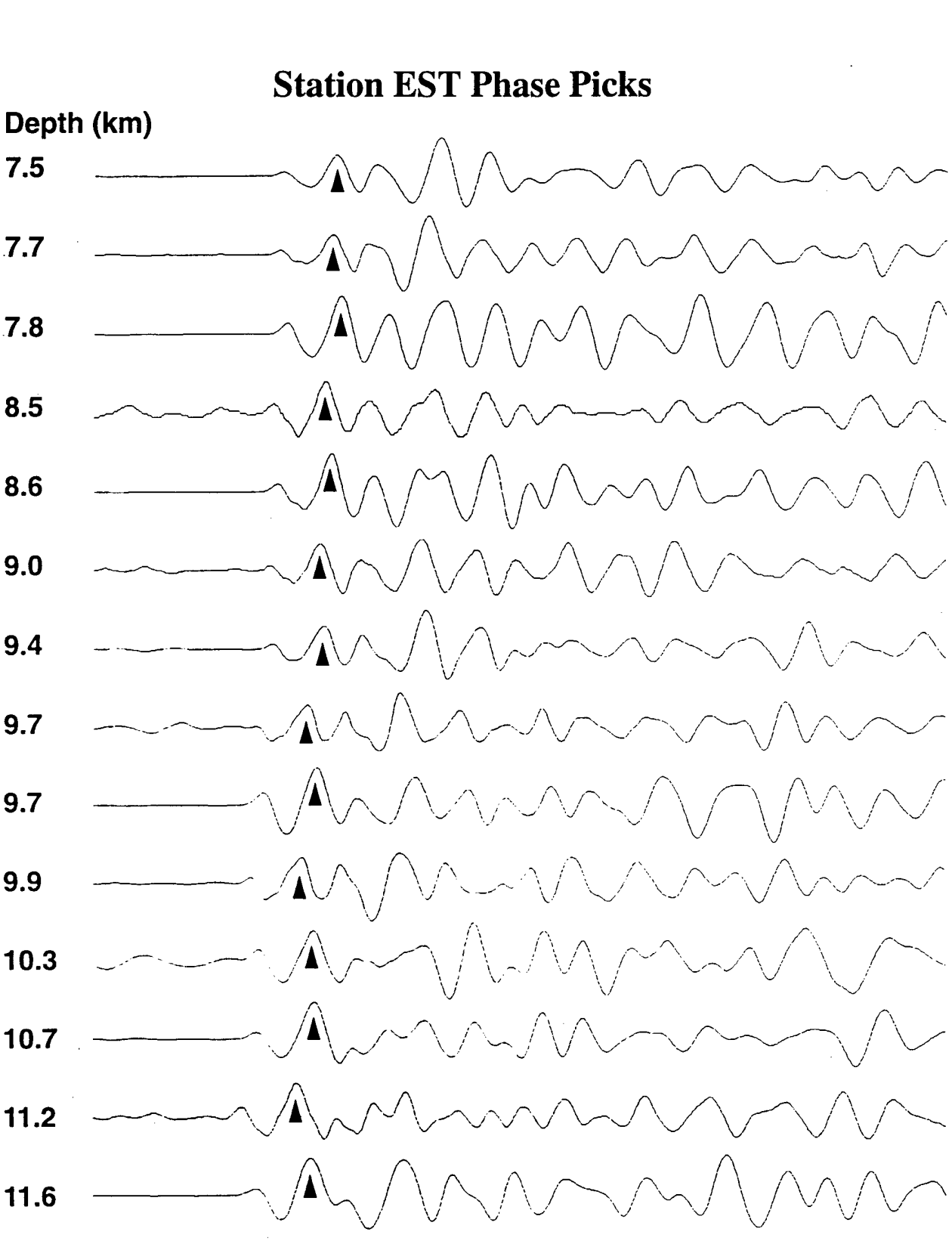

Figure 3-4. Seismograms and phase picks from station EST plotted in order of increasing hypocenter depth. Depths (in km) are listed to the left of the traces. Traces are: bandpassed at 1 to 3 Hz with a two pole Butterworth filter; 6 seconds in length; amplitude normalized; and aligned according to calculated P_g arrival times using a velocity of 6.0 km/s.

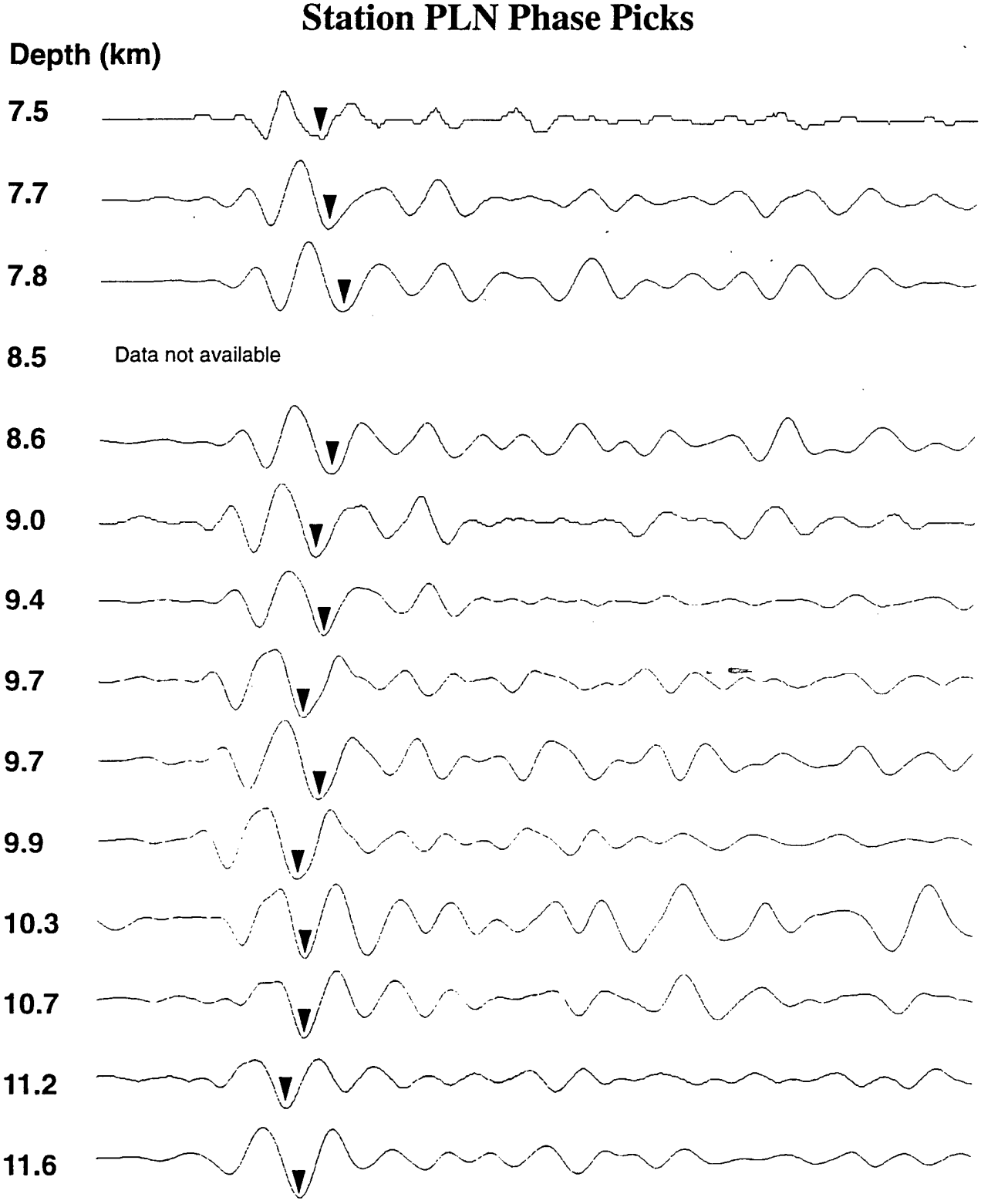

Figure 3-5. Seismogram and phase picks from station PLN plotted in order of increasing hypocenter depth. Depths (in km) are listed to the left of the traces. Traces are: bandpassed at 1 to 3 Hz with a two pole Butterworth filter; 6 seconds in length; amplitude normalized; and aligned according to calculated P_g arrival times using a velocity of 6.0 km/s.

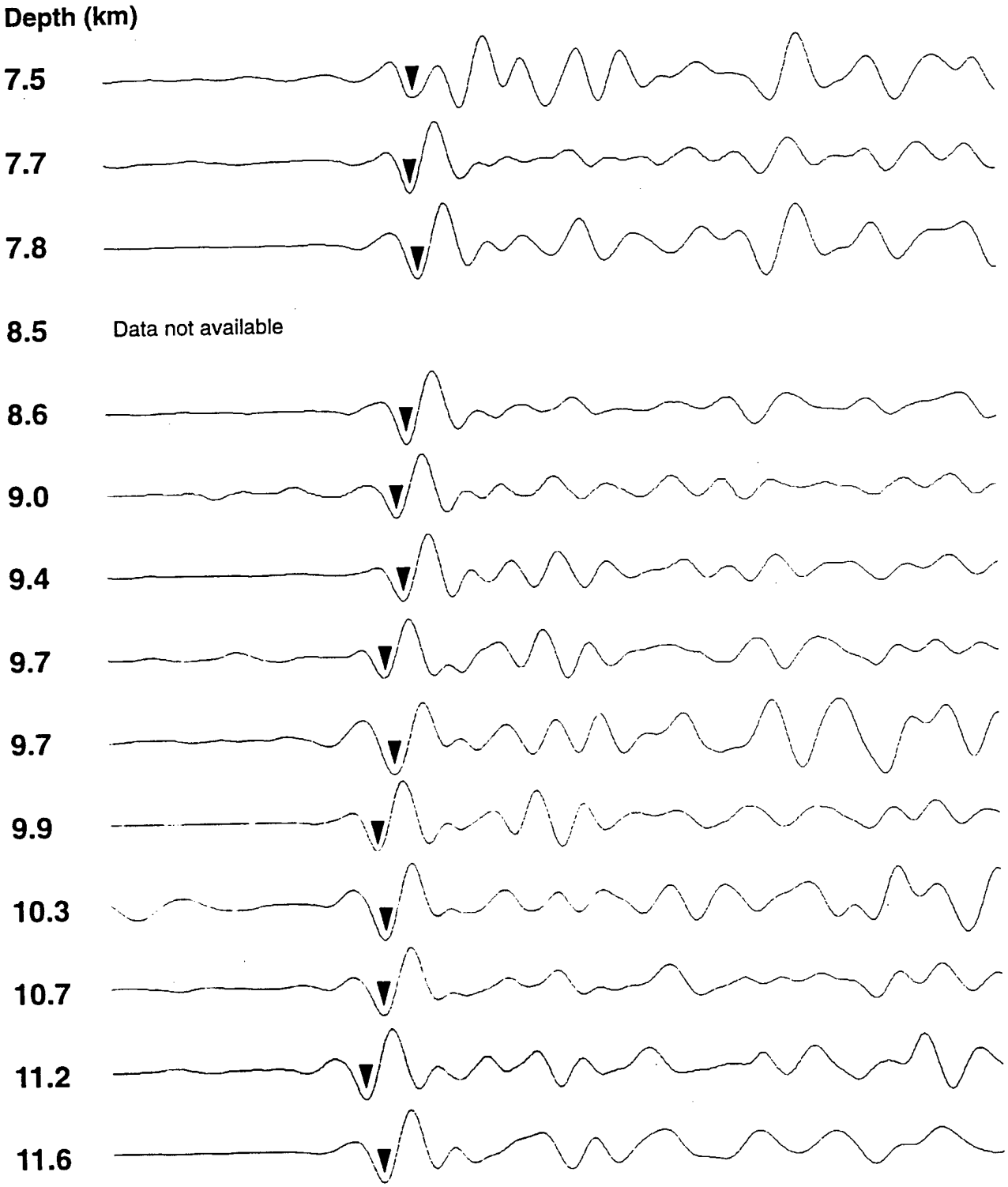

Figure 3-6. Seismogram and phase picks from station FPW plotted in order of increasing hypocenter depth. Depths (in km) are listed to the left of the traces. Traces are: bandpassed at 1 to 3 Hz with a two pole Butterworth filter; 6 seconds in length; amplitude normalized; and aligned according to calculated P_g arrival times using a velocity of 6.0 km/s.

3. EMPIRICAL IDENTIFICATION OF DEPTH-RELATED PHASES

Since the forward modelling described in the previous section appears to hold only modest promise, we attempted a more direct empirical approach. Since the Elk Lake earthquakes are well-located in a relative sense, we plotted seismograms in depth order at individual stations. The seismograms were arbitrarily aligned on the expected time of the P_g phase, whose travel time is virtually insensitive to depth at distances greater than a few focal depths. We found that of the 34 stations examined, 15 had arrivals that appear to be functions of focal depth. A selection of these seismograms at six stations is shown in Figures 3-1 through 3-6. We note that the depth-related phases are usually negative functions of increasing depth; this may be diagnostic of either reflections or refractions but not of direct waves. We have not attempted to positively identify the observed depth-related phases at this time; we are not optimistic of success in doing so in light of the forward modelling results. We note that the University of Washington stations are too widely separated to attempt identification based on apparent velocity.

At nearly all stations at which depth-related phases were observed, only one such phase was apparent. Since P_n and P_g were recorded poorly (if at all) at most of these stations, it appears that the hoped-for depth information can only rarely be developed from time differences between various P phases observed at a single station. At the stations where two depth-related P phases were noted, the relative time resolution was too low for these stations to be used for single-station depth estimates. A two-station methodology appears to offer some promise under the right conditions, however.

Two-Station Time Differences

We sought pairs of stations having observed depth-related phases and which were each situated at different distances along nearly the same azimuth from Elk Lake. The time differences between individual events' depth-related phases at these stations are themselves functions of focal depth, as long as the depth-related phase observed at both stations is not the same one (P_n time differences, for instance, would tend to be essentially constant). The effects of minor differences in the stations' azimuths were computed and corrections made to the observed time differences,

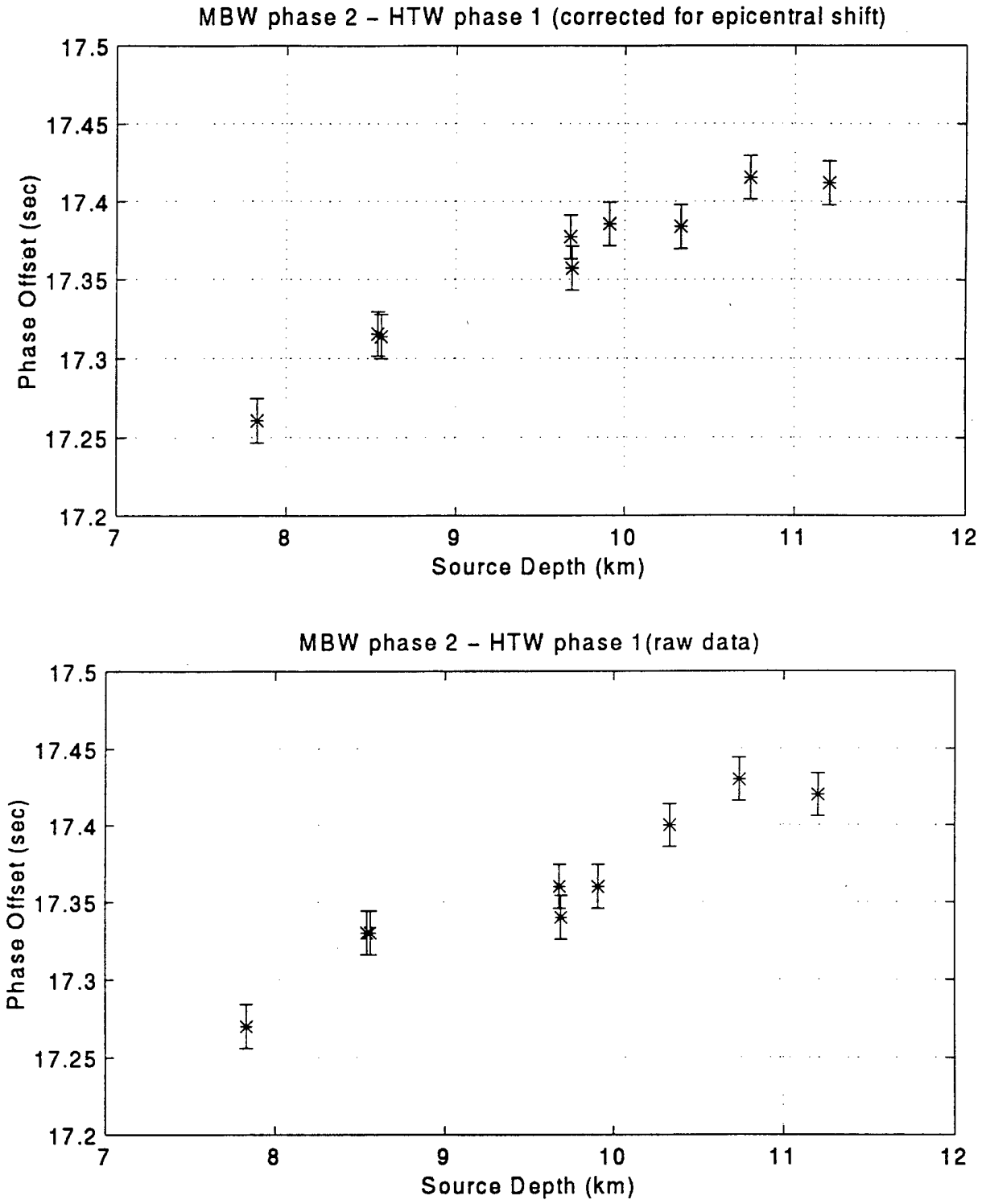

Figure 3-7. Phase offset plots between station MBW phase 2 and station HTW phase 1, corrected for epicentral shift (top) and uncorrected raw data (bottom). Error bars represent a standard deviation of +/- .014 s. Notice clear linear depth-dependent trend where phase offset increases with depth.

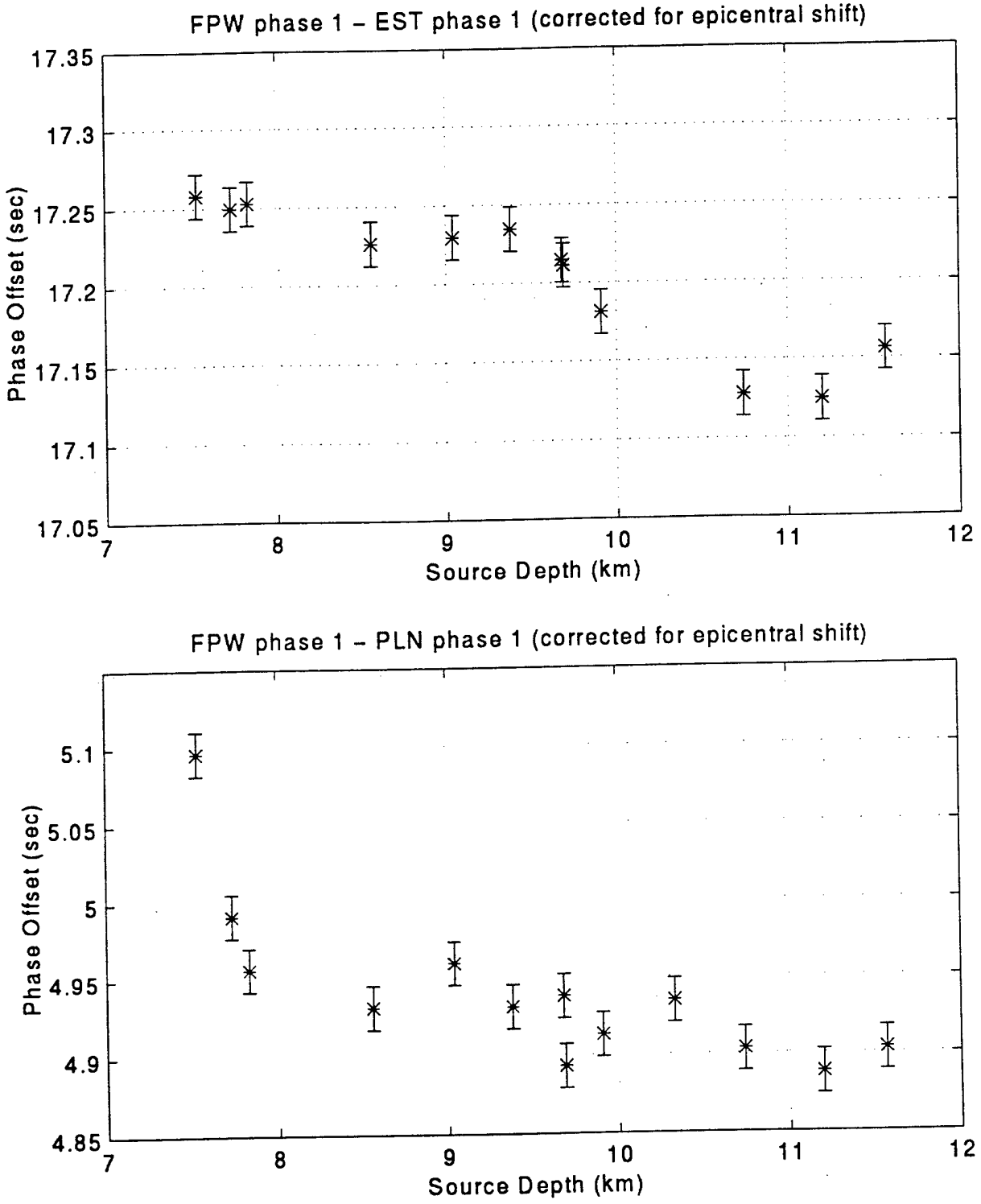

Figure 3-8. Phase offset plots between station FPW phase 1 and station EST phase 1 (top), and FPW phase 1 and PLN phase 1 (bottom). Error bars represent a standard deviation of +/- .014 s. Both plots are corrected for epicentral shift. Notice clear linear depth-dependent trend where phase offset decreases with depth.

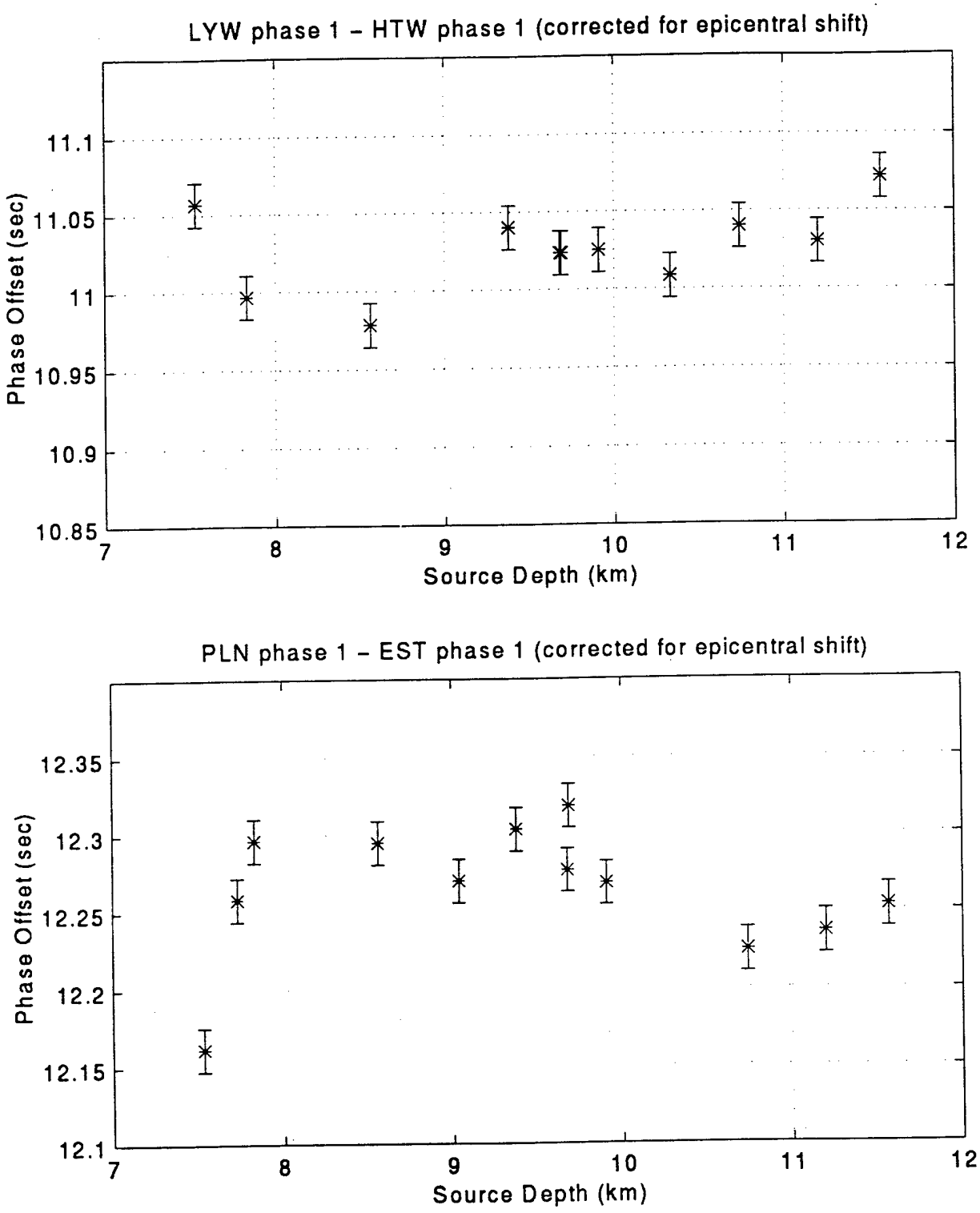

Figure 3-9. Phase offset plots between station LYW phase 1 and station HTW phase 1 (top), and PLN phase 1 and EST phase 1 (bottom). Error bars represent a standard deviation of +/- .014 s. Both plots have been corrected for epicentral shift. Notice lack of depth dependence, perhaps due to the fact that the same phase is seen at each station pair.

but for the station pairs selected this was always a second order effect (see Figure 3-7) and our conclusions would not be affected if this correction were not made.

Figure 3-7 shows an excellent example of a depth-related time difference which is a monotonic function of focal depth. The change in time difference with depth is small, but well within the observable range. Assignment of relative focal depths to an accuracy of the order of 0.5 km would appear to be possible using this curve as a calibration; the accuracy could possibly be increased if methods such as cross-correlation were employed rather than direct picking by an analyst. We hope to undertake work with both these objectives in the coming year.

Figure 3-8 shows two other station pairs that resulted in good trends. Not all stations show clear trends, as is evidenced by the two station pairs shown in Figure 3-9. A possible explanation for these trendless difference plots is that the observed depth-related phase in each pair is the same at both stations.

Not all the plots are directly interpreted. We observed some that show strong maxima or minima (see Figure 3-10 for examples). These plots are disturbing because a given time difference may correspond to two different focal depths. We have not yet attempted to explain how these time differences might arise from the travel times of different phases, or whether time differences at multiple pairs of stations might resolve the ambiguity.

DISCUSSION

The empirical approach to identification of depth-related phases from a calibration set, coupled with the use of the two-station time-difference method, appears to hold promise as a method for improving focal depth determination using a limited number of stations. So far, we see a limitation in the need to observe similarity between the waveforms for different events at the same station, which almost certainly will limit the depth range over which precise time differences may be determined. Another limitation is the need for a calibration set of events with known focal depths. We are nevertheless encouraged that development of robust methodology

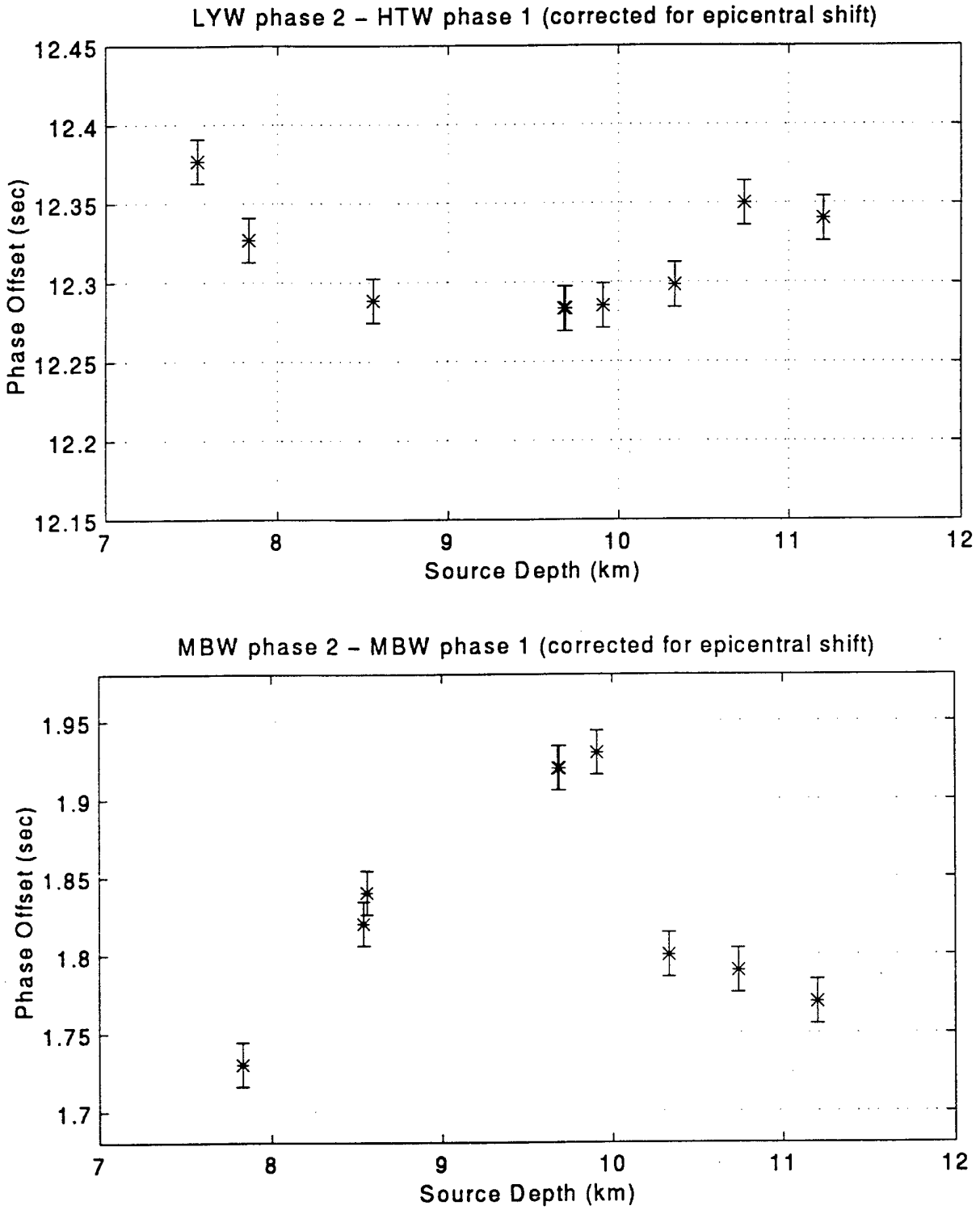

Figure 3-10. Phase offset plots between station LYW phase 2 and station HTW phase 1 (top), and MBW phase 2 and MBW phase 1 (bottom). Error bars represent a standard deviation of +/- .014 s. Both plots have been corrected for epicentral shift. Notice that equal phase offsets may correspond to two different depths.

that can be of practical use appears to be possible.

Appendix A. Seismogram Filtering

Seismogram filtering performs two useful functions. First, it suppresses background and telemetry noise that interferes with the desired signal. The analog telemetry systems employed by the University of Washington add significant high frequency electronic noise to the recorded signals and some of the stations occasionally record wind noise. Low pass and bandpass filtering often improved the observed signal. Second, low pass filtering enhances the similarity of events located in nearly but not quite the same place, as observed at a given station. All usable data we examined were the result of bandpass filtering the recorded data.

Filtering was performed using a two pole Butterworth filter, part of the University of Washington's interactive phase picking program *PING*. Stations were examined in a variety of frequency bands. For matching observed data with predicted arrivals we found that bandpassing between 1 and 10 Hz was optimum. The 10 Hz high cut allowed enough high frequency content to resolve separate phases while eliminating most of the unwanted high frequency noise. Examples of different filter settings are shown in Figure A-1 (bandpasses of 1-39 and 1-15 Hz), and Figure A-2 (bandpasses of 1-10 and 1-5 Hz), for arrivals of the 14 February 1981 2127 UTC aftershock (magnitude 3.8, depth 7.8 km) at the eastern Washington station group. The modelled travel time plots required the resolution of up to seven phases in time windows ranging from 1 to 3 seconds. High cuts below 10 Hz reduced our resolving power whereas high cuts above 15 Hz were complicated by their excessive high frequency component.

When the objective was to improve similarity from one event to the next at a single station in order to correlate phases across the entire depth range, the 1 to 3 Hz band proved to be the most effective. In Figures A-3 and A-4 depth order plots aligned upon the theoretical P_g arrival time are shown for station HTW for several bandpasses (1-39 Hz, 1-10 Hz, 1-5 Hz and 1-3 Hz). In Figure A-3 (bandpasses of 1-39 and 1-10 Hz) there appears to be some underlying similarity for up to 3 to 4 events. In contrast, in Figure A-4 (bandpass of 1-5 Hz) it can be seen that a single

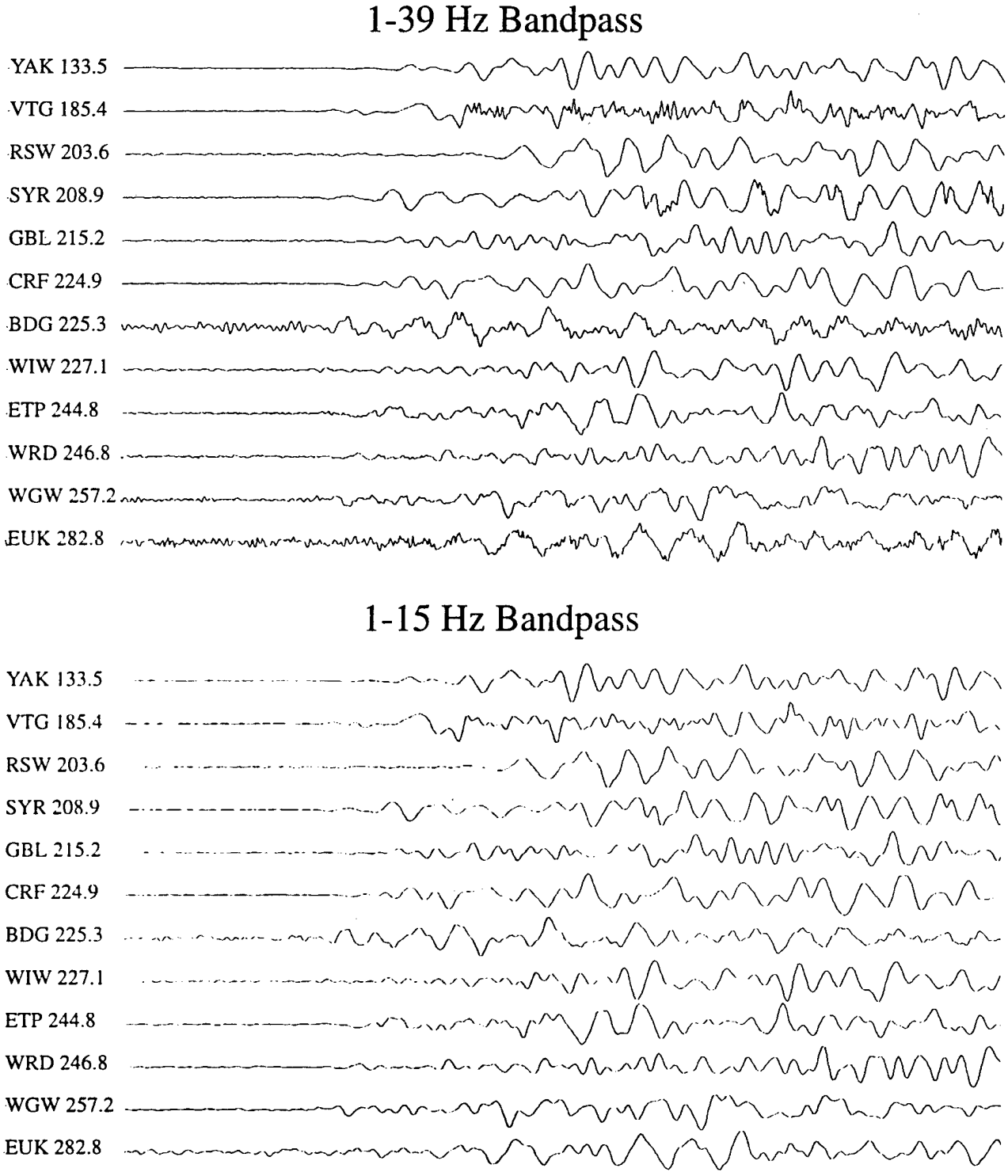

Figure A-1. Eastern Washington station group plotted at different bandpasses with respect to increasing epicentral offsets for the Elk Lake aftershock, 14 February 1981 2127 UTC (magnitude 3.8, depth 7.8 km). Traces are 6 seconds in length, aligned by time of first arrival and amplitude normalized. Station name and epicentral offset (km) are listed to the left of each trace.

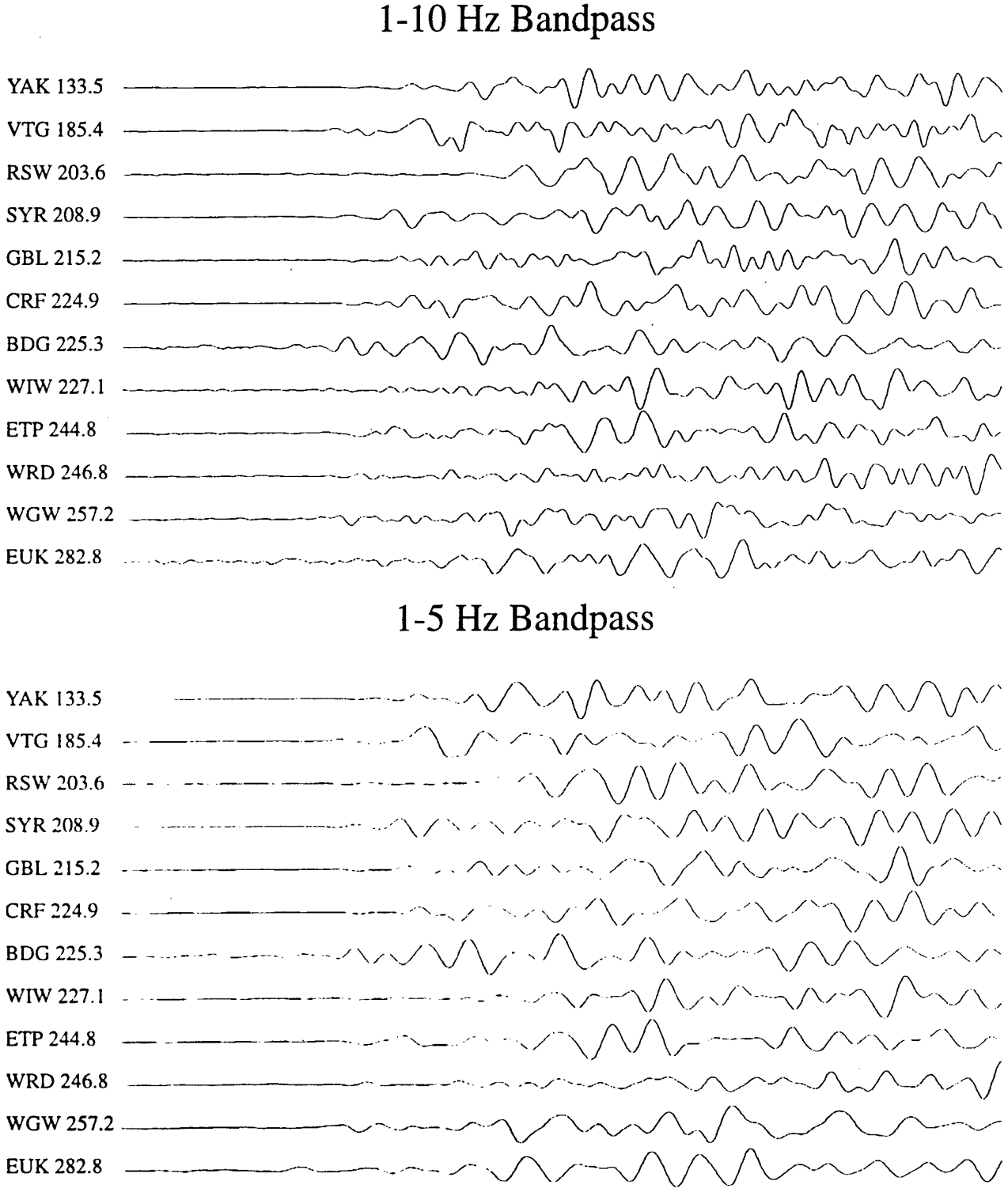

Figure A-2. Eastern Washington station group plotted at different bandpasses with respect to increasing epicentral offsets for the Elk Lake aftershock, 14 February 1981 2127 UTC (magnitude 3.8, depth 7.8 km). Traces are 6 seconds in length, aligned by time of first arrival and amplitude normalized. Station name and epicentral offset (km) are listed to the left of each trace.

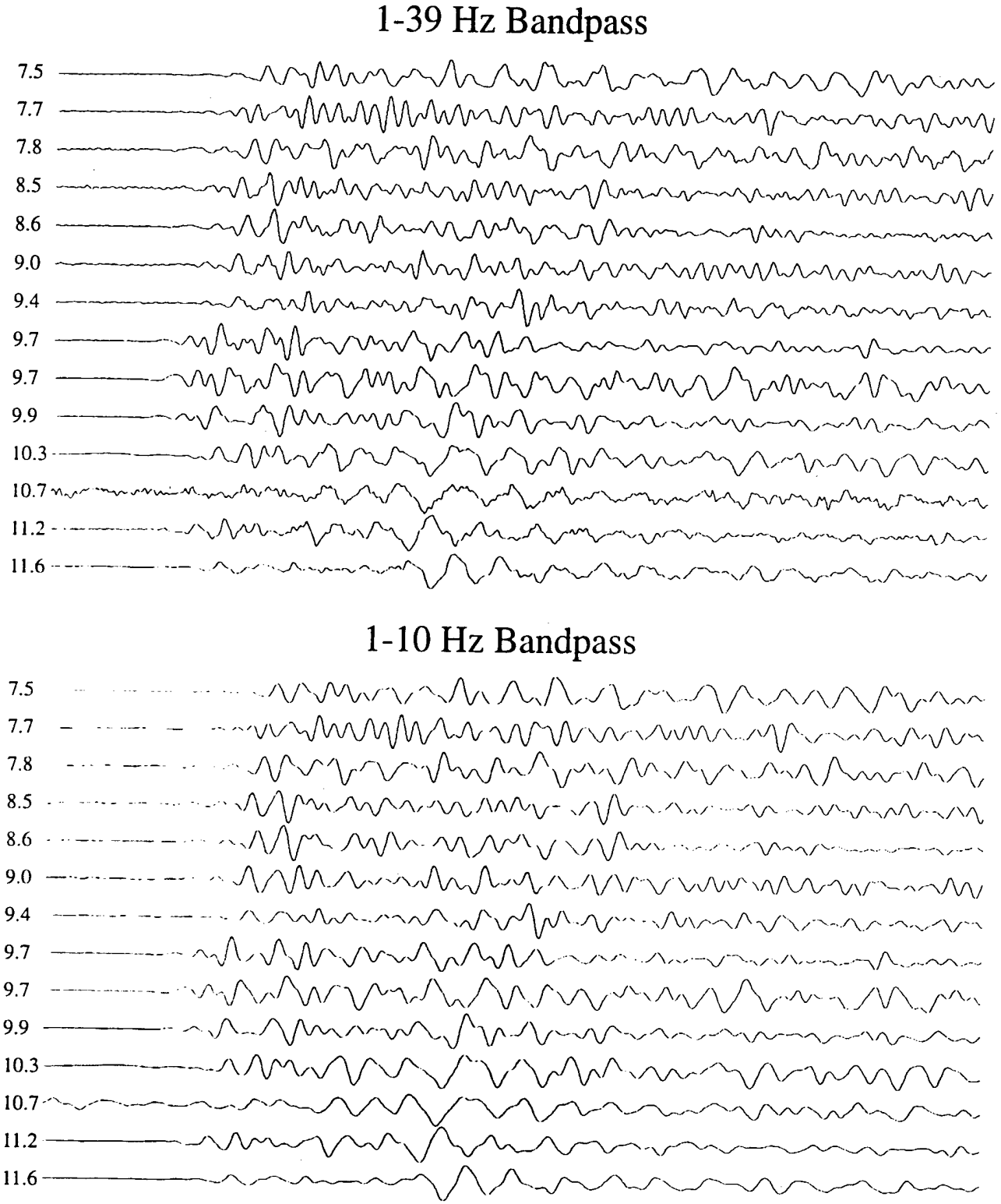

Figure A-3. Station HTW plotted with respect to increasing hypocenter depth at different bandpasses. Traces are 6 seconds in length, amplitude normalized and aligned according to calculated P_g arrival times using a velocity of 6.0 km/s. Hypocenter depths are listed to the left of the traces in km. Notice that though there is some phase correlation across 2-3 events no phase correlates across the entire depth range.

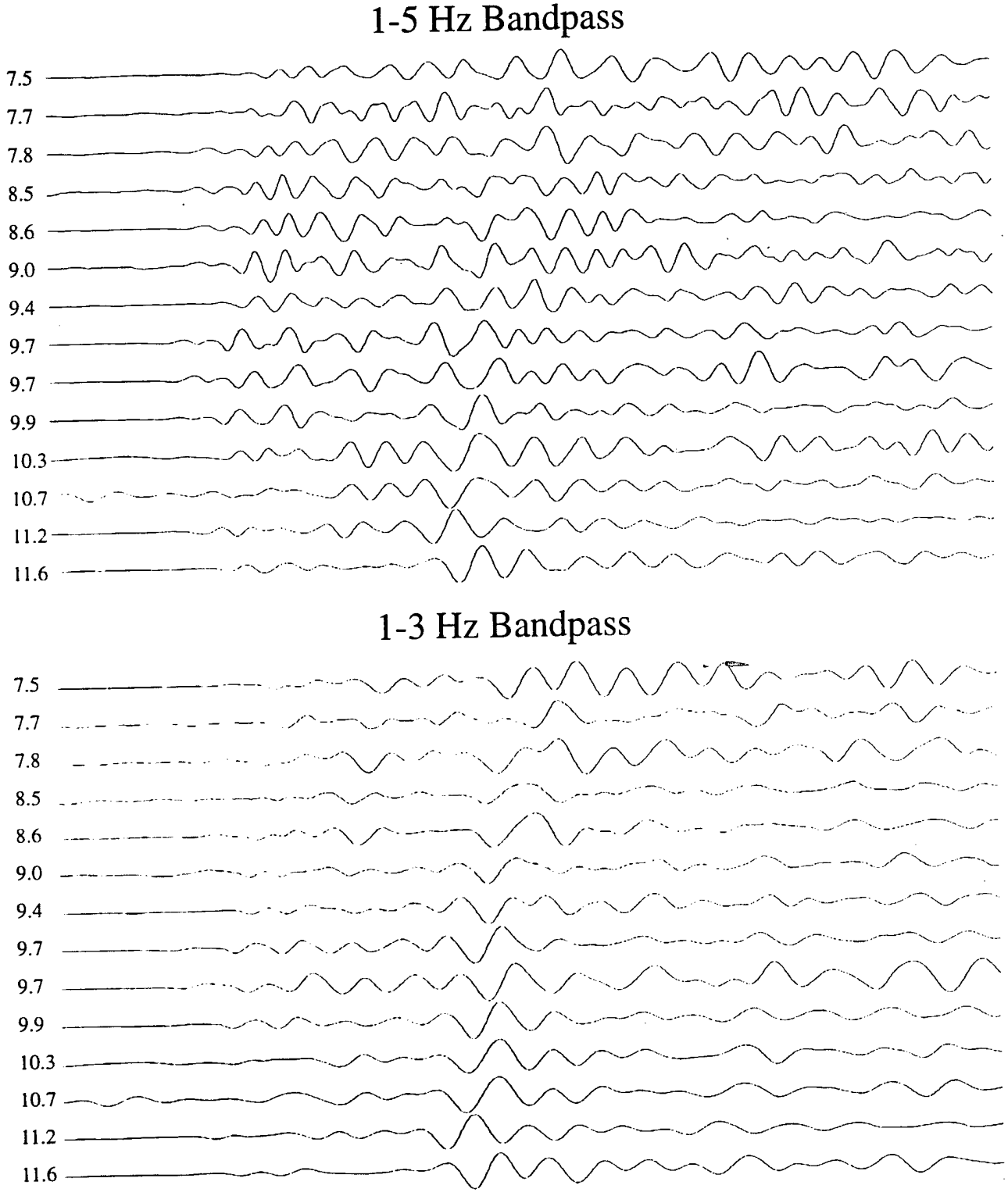

Figure A-4. Station HTW plotted with respect to increasing hypocenter depth at different bandpasses. Traces are 6 seconds in length, amplitude normalized and aligned according to calculated P_g arrival times using a velocity of 6.0 km/s. Hypocenter depths are listed to the left of the traces in km. Notice the appearance of phase correlation at 1-5 Hz bandpass and the improvement at 1-3 Hz bandpass. A 1-3 Hz bandpass appears to be optimum.

phase begins to correlate across most of the depth range. In the 1-3 Hz band, this phase is readily apparent across the entire depth range. Such phase enhancement using a 1-3 Hz bandpass has been observed to date at 15 stations (HTW, MBW, LYW, RPW, FPW, EST, PLN, BDG, ELL, ETP, ETT, TBM, WEN, WGW and YAK), out of 34 whose data we have examined.

REFERENCES

Catchings, R. D., and W. D. Mooney (1988), Crustal structure of the Columbia Plateau; Evidence for continental rifting, *Journal of Geophysical Research* **93**, 459-474.

Glover, D. W. (1985), *Crustal Structure of the Columbia Basin, Washington from Borehole and Refraction Data*, M. S. Thesis, University of Washington.

Grant, W. C., C. S. Weaver, and J. E. Zollweg (1984), The 14 February 1981 Elk Lake, Washington, earthquake sequence, *Bulletin of the Seismological Society of America* **74**, 1289-1309.

Leaver, D., W. D. Mooney, and W. M. Kohler (1984), A seismic refraction study of the Oregon Cascades, *Journal of Geophysical Research* **89**, 3121-3134.

Miller, K. C., G. R. Keller, J. M. Gridley, J. H. Luetgert, W. D. Mooney, and H. Thybo (1995), Crustal velocity structure in western Washington: Relationship to geology and seismicity, *Seismological Research Letters* **66**, 40.

Miller, K. C. and G. R. Keller (1993), *Proposal to Collaborate with the USGS Deep Continental Studies Group on the North Deployment of the Pacific Northwest Refraction Experiment*, Technical Report, 232 p.

Zelt, C. A., and R. B. Smith (1992), Seismic traveltime inversion for 2-D crustal velocity structure, *Geophysical Journal International* **108**, 16 - 34.